JYU DISSERTATIONS 136

Enni Nygrén

Recovery of Rubidium from Power Plant Fly Ash

UNIVERSITY OF JYVÄSKYLÄ
FACULTY OF MATHEMATICS
AND SCIENCE

JYU DISSERTATIONS 136

Enni Nygrén

Recovery of Rubidium from Power Plant Fly Ash

Esitetään Jyväskylän yliopiston matemaattis-luonnontieteellisen tiedekunnan suostumuksella
julkisesti tarkastettavaksi yliopiston Ylistönrinteen salissa YlistöKem4
lokakuun 4. päivänä 2019 kello 12.

Academic dissertation to be publicly discussed, by permission of
the Faculty of Mathematics and Science of the University of Jyväskylä,
in Ylistönrinne, auditorium YlistöKem4, on October 4, 2019 at 12 o'clock noon.

JYVÄSKYLÄN YLIOPISTO
UNIVERSITY OF JYVÄSKYLÄ

JYVÄSKYLÄ 2019

Editors
Ari Väisänen
Department of Chemistry, University of Jyväskylä
Ville Korkiakangas
Open Science Centre, University of Jyväskylä

Permanent link to this publication: http://urn.fi/URN:ISBN:978-951-39-7852-5

ISBN 978-951-39-7852-5 (PDF)
URN:ISBN:978-951-39-7852-5
ISSN 2489-9003

ABSTRACT

Nygrén, Enni
Recovery of rubidium from power plant fly ash
Jyväskylä: University of Jyväskylä, 2019, 98 p.
(JYU Dissertations,
ISSN 2489-9003; 136)
ISBN 978-951-39-7852-5 (PDF)

Although valuable rubidium (Rb) is present in large quantities in many natural sources, its concentration is low, and recovery are often uneconomical. Rubidium can concentrate on power plant fly ash when peat and wood residue is used as fuel. Accurate determination of rubidium and recovery from fly ashes originating from two Finnish combustion power plants were studied in this thesis.

Three different analysis methods based on ICP-OES (inductively coupled plasma – optical emission spectrometry), GFAAS (graphite furnace atomic absorption spectrometry), and ICP-MS (inductively coupled plasma – mass spectrometry) for determination of rubidium from different fly ash derived matrices were developed and evaluated. ICP-OES was found to be a useful analysis technique at ppm concentration levels when the observed ionization interference was corrected using the MLR-method. The GFAAS and ICP-MS analysis methods were found to be most suitable for the analysis of low rubidium concentrations. For the multi-elemental analysis of several elements, ICP-techniques are preferred.

Properties of fly ashes originating from different fuel contents were investigated by sieving the ashes into fractions by their particle size and determining their elemental content. The highest Rb concentrations (114 ± 3 mg kg^{-1}) were in fly ashes of 50% peat and 50% wood residue as fuel. Sieving the fly ash before the recovery of Rb did not offer any real benefit. The concentration of rubidium in different sized ash particles presumably depends on the origin of the fuel and the design of the power plant.

The developed recovery technique for Rb consists of oxalic acid leaching of fly ash, preparatory treatments of the leachate (recovery of oxalate and pH-adjustment) and liquid-liquid extraction using chlorophene. The oxalic acid leaching procedure is part of a patented method for recovery of rare earth elements (REEs) and platinum group metals (PGMs) from fly ash. The capability of oxalic acid to leach Rb from fly ash was compared to the total digestion results, and pH-adjustment prior to the liquid-liquid extraction was optimized. Using 1 mol L^{-1} chlorophene in chloroform as an organic phase with an A:O phase ratio of 1 and four extraction steps, 94% recovery of Rb was achieved. For stripping of Rb, 0.01-1 mol L^{-1} HCl was applied with excellent recoveries (96-100%). After using 0.01 mol L^{-1} HCl as a stripping solution, the extraction cycle was repeated three times to ensure low matrix content in the final solution.

In addition, the feasibility of potassium copper(II) hexacyanoferrate sorbent for the recovery of Rb was investigated. The synthesized sorbent was 3D-printed into a functional filter, which was found effective for the recovery of Rb from synthetic samples mimicking oxalic acid leached fly ash. However, the desorption of Rb from the functional filters was challenging, resulting in only a 60% recovery of Rb with 1 mol L^{-1} ammonium chloride solution. Desorption of Rb from the filters requires further investigations.

Keywords: Rubidium, fly ash, recovery, digestion, leaching, liquid-liquid extraction, chlorophene, potassium copper hexacyanoferrate, functional filter, ICP-OES, ICP-MS, GFAAS

Author's address

Enni Nygrén
Department of Chemistry
Renewable Natural Resources and Chemistry of Living Environment
P.O. Box 35
FI-40014 University of Jyväskylä
Finland
enni.k.nygren@jyu.fi

Supervisors

Professor Ari Väisänen
Department of Chemistry
University of Jyväskylä
Finland

Postdoctoral researcher Siiri Perämäki
Department of Chemistry
University of Jyväskylä
Finland

Reviewers

Professor Paavo Perämäki
Research Unit of Sustainable Chemistry
University of Oulu
Finland

Postdoctoral researcher Sami Virolainen
School of Engineering Science
LUT University
Finland

Opponent

Professor Ulla Lassi
Research Unit of Sustainable Chemistry
University of Oulu
Finland

PREFACE

The work presented in this doctoral thesis was conducted at the Department of Chemistry at the University of Jyväskylä between 2015-2019.

I own my deepest gratitude to my supervisors Prof. Ari Väisänen and Ph.D. Siiri Perämäki for the support and encouragement throughout these years. I would like to thank Ari for the opportunity to work in his research group and Siiri for her adept and patient guidance during this work. I also would like to thank referees Prof. Paavo Perämäki and Postdoctoral researcher Sami Virolainen for their valuable comments regarding this dissertation.

I am grateful for the financial support provided by Jyväskylän Energia Oy and for the expertise and collaboration of the Development Manager Risto Ryymin, who steered this project forewords. M.Sc. Antti Tiihonen is especially recognized for collaboration and preliminary work concerning this project. Special thanks go to M.Sc. Virva Kinnunen for her assistance with ICP-MS measurements and to M.Sc. Elmeri Lahtinen for his services by the 3D-printer. I also would like to thank all my colleges in the Chemistry Department for inspiring conversations and good memories.

Last, I would like to thank my family, my mother Ritva and my sisters Iina and Anna for their unconditional support and love. Also, I would like to honor the memory of my father Jari by acknowledging the support he gave me during my studies. And my dear friends, even if you are far away and we do not see often, I know I always have your love. Finally, my deepest gratitude goes to my loving spouse and best friend Mika, whose endless love and encouragement have kept me going. I am grateful to have you in my life.

Jyväskylä 20.9.2019

Enni Nygrén

CONTENTS

ABBREVIATIONS

α	Separation factor
AAS	Atomic absorption spectrometry
AC	Time-dependent alternating current
AMP	Ammonium molybdophosphate
AMP-PAN	Ammonium molybdophosphate with polyacrylonitrile
A:O	Aqueous to organic
BAMBP	4-*sec*-butyl-2-(α-methylbenzyl) phenol
BEC	Background equivalent concentration
c	Concentration
CCD	Charge-coupled device
CHN	Carbon, hydrogen and nitrogen
CPh	Chlorophene
CRM	Certified reference material
D	Distribution ratio
DC	Direct current
DOE	The U.S. Department of Energy
E%	Extraction efficiency
ecoba	European Coal Combustion Products Association e.V.
EIE	Easily ionized elements
EPA	Environmental Protection Agency
FAAS	Flame atomic absorption spectrometry
GFAAS	Graphite furnace atomic absorption spectrometry
GPS	Global positioning systems
HGA	Cylindrical graphite tube
ICP-MS	Inductive coupled plasma – mass spectrometry
ICP-OES	Inductive coupled plasma – optical emission spectrometry
IDL	Instrumental detection limit
ISTD	Internal standard
IUPAC	International Union of Pure and Applied Chemistry
KCuFC	Potassium copper hexacyanoferrate
KCoFC	Potassium cobalt hexacyanoferrate
K_D	Distribution coefficient
K(M)FC	Potassium (metal) hexacyanoferrate
KCuFC-PAN	Polymer encapsulated potassium copper hexacyanoferrate
Le	Oxalic acid leachate after recovery of oxalate
LOD	Limit of detection
LOQ	Limit of quantification
m	Mass
m_0	Characteristic mass
m/z	Mass to charge ratio
MDL	Method detection limit

MLR	Multiple linear regression
MW	Microwave
n.d.	Not detected
OxLe	Oxalic acid leachate
PFA	Perfluoroalkoxy alkane
PGM	Platinum group metal
pHad	pH adjusted leachate
ppm	Parts per million
ppt	Parts per trillion
QC	Quality control
QID	Quadrupole ion deflector
t-BAMBP	4-*tert*-butyl-2-(α-methylbenzyl) phenol
r	Correlation coefficient
rcf	Relative Centrifugal Force (G-force)
REE	Rare earth element
RF	Resorcinol-formaldehyde
RF power	Radiofrequency power
RSD	Relative standard deviation
RSD_L	Relative standard deviation from long-term measurements
RSD_S	Relative standard deviation from short-term measurements
s	Standard deviation
SCD	Segmented-array charge-coupled-device detector
SRM	Standard reference material
SWRO	Seawater reverse osmosis
SynpHad	Synthetic samples mimicking acid leached fly ash
TGHA	Transverse heated graphite tube
US	Ultrasonic
v/v	Volume to volume ratio
w/w	Weight to weight ratio

1 INTRODUCTION

Since 2018 the U.S. Department of the Interior and other executive branch agencies have listed rubidium as one of 35 critical materials, and they want to ensure secure and reliable supplies for the materials.[1] At present, rubidium and its compounds are mostly used in research and in some technical applications, and the market for rubidium is minor. However, the demand for rubidium is expected to rise due to the development of quantum mechanics -based computing devices. In the future, these applications can have the potential for relatively high consumption of rubidium. One of these applications is a quantum computer, which is expected to be in prototype phase in 2025.[2]

Although rubidium has 90 mg kg^{-1} of abundance in the Earth's crust, it is not a major constituent in any mineral.[3] Traditionally, rubidium is produced as a by-product of lithium, potassium, and cesium extraction from ores. If the demand for rubidium increases, alternative sources for rubidium are needed.

Increasing energy demand worldwide induces fly ash production in combustion process -based power plants. All the valuable non-volatile metals of the fuel used, including rubidium, can concentrate in fly ash. The particle size of fly ash is initially very small, and this reduces the need for pretreatment before its use in hydrometallurgical recovery process compared to mining where crushing and grinding of the ore are needed. The extraction of rubidium, among other elements, from fly ash is not only efficient due to minor pretreatment costs but it also utilizes material, which is usually considered as waste. Therefore, fly ash can be considered as a lucrative source for rubidium.

The recovery of valuable elements from fly ash can involve the extraction of the elements from the ash by acid leaching followed by the separation of the desired elements. Currently, precipitation, ion exchange, and liquid-liquid extraction are the most common methods for the separation of rubidium. In liquid-liquid extraction, substituted phenols, such as 4-*sec*-butyl-2-(α-methylbenzyl) phenol (BAMBP) and 4-*tert*-butyl-2-(α-methylbenzyl) phenol (*t*-BAMBP), have efficiently been utilized for selective extraction of Rb^+ and Cs^+ ions.[4-9] Chlorophene (2-benzyl-4-chlorophenol) has properties similar to BAMBP compounds, and it could be used for the extraction of rubidium.

Previously, ion exchange resins like potassium metal hexacyanoferrate sorbents have been used for removal of radioactive cesium from nuclear waste brine, and the same method has been used for the extraction of rubidium.[10,11] Potassium metal hexacyanoferrate powder is difficult to handle, and other more practical methods for the use of the sorbent have been investigated previously. For example, polymer encapsulated copper-based potassium hexacyanoferrates ($K_2[CuFe(CN)_6]$) have been used for the extraction of rubidium from seawater reverse osmosis (SWRO) brine.[12] Hexacyanoferrates have great potential for selective recovery of rubidium from different waste streams.

2 REVIEW OF LITERATURE

2.1 Rubidium

Robert Bunsen and Gustav Kirchhoff discovered rubidium in 1861, and it was named after the Latin word *rubidus*, meaning dark red as the red lines in its spectrum. Rubidium's chemical symbol is Rb, and it is positioned in group 1 of the periodic table between potassium (K) and cesium (Cs).[13]

2.1.1 Properties

Rubidium is a soft, ductile, silvery-white alkali metal that has a melting point of 39 °C. It´s most common oxidation state is +I, and it has a very low ionization energy of only 406 kJ/mol. After cesium, rubidium is the second most electropositive and alkaline element.[13]

The chemical properties of rubidium are typical of alkali metals. Rubidium is very reactive and can ignite spontaneously in the air with a violet flame. Its reaction with water can be explosive due to the release of hydrogen. In nature, rubidium exists in two isotopes: isotope 85 (72.2%) with isotopic mass 84.9118 u, and isotope 87 (27.8%) with isotopic mass 86.9092 u. In addition, 24 other isotopes have been manufactured artificially. Of naturally occurring isotopes, ^{87}Rb is slightly radioactive with a half-life of 49 billion years, and all artificial isotopes are radioactive.[14]

The rubidium ion is monovalent, and its most common compounds and their properties are presented in table 1. Rubidium can form water-soluble compounds like acetate, bromide, carbonate, chloride, chromate, fluoride, formate, hydroxide, iodide, nitrate, and sulfide. Rubidium forms double halide salts with antimony, bismuth, cadmium, cobalt, copper, iron, lead, manganese, mercury, nickel, thorium, and zinc. These compounds are generally water-insoluble. Rubidium metal can form alloys with other alkali and alkaline earth metals, antimony, bismuth, gold, and mercury. Rubidium can also form a number of chelates with ethers, thiols, and amine ligands.[13]

TABLE 1 Properties of rubidium and its most common solid compounds.[14]

Compound	Formula	Atomic/ molecular weight g mol^{-1}	Melting point °C	Boiling point °C	Density g cm^{-3}	Solubility in water g/100g
Rubidium	Rb	85.468	39.30	688	1.53	-
Rubidium bromide	RbBr	165.37	682	1,340	3.35	116 (25 °C)
Rubidium carbonate	Rb_2CO_3	230.95	837	-	-	223 (20 °C)
Rubidium chloride	RbCl	120.92	715	1,390	2.76	93.9 (25 °C)
Rubidium fluoride	RbF	104.47	833	1,410	3.2	300 (20 °C)
Rubidium hydrogen carbonate	$RbHCO_3$	146.49	175 (decomp.)	-	-	116 (20 °C)
Rubidium hydroxide	RbOH	102.48	382	-	3.2	173 (30 °C)
Rubidium iodide	RbI	212.37	642	1,300	3.55	165 (25 °C)
Rubidium nitrate	$RbNO_3$	147.47	305	-	3.11	65 (25 °C)

2.1.2 Abundance, occurrence, and production

Rubidium is the sixteenth most abundant metal in Earth´s crust with a concentration of 90 mg kg^{-1},[3] but it is usually widely spread and not found in high concentrations in any minerals.

Rubidium does not form any minerals of its own, but it is found in several common minerals were it has replaced other alkali metals.[15,16] The Rb^+ ion can substitute the K^+ ion in mica, such as muscovite $KAl_2(AlSi_3O_{10})(F,OH)_2$, and in feldspars, such as microcline ($KAlSi_3O_8$) and orthoclase ($KAlSi_3O_8$).[15,16] In rare minerals like lepidolite and pollucite, rubidium can replace potassium and cesium. Lepidolite $KRbLi(OH,F)Al_2Si_3O_{10}$ is a potassium lithium mica and contains up to 3.5% rubidium oxide. Pollucite $Cs_2O \cdot Al_2O_3 \cdot 4SiO_2$ is a cesium aluminium silicate that may contain up to 1.5% rubidium oxide.[2]

World resources of rubidium are not fully known. Although mineral sources of rubidium exist globally, the extraction of rubidium is not economically feasible due to the low concentrations in ores.[2] It is estimated that 2-4 tons of rubidium are globally obtained annually as a by-product of lithium and cesium extraction.[12] Rubidium-bearing pegmatite can be found in Afghanistan, Australia, Canada, China, Denmark, Germany, Japan, Kazakhstan, Namibia,

Peru, Russia, the United Kingdom, the United States, and Zambia.[2] Minor amounts of rubidium are reported in evaporates in France, Germany, and the United States and in brines in northern Chile and China. The mining of pollucite was known to take place periodically in Canada, Namibia, and Zimbabwe, but production in Canada ceased at the end of 2015. However, rubidium concentrate probably would continue to be produced as a byproduct of processing pollucite rocks from stocks.[2]

Traditionally, rubidium is recovered from ore by sulfuric acid leaching to form mixed alkali alums. The ore is usually calcined before leaching to increase the yield. The leaching is followed by filtration and wash of the residue. Different alkali alums are separated and purified by fractional recrystallizations. Rubidium alum can be converted to rubidium hydroxide by neutralization and precipitation of aluminium. The sulfate can be precipitated by barium hydroxide.[13]

Rubidium is also recovered from mixed alkali metal carbonates that are by-products generated during the processing of lepidolite and pollucite to extract lithium. In the chlorostannate method, dissolved carbonates are first converted to chlorides. Less soluble cesium chlorostannate is precipitated by stannic chloride and removed from the solution before more soluble rubidium chlorostannate precipitates. Rubidium chlorostannate can be purified by pyrolytic, electrolytic, or chemical methods.[13]

Methods that are more selective to recover rubidium are liquid-liquid extraction methods by substituted benzenes or crown ethers as extractants and methods based on solid cation exchangers like complex salts, such as hexacyanoferrates or nitrated and sulfonated polystyrenes.[14]

2.1.3 Applications

The main use of rubidium and its compounds is in research, but some applications, including biomedicine, electronics, specialty glass, and pyrotechnics, utilize rubidium. Rubidium salts are used in antishock agents and in the treatment of epilepsy and thyroid disorder. The radioactive isotope ^{82}Rb is used as a blood-flow tracer in positron emission tomographic imaging, and rubidium chloride is used as an antidepressant. Stability and durability in fiber optic telecommunications networks can be improved by rubidium carbonate, which reduces electrical conductivity.[2,13]

Ultra-cold rubidium atoms are used in a variety of applications in quantum computing research. Applications like quantum mechanics -based computing devices have the potential for relatively high consumption of rubidium in the future.[2] The photo-emissive properties of rubidium, which originate from surface-emitting free electrons induced by electromagnetic radiation, make it ideal for electrical-signal generators in night-vision devices, photoelectric cells, motion-sensor devices, and photomultiplier tubes. Rubidium also plays a vital role in global positioning systems (GPS) where it is used as an atomic resonance-frequency-reference oscillator for telecommunications network synchro-

nization.[2] Rubidium is also used in atomic clocks as an atomic resonance frequency standard.[13]

2.1.4 Price

There are no bulk prices available for rubidium metal or its compounds, but the value of rubidium can be estimated by commercial prices. Table 2 presents different prices of rubidium products offered by Alfa Aesar, manufacturer and supplier of chemicals, metals, and life science products for research and development, owned by Thermo Fisher Scientific.

TABLE 2 Commercial prices of rubidium and its compounds in March 2019.[17]

Compound	Package size (g)	Grade	Price (€)
Rubidium metal	1	99.75 %	124
	5	99.75 %	271
	100	99.75 %	2,038
Rubidium carbonate	100	≥99 %	228
Rubidium chloride	100	≥99 %	432
Rubidium nitrate	100	≥99 %	274
Rubidium sulfate	100	≥99 %	202

Prices of rubidium metal and its compounds depend on package size and purity of the product, and there is some difference with different suppliers. The price of the rubidium metal includes challenging handling and packing conditions due to the reactivity of the metal. Calculated from the price of the 100 g package, the price of rubidium metal is 20,380 €/kg, which is approximately half of the price of gold, at 37,000 €/kg.[18] The prices for rubidium compounds of ≥ 99% purity in a 100-gram container vary between 200 and 430 €.[17] Rubidium compounds are often more important commercially than the rubidium metal.

2.2 Fly ash

2.2.1 Properties

Energy production based on the combustion process generates combustion products like boiler slag, gypsum, flue gases, coarse bottom ash and fly ash. Fly ash is a fine powder of spherical glassy particles that is filtered from flue gases by electrostatic precipitators or mechanical filters. Fly ash is formed during combustion in a furnace at 1,100-1,400 °C when coal or biomass is used as fuel. Coal fly ash particles have an average size under 20 µm and a light texture. Bulk density of fly ash varies from 0.54 to 0.86 g cm^{-3}, and it has a high surface area (300-5010 m^2 kg^{-1}).[19]

2.2.2 Composition

The composition of fly ash depends mostly on the fuel used in the combustion process. Fly ash consists mainly of metal oxides, but the composition can variate widely even with the same fuel group as seen in table 3. However, there are significant differences between fly ashes from different fuels. Silicon dioxide and aluminium oxide are the major components in coal fly ash while calcium oxide, silicon dioxide, and potassium oxide cover over 75% of the weight percentages of wood and wood residue fly ash. In peat fly ash, the major components are SiO_2, Al_2O_3, Fe_2O_3, SO_3 and CaO covering over 90% of the oxides, but this result relies only on one sample.[20]

After combustion, trace elements of the fuel can concentrate in fly ash. Many potentially harmful elements, such as Cr, Pb, Ni, Ba, Sr, V, and Zn, can be present in fly ash, but valuable elements, like rare earth elements and platinum group metals, can also be found in recoverable concentrations.[19,21-23]

Rubidium concentration in coal ash is 48-110 mg kg^{-1} [24] and in plant ash 100 mg kg^{-1} [25], which is a higher concentration than in the Earth's crust.

TABLE 3 Composition of fly ash as weight percentages when coal[26], wood and wood residue[20], or peat[20] is used as a fuel.

	Coal				Wood and wood residue				Peat
	Mean	Min	-	Max	**Mean**	Min	-	Max	
SiO_2	**54.1**	32.0	-	68.4	**22.2**	1.86	-	68.2	**37.5**
Al_2O_3	**23.2**	11.3	-	35.2	**5.09**	0.12	-	15.1	**20.1**
Fe_2O_3	**6.85**	0.79	-	16.4	**3.44**	0.37	-	9.54	**13.8**
CaO	**6.57**	0.43	-	27.8	**43.0**	5.79	-	83.5	**9.97**
SO_3	**3.54**	0.27	-	14.4	**2.78**	0.36	-	11.7	**12.1**
MgO	**1.83**	0.31	-	3.98	**6.07**	1.10	-	14.6	**2.14**
K_2O	**1.60**	0.29	-	4.15	**10.8**	2.19	-	32.0	**1.12**
TiO_2	**1.05**	0.62	-	1.61	**0.29**	0.06	-	1.20	**0.31**
Na_2O	**0.82**	0.09	-	2.90	**2.85**	0.22	-	29.8	**0.10**
P_2O_5	**0.50**	0.10	-	1.70	**3.48**	0.66	-	13.0	**2.75**
Sum	**100**				**100**				**100**
Samples	37	37		37	28	28		28	1

2.2.3 Production

In 2016, fly ash covered 64% of coal combustion products in Europe.[26] Today, estimation for coal fly ash production worldwide is over 900 million tons annually.[19,26] In addition to coal, different biomass products can also be used as a fuel in combustion processes. Biomass contributes 8–15% of the world energy supplies, and estimation for bio fly ash production is 470 million tons per year.[20]

2.2.4 Utilization

The estimated global average utilization rate of fly ash is 25%.[19,27] For the largest fly ash producers, current utilization rates have been estimated to be 50% for the USA, 44% for the EU[26], and 60% for India. For China, estimations between 30-70% have been made from different sources.[19]

The utilization of fly ash is mostly defined by its elemental content. If fly ash has a low content of toxic elements, suitable pH, and high water-holding capacity, it is a good source for essential plant nutrients and can be used in soil improvement. If valuable metals of the fuel used will concentrate in fly ash, it can be used as an alternative source for those metals compared to mining. In the cement industry, fly ash has been used as a raw material or as an additive, depending on its CaO content.[19] In Europe, most of the utilized fly ash is used in concrete and cement products as can been seen in table 4.

TABLE 4 Production and utilization of coal combustion fly ash as kilotons (kt) and percentages (%) in Europe in 2016 (modified from [26]).

Production of fly ash	**kt**	**(%)**
	25700	100
Utilization of fly ash	**kt**	**(%)**
Concrete addition	4,640	18.0
Blended cement	1,930	7.50
Cement raw material	1,890	7.33
Road construction	1,860	7.24
Concrete Blocs	625	2.43
Other	420	1.63
Total utilization	11,400	44.1

2.3 Recovery of rubidium

Compounds of alkali metals are highly soluble in water and do not easily form precipitates or complex ions. They all have similar aqueous chemistry, which makes separation and purification of rubidium from other alkali metals difficult. Most of the separation methods are size-selective and are based on the different ionic or hydrated ionic radii of alkali metals ions or the electron potentials of the ions. At present, the main methods for separation of rubidium are precipitation, ion exchange, and liquid-liquid extraction methods.

2.3.1 Liquid-liquid extraction

Liquid-liquid extraction or solvent extraction is a method where the solute is transferred from one phase to another.[28 pp. 538-342] Transfer takes place between two different immiscible liquids, usually water (polar) and an organic solvent (non-polar). In most cases, liquid-liquid extraction is done either to isolate or concentrate the desired ions or separate them from undesired matrix elements. Usually, ions are selectively extracted from the water phase into the organic phase. After possible scrubbing stages where impurities are extracted from loaded organic phase, ions are stripped back into a water phase by a stripping solution.

Despite the variation in the experimental conditions, distribution of the analyte ions between the water and organic phases can be described by distribution ratio D. It is the ratio of the total concentration of an ion (M^+) in the organic phase to the concentration in the aqueous phase at equilibrium:[28 pp. 538-342]

$$D = \frac{c(M^+)_{org}}{c(M^+)_{aq}} = \frac{(c_i - c_f)}{c_f} \cdot \frac{V_{aq}}{V_{org}} \quad (1)$$

In equation 1, c_i and c_f are the initial and final concentrations (mg L^{-1}) of the analyte ions in the aqueous phase at equilibrium, and V_{aq} and V_{org} are the volumes (mL) of the phases. Often, it is beneficial to use extraction efficiency $E(\%)$ to describe the amount of analyte ions extracted from the water phase to the organic phase (or vice versa):

$$E(\%) = \frac{(c_i - c_f)}{c_i} \cdot 100\% \quad (2)$$

The separation of two different ions (ion A and ion B) after liquid-liquid extraction can be illustrated by separation factor α:

$$\alpha = \frac{D_A}{D_B}, \quad (3)$$

where D_A and D_B are distribution ratios of ions A and B, respectively. The more the separation factor α differs from one, the more effective the separation of ions A and B is.

In the solvent extraction, the most common extractants for recovery of rubidium are substituted phenols, crown ethers, and other cyclic ethers.

Phenolic compounds

Substituted phenols have been utilized efficiently for the selective extraction of alkali metals.[29 p. 96] The extraction takes place only in a moderate-to-strong basic aqueous solution where substituted phenols behave as weak acids. Therefore, by increasing the pH, the cation exchange capacity increases. Also, the lower the hydrated ionic radius is, the more effectively the metal is extracted. Ionic

and hydrated ionic radii of selected ions can be seen in table 5. During extraction, salt is formed through cation exchange, and the solvent interacts with additional extractant molecules. However, at the highest pH values, competition often occurs between the ions to be extracted and the cations of the base used for pH adjustment. This can decrease the cation exchange capacity.

TABLE 5 Ionic and hydrated ionic radii of selected ions. [30]

Ion	Ionic radius (nm)	Hydrated ionic radius (nm)
Li^+	0.094	0.382
Na^+	0.117	0.358
NH_4^+	0.148	0.331
K^+	0.149	0.331
Rb^+	0.163	0.329
Cs^+	0.186	0.329
Mg^{2+}	0.072	0.428
Ca^{2+}	0.100	0.412

Phenolic extractants, such as 4-*sec*-butyl-2-(α-methylbenzyl) phenol (BAMBP) and 4-*tert*-butyl-2-(α-methylbenzyl) phenol (*t*-BAMBP) have high selectivity towards Rb^+ and Cs^+ ions.[4-9] With these extractants, selectivity is usually $Cs^+ > Rb^+ > K^+ > Na^+ > Li^+$ among alkaline metals. The structures of BAMBP and *t*-BAMBP are shown in figure 1.

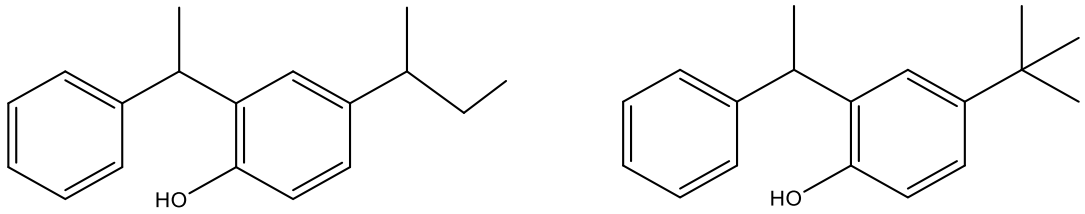

BAMBP *t*-BAMBP

FIGURE 1 Structures of BAMBP (4-*sec*-butyl-2-(α-methylbenzyl) phenol) and *t*-BAMBP (4-*tert*-butyl-2-(α-methylbenzyl) phenol).

Nowadays, *t*-BAMBP is used more in the extraction of alkali metals due to its higher synthesis yield, and it has been used especially for solvent extraction of rubidium and cesium from brines.[4-9]

Recently, Li *et al.* conducted a comprehensive study on separation of cesium and rubidium from potassium with *t*-BAMBP from synthetic brine.[5] They found that the optimal conditions for cesium and rubidium extraction were

from 0.1 mol L^{-1} NaOH feed solution at the A:O phase ratio of one with five extraction stages at room temperature. The *t*-BAMBP was diluted to ShellSol D70, a commercial aliphatic mineral spirit, and the loaded organic phase was stripped by 0.1 mol L^{-1} HCl solution. Over 99% of cesium and rubidium were extracted with 19% potassium co-extraction.

The *t*-BAMBP solvent extraction was also employed for the separation of rubidium from potassium in rubidium ore liquor. The efficient separation of Rb from ore liquor at high alkalinity was achieved via fractional extraction. The optimal parameters for Rb extraction and scrubbing of potassium with water were an organic phase of 1 mol L^{-1} *t*-BAMBP in xylene, a contact time of 1.5 min, and an A:O phase ratio of 1:3 for extraction/scrubbing. Three stages for extraction and 10 stages for scrubbing were conducted to achieve 98% extraction efficiency. Potassium scrubbing efficiency with water was more than 99%. After two stages of countercurrent stripping with 1 mol L^{-1} HCl (A:O of 4:1), a 97% total recovery of Rb was achieved.[31]

Despite the usability of BAMBP-compounds, BAMBP is quite expensive, and *t*-BAMBP is not broadly commercially available, which creates demand for less-expensive alternative extractants for rubidium extraction. Chlorophene (2-benzyl-4-chlorophenol) has a moderate price and could be used as an extractant for rubidium (figure 2). Only a few reports are available about the usage of chlorophene for the extraction of cesium by Oak Ridge National Laboratory,[32,33] but it can be expected to perform similar cation exchange with a phenolic proton to form phenolate with rubidium as in the case of BAMBP.[3,8] One phenolic molecule has lost a proton to become a phenolate anion, and the suggested cation-to-ligand ratio is 1:4. The proposed structure between solvating phenols and alkali metal ion is presented in figure 3.[9]

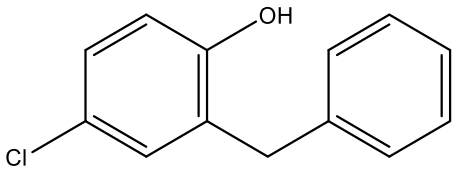

FIGURE 2 Structure of chlorophene (2-benzyl-4-chlorophenol).

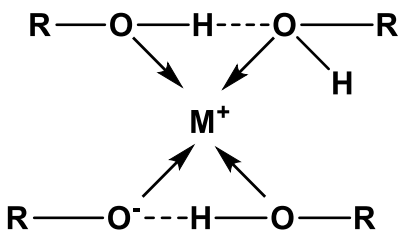

FIGURE 3 Suggested structure for alkali metal ion and solvating phenols. Modified from Bryan *et al*.[9]

Crown ethers

Macrocyclic polyethers called crown ethers have the ability to form stable complexes with alkali and alkaline-earth metals and with ammonium ions.[34] Alkali metals can potentially be separated from each other or from other metals with crown ether complexes.[13] The stability and formation constant of the crown ether complexes depend on many factors, such as solvent systems, the size of the alkali metal, and the size of the crown ether cavity. Especially, 18-crown-6 (figure 4) and its derivatives have suitable cavity size (0.26-0.32 nm) to form complexes with the rubidium ion.[35]

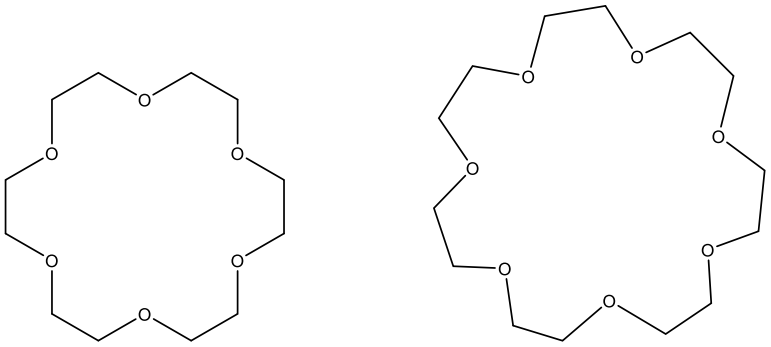

FIGURE 4 Structures of 18-crown-6 and 21-crown-7.

There are a number of examples in the literature since the 1960s of extraction and concentration of rubidium by crown ethers.[36-38] The subject is still popular among researchers, and new applications of the usage of crown ethers are published regularly.

Galina *et al.* investigated single species and competitive solvent extraction of alkali metals picrates from aqueous solution into chloroform by selected 18- to 24-membered benzo- and cyclohexane-group-containing crown ethers in 1999.[39] They noticed that separation factor values of competitive solvents were greater than single species values in nearly every case. For rubidium, 21-membered benzo- and cyclohexano-group-containing crown ethers had the highest separation factors.

A room temperature ionic liquid system containing 18-crown-6 has been optimized for the extraction of rubidium and cesium from a high potassium brine solution by Huan *et al*.[40] After extraction and stripping, 84% of rubidium and 95% of cesium were recovered with a 9.6% recovery of potassium.

Rubidium has also been successfully extracted from mining waste, boron-containing clay, after sulfuric acid leaching and tetraphenylborate precipitation by solvent extraction with 18-crown-6 in nitrobenzene.[41] The boron clay contains 1,292 mg kg^{-1} of rubidium, and under optimized conditions, a maximum 89.5% rubidium extraction was achieved.

2.3.2 Ion exchange

Solid ion exchangers can be used to extract cationic or anionic ions from solutions by replacing them with other ions of similar characteristics. Cation exchange materials contain surface groups that are negatively charged and attract positive metal ions. Contrariwise, anion exchange materials positively charged surface groups attract negative anions. Ion exchange media can absorb extracted ions inside the media, or the ions can be adsorbed to the surface of the media. In both cases, the media, where the ion is transferred to, is called sorbent. An ion-exchange resin is a resin or polymer that acts as a medium for ion exchange.[42 pp. 1-5]

The efficiency of the ion exchange resins to remove ions from a liquid solution can be described by the distribution coefficient K_d. It is defined as the ratio of metal ion concentration in the solid ion exchanger resin to metal ion concentration in the solution at equilibrium. By measuring analyte concentration in the solution before and after contact with the resin, K_d can be calculated according to the following equation:[43 pp. 17-18]

$$K_d = \frac{(c_i - c_f)}{c_i} \cdot \frac{V_s}{m_e}. \quad (4)$$

Here, c_i and, c_f are the initial and final concentrations of metal ions in the solution, V_s is the volume of the solution, and m_e is the mass of the ion exchanger used. High K_d value indicates a strong capacity of the resin to sorb the desired ions. The K_d is specific to the temperature and concentration of the other ions in the solution, and changes in the physical and chemical parameters can affect the ion exchange process.[43 pp. 17-18]

The extraction efficiency of the resin *E(%)* can also be described by equation 2, where c_i is the initial concentration (mg L^{-1}) of the analyte ions in the liquid sample before contact with the resin, c_f is the concentrations of the analyte ions in the sample after contact, and V_{aq} is the volume (mL) of the liquid sample.

Inorganic sorbents

Inorganic ion-exchange sorbents are often a well-defined chemical species.[44 pp. 6-9] The method of preparation can have a great influence on the structure of the sorbents, and their composition and structure have a significant effect on their sorption properties. Inorganic sorbents are also often more chemically unstable than organic resins.

Inorganic sorbents like ferrocyanides have been employed for the extraction of rubidium and cesium from various sources. Hexacyanoferrates are insoluble complex cyanides of transition metals that can capture alkali metal ions into their crystal lattice. Hexacyanoferrates exhibit in a great variety of compositions and structures, which are influenced by the method of the preparation of the hexacyanoferrates. It has also been shown that the sorption process strongly depends on the composition and structure of the starting solids.[45-49] The most often observed structure for transition metal hexacyanoferrate is face-center

cubic lattice with octahedral coordination of the transition metal with Fe ions and -CN ligands.[50] In these structures, alkali metal cations are located in the tetrahedral sites. The oxidation state and size of the transition metal influences the stoichiometry of the compounds, but the octahedral coordination geometry of the $[Fe(CN)_6]$ group is not significantly perturbed in size by the Fe's oxidation state.

In 1990, Lehto *et al*. showed that the specific surface areas of the $K_2[CoFe(CN)_6]$ with cubic lattice correlated directly with cesium uptake. Only the outermost surface layer of their crystals was involved in the exchange process, i.e., only potassium (or cobalt) ions inside the elementary cubes closest to the surface of the crystals are exchanged for cesium ions.[51] The structure of hexacyanoferrates has been studied by Ayrault *et al.* since the 1990s, and they discovered that copper hexacyanoferrates have different structures as a result of different preparation methods.[45,46] In 2004, Loos-Neskovic *et al*. prepared potassium copper hexacyanoferrate (II) $K_2CuFe(CN)_6$ by local growth and observed a triclinic *P*-1 structure for the sorbent.[49] They discovered that in a neutral solution, the initial crystal structure was maintained during the ion exchange between potassium and cesium, but in an acidic solution, the structure is destroyed.

Transition metal hexacyanoferrates have been employed for the extraction of cesium from radioactive liquid waste streams, and there are a number of publications on the subject.[52-60] Similarities between cesium and rubidium have inspired researchers to use the same methods for extraction of rubidium.

The University of Helsinki in collaboration with Fortum Nuclear Services Oy developed very effective inorganic ion exchangers for cleaning radioactive waste streams. The hexacyanoferrate-based ion exchanger CsTreat® was developed for extracting cesium from radioactive waste and to concentrate it to a smaller volume.[61-64] The same ion exchanger has been used for recovery of rubidium from brine rejected from seawater reverse osmosis (SWRO) plants.[10,65,66] SWRO is a process where seawater is turned into a drinkable supply by a desalination process. This process generates concentrated brine that has high salinity and elevated concentrations of valuable metals.[67]

Naidu *et al*. studied selective sorption of rubidium by different metal hexacyanoferrates.[10,12,68] They developed a method for preparation of sorbents of potassium metal hexacyanoferrates K(M)FC encapsulated in an organic polymer and identified from copper, cobalt, iron, and nickel that potassium copper hexacyanoferrate was most suitable for rubidium sorption.[10,12] From saline SWRO brine with a wide range of co-existing ions, polymer encapsulated potassium copper hexacyanoferrate (KCuFC-PAN) indicated selectivity towards rubidium and suited well for a dynamic column. The KCuFC-PAN could also be regenerated for rubidium sorption/desorption cycles.

Gilbert *et al*. used commercial sorbents for the recovery of valuable metal ions, including rubidium, from brine rejected from the SWRO plant.[65,66] Their results showed that the commercial ion exchanger CsTreat® displayed a high sorption capacity for rubidium. The same research group performed batch experiments with CsTreat, which showed that the sorption capacity did not de-

pend very much upon the presence of other ions, and CsTreat presented high selectivity towards Cs and Rb.[65,66]

Zeolites are crystalline hydrated aluminosilicate minerals with a three-dimensional framework structure constructed of SiO_4 and AlO_4 tetrahedra linked through oxygen atoms.[69] The aluminosilicates are negatively charged and can interact with positively charged cations. Zeolites readily bind cations of alkali metals and alkali earth metals into large spaces and channels in its structure. In addition, water molecules are present in zeolite channels, mainly coordinated by cations or protons. Studies about the removal of radioactive Cs^+ by zeolites have been made by many authors,[70-73] and the same methods could be applied for the recovery of rubidium. Unfortunately, selective desorption of rubidium from zeolites brings new unresolved challenges and generates a need for more development.

Ammonium molybdophosphate, $(NH_4)_3P(Mo_3O_{10})_4 \cdot 3H_2O$, AMP), has demonstrated high capacity and selectivity for the cesium ion (Cs^+).[74] In the 1990s, Sebesta and Štefula[76] developed AMP-PAN resin by combining ammonium molybdophosphate (AMP) with polyacrylonitrile (PAN), and after that, many publications about Cs^+ removal from radioactive waste streams have followed.[76-78]

Bao *et al*. studied selective preconcentration and separation of rubidium by the composite adsorbent AMP-PAM from salt lake brine. They investigated several experimental parameters and discovered that under optimal conditions, maximum sorption capacity for the Rb^+ ion by the sorbent was 500 mg g^{-1}. The adsorption of rubidium was not interfered by the presence of co-existing ions. Rubidium was desorbed from the AMP-PAN adsorbent effectively by 0.5 mol L^{-1} NH_4Cl solution, and regeneration and reuse of the adsorbent was achievable.[79]

Organic resins

Organic ion exchange resins have a three-dimensional covalent network that includes exchangeable ions associated with fixed acid or basic groups. The cation exchangers have fixed acid groups and exchangeable cations (usually H^+ or Na^+), and they are described as in the H form and Na form. Those with fixed base groups and exchangeable anions (OH^- or Cl^-) are anion exchangers in the OH form and Cl form, respectively.[80] Organic ion exchangers, like resorcinol formaldehyde resins, have been used for fractional separation of alkali metals.

Resorcinol-formaldehyde (RF) resins are organic resins developed by Ebra and Wallace in 1983 for selective removal of cesium from aqueous alkaline nuclear waste solutions.[81,82] RF resin is prepared by condensation polymerization of resorcinol and formaldehyde.[83] At elevated pH, two weakly acidic hydroxyl groups on the resin resorcinol ring deprotonate and become functional. The resin has shown high selectivity towards cesium ions, and it is estimated that the relative affinities of RF resin for ion-exchange are $H^+ > Cs^+ > Rb^+ > K^+ > Na^+$. Due to the resins "weak acid nature", Cs^+ and its competitors can be removed from the resin by elution using acid.

The study of resorcinol-formaldehyde resins has continued from the 1980s until recent years. Most of the studies consider cesium separation and recovery from radioactive waste. Especially, the separation of cesium from other alkali metals have been the main interest.[84-91]

Favre-Réguillon *et al.* studied the extraction of cesium by RF resin from simulated radioactive waste in the presence of a large excess of sodium at different acidities. They detected that the alkali-metal cation sorption selectivity series is strongly influenced by the pH of the solution and high pH selectivity is towards Cs^+ ions. RF resins had significantly greater selectivity towards rubidium and cesium ions than other phenolic ion-exchange resins.[84]

The U.S. Department of Energy (DOE) stores millions of gallons of high-level radioactive waste slurries at the Hanford and Savannah River Sites. The suitability of the granular and spherical form of resorcinol formaldehyde resins for the ion-exchange separation of Cs^+ from liquid nuclear waste at the sites has been studied extensively.[85-81] The spherical RF resin had excellent morphology for ion exchange processing, and due to its effectiveness in absorbing cesium, RF resin was found to be suitable for cesium recovery.[86,87,89,91] After loading cesium to the resin, Cs could be separated from sodium by sequential elution, resulting in a concentrate of very high Cs and low Na.[90]

Shelkovnikova *et al.* studied the selectivity of ion exchange between Cs^+ and Rb^+ ions on RF resin and sorbent based on resorcinarene and compared the result to the literature values of phenyl formaldehyde. According to their investigations, RF resin had the highest capacity up to pH 13, but there was very little difference in the selectivity of ion exchange resins towards cesium and rubidium ions.[92]

Due to the RF resin's selectivity towards large alkali metal ions at a high pH, selective recovery of rubidium could be possible by sequential elution after extracting rubidium from the sample solution.

2.4 Analytical techniques

2.4.1 ICP-OES

Inductively coupled plasma - optical emission spectrometry (ICP-OES) is a widely used instrumental technique for elemental analysis. The main advantages of the technique are the moderate price, determination of 70 elements simultaneously, and wide working range from $\mu g\ L^{-1}$ up to $g\ L^{-1}$ concentrations, depending on the analytes.[93 pp. 1-3] In ICP-OES, a liquid sample is introduced into a hot plasma as a fine aerosol. Sample droplets dry up and elements of the sample are excited to emit electromagnetic radiation that is processed and detected. Every element emits radiation in a wavelength characteristic to the element. The intensity of the emission signal has a linear relationship to the concentration of the analyte.

General instrumentation and principle of operation

The function of the sample introduction system is to convert the liquid sample to fine droplets before entering the plasma. This can be achieved with a nebulizer that mixes the liquid sample with carrier gas, also called nebulizer gas, and converts the sample to an aerosol. A typical nebulizer gas is argon with 0.6-1 L min^{-1} flow rate. The nebulizer is connected to a spray chamber where larger droplets are removed and only the smallest droplets reach the plasma without destabilizing it. The plasma is generated inside a quartz or ceramic torch, and the sample is introduced into the plasma via an injector tube.[93 pp. 39-55]

Plasma is ionized argon gas and is maintained with radio frequency (RF) power. By altering the electromagnetic field inside the induction coil or flat plates by RF power, the energy is coupled to the plasma; hence, the name inductively coupled plasma. Plasma gas provides argon for the plasma but also cools the outer part of the torch. The plasma gas flow is typically between 8-17 L min^{-1}. Auxiliary gas flows tangentially inside the torch, cools the injector, and pushes the plasma away from the injector tip to prevent precipitations of solids. Auxiliary gas is also usually argon with a flow rate between 0-2 L min^{-1}. The temperature of the plasma varies from 5,000-10,000 K in different parts of the plasma, but in a normal analytical zone optimal for ionization of most elements, the temperature of 5,000-8,000 K is common.[93 pp. 11-32]

After the sample droplets reach the plasma, the energy from the plasma is transferred to the sample in several steps. First, the solvent of the sample is evaporated and the remaining solid is melted and vaporized. The molecules of formed gases are atomized, and most of the elements are also ionized. Finally, atoms and ions are excited to higher energy levels. The transition from excited states to lower energy states creates light emissions in UV or visible wavelength regions characteristic for the exited atom or ion. The atomic and ionic transitions are designated as I and II Roman numbers, respectively, to separate the two species.[93 pp. 11-32]

Emission from the plasma can be viewed from the side of the plasma (radial viewing) as well as lengthways (axial viewing). In radial viewing, the measurement is not prone to interferences, but it has lower sensitivity and higher detection limits for most elements. In axial viewing, the measurement has higher sensitivity, but it is more prone to interferences due to the different temperature zones of the plasma, although a shear gas removes the tail of the plasma. When measuring easily ionizable elements (EIE), like alkali metals with axial viewing, excitation interferences are very common. Alkali metals increase electron density in the plasma and decrease the ionization of other alkali metals while the intensity of the atomic transition increases. This phenomenon is called the alkali effect, and it can be seen as an incorrectly high concentration of alkali metal in the presence of other alkali metals when measuring the atomic line and viewing the plasma axially. With radial viewing, the alkali effect can be avoided.[93 pp. 32-36]

The light emitted by the atoms and ions is spectrally separated by the optics, and the elements being analyzed are characterized by their wavelengths by one or more detectors. Spectral separation is often conducted by diffraction gratings and prisms before entering the detector. Often an echelle polychroma-

tor with a solid-state detector, like a charge-coupled device (CCD), is used with ICP-OES.[93 pp. 65-97]

Interferences in ICP-OES

Common interferences in the ICP-OES technique are spectral or non-spectral interferences. Spectral interferences originate from sample components or background emission near the analytical line emission. Interfering emission can overlap the analytical line partially or completely.[93 pp. 118-147]

The best solution for the correction of spectral interferences usually is to use an interference-free emission line if possible. If an interference-free emission line is not available, there are many methods for the correction of spectral interferences. Optimized background correction points can be used to correct a simple background shift or sloping of the background, and inter-element correction works for direct spectral overlap. Multivariate regression techniques can correct partial spectral overlaps and complex background shifts. Detailed descriptions of these methods can be found elsewhere.[93 pp. 118-147]

Non-spectral interferences arise from the physical properties of the samples and cause changes in sample transport, nebulizer properties, spray chamber aerodynamics, and excitation conditions of the plasma. Differences in the physical properties (viscosity, density, and surface tension) of the sample and calibration solutions can lead to incorrectly high or low results, depending on how the sample introduction system is affected by the difference. Interferences arising from the sample introduction system are often referred to as matrix interferences, but the matrix of the sample can also cause spectral interference to the background emission by decreasing or increasing it..[93 pp. 147-153]

Non-spectral interferences can be corrected by matrix matching and by the use of an internal standard. In matrix matching the matrix of the samples and calibration standards are adjusted to be as similar as possible. This can be done by diluting the samples and matching, the acid matrix and/or matrix elements of the samples, standards, and blanks. When using an internal standard, a constant amount of an element is added to all samples and standards during sample preparation, and the change in the intensity of that element can be used as a correction factor for all analytes. The element used as an internal standard, should be absent from the samples and be affected by the non-spectral interference the same way as all the analytes to be measured. In addition, it is preferred that the emission line of the internal standard is free from spectral interferences and has excitation energies similar to the selected analytical lines.[93 pp. 147-153]

Easily ionizable elements cause changes in excitation conditions and induce significant variation in the analytical signal. The concentration and nature of the interfering element, the characteristics of the emission line, plasma operation conditions, and the plasma observation zone affect the severity of EIE interference.[94 pp. 162-172] The absolute concentration of the interfering element has more influence on excitation conditions than the relative concentration compared to that of an analyte. Therefore, the simplest method to treat EIE interferences is to dilute the sample, add an ionization buffer to the samples and calibration solutions, or use radial viewing. EIE interferences also become less se-

vere, when using robust plasma conditions. If the concentration of the analyte is very low, dilution is infeasible and axial plasma viewing might be needed. The most used mathematical methods to overcome EIE interferences are multivariate calibration techniques, like multiple linear regression (MLR), principal-component regression (PCR), and partial least square regression (PLS).[94 pp. 178-181]

Robust conditions of the plasma

The term robustness of the plasma is used to describe the excitation and atomization conditions of the plasma when encountering the sample matrix.[93 pp. 11-32] The ratio of magnesium emission of ionic (MgII 280.270 nm) and atomic (MgI 285.213 nm) transitions is commonly used to quantify the robustness. When MgII/MgI is 8 or greater, the plasma is considered to be robust and not prone to changes in the analytes' emission signal even if there are small changes in the sample matrix.[95] Robustness indicates the absence of excitation interferences and depends on parameters like RF power, plasma, auxiliary, and especially nebulizer gas flow and plasma height for radial viewing. By systematic optimization of these parameters, robust plasma conditions can be achieved.

2.4.2 GFAAS

Atomic absorption spectrometry (AAS) is based on the capability of gaseous free atoms to absorb radiation energy. Ground-state atoms absorb the energy of a specific wavelength and are elevated to an excited state. The amount of radiation energy absorbed at this wavelength is directly proportional to the number of atoms of the selected element in the light path and their concentration in the sample. The atomization of the sample can take place in a flame (FAAS) or in a graphite furnace (GFAAS; also known as electrothermal atomic absorption spectroscopy, or ETAAS). GFAAS is significantly more sensitive than FAAS with detection limits typically 100 to 1,000 times lower.[96 pp. 1-42]

General instrumentation and principle of operation

The instrumentation of the AAS technique contains a primary light source for the production of the radiation to be absorbed, an atomization source for atomization of the sample, a monochromator for isolation of the specific wavelength of radiation to be measured, a detector to measure the radiation accurately, and electronics to process the data signal and produce the results.[96 pp. 1-42] Commonly, a single- or multi-element hollow cathode lamp or electrodeless discharge lamp is used as a radiation source providing a bright, stable, and narrow line spectrum of the element to be determined. Most elements have their absorption lines between wavelengths of 190 nm and 850 nm. The volatilization and atomization of the sample can take place in a flame in FAAS or in a graphite furnace in GFAAS. Nowadays, most modern instruments use solid-state detectors; photomultiplier tubes are rarely used.

In contrast to FAAS, where a sample is dried and atomized in a flame, the GFAAS technique sample is heated electrically in a small graphite tube. A fixed amount of liquid or solid sample is deposited in the tube, and with the tempera-

ture program, the sample is dried, decomposed, and atomized before analysis. The analyte is then atomized, and radiation from the lamp passes through the tube. After analysis, the furnace is cleaned by heating.[97]

Usually, 1-50 µL of the liquid sample (or 1-2 µg of the solid sample) is introduced to a 20-30 mm long and 4-6 mm in diameter graphite tube via an autosampler.[96 pp. 1-42] In the tube, the sample is placed on a surface called L'vov platform[98] that delays volatilization and atomization of the sample until thermal equilibrium is achieved in the tube environment. This reduces interferences originating from temperature differences in the tube. Two popular designs of the graphite tubes are the cylindrical graphite tube HGA with contacts at the end of the tube and the transverse heated graphite tube THGA. Newer designs of THGA tubes have end caps that reduce the tube diameter at the end without restricting the light throughput. This design has increased sensitivities and improved detection limits compared to THGA tubes without end caps.[99] The limited lifetime of the graphite tubes is usually 50-200 determinations, depending on the sample matrices, especially acid concentrations.

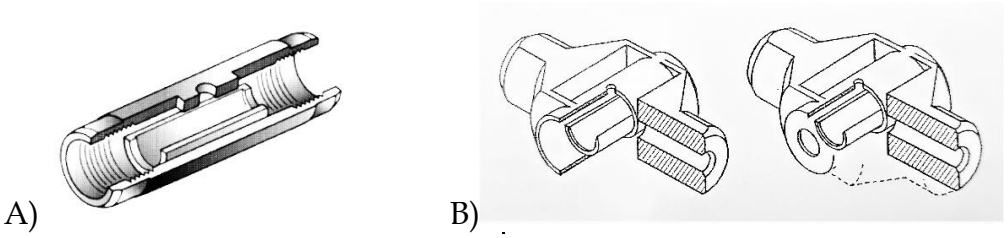

FIGURE 5 A) Cylindrical graphite tube HGA. B) Transverse heated graphite tube THGA without end caps (left) and with end cap (right).[100]

After the sample deposition, the furnace is heated gradually and the atomization of the sample is controlled by the furnace program. The furnace program usually consists of four steps: drying, pyrolysis, atomization, and cleanout. At the beginning of the temperature program, before sampling, the furnace should be at room temperature. In the drying step, the solvent of the sample is evaporated. This is typically 20–40 °C above the boiling point of the solvent. The ramp time should be adequate to prevent the splattering of the sample. With the THGA graphite tube, a furnace two-step drying procedure is recommended to ensure even and smooth drying. In the pyrolysis step, most of the matrix components are removed. This step depresses the background signal and reduces possible chemical interferences. In the atomization step, the elements of the remaining sample are atomized and absorption of the lamp's radiation is detected. The optimal atomization temperature depends upon the properties of the compound of the element, and it should be high enough to volatilize all of the analyte's elements. The optimum atomization temperature is reached when the maximum integrated absorbance and optimal peak shape is achieved.[98]

An inert atmosphere is a requirement for graphite furnace analysis. Passing inert gas like argon around the tube, the surface of the tube is protected from combustion at high temperatures. The same gas can be used for purging

the interior of the furnace to remove solvent and matrix components after the drying and pyrolysis steps. The closed-circulated water system is often used for cooling the furnace to room temperature after the furnace program and determinations have ended.[97]

Interferences in GFAAS

Spectral interferences appear when the measured radiation absorption is partially from elsewhere than from the absorption of the analyte element. Interference, where other elements' absorption profiles overlaps with an emission line of the analyte's element, is rare. With the graphite furnace AAS, the matrix materials of the sample often cause broadband absorption spectra and induce interferences to the background absorption. Background correction is required for all samples to remove absorption signals that do not originate from the analyte. Often the applied method for correction is the Zeeman Effect background correction, where the external magnetic field is used for the splitting of the atomic spectral lines and atomic species of the analyte can be separated from non-atomic species of the background absorption.[96 pp. 17-30]

In GFAAS, non-spectral interferences can be from chemical or physical origins. Common chemical interferences in GFAAS that reduce the analytes' signal are the formation of volatile compounds that evaporate before atomization as well as formation of thermally stable compounds during atomization.[96 pp. 58-61] Both interferences can be reduced by matrix modifiers, and evaporation can be controlled by optimizing the pyrolysis. Changes in viscosity and surface tension of the sample can generate physical interferences and affect the deposition of the liquid sample. Elements with high atomization temperatures can experience incomplete atomization, which affects the absorption of the analyte and causes memory effects. Matrix modifiers can also correct most physical interferences.

Matrix modifiers are frequently used in the GFAAS technique to diminish interferences and to improve the quality of the analysis. Often a high concentration of the modifier salt is added directly to the sample before analysis to transform the analyte element to the desired compound whose behavior in pyrolysis is known.[97] Modifiers can be used either to make the matrix more volatile or to stabilize the analyte element to endure high temperatures during pyrolysis.

Characteristic mass

In GFAAS, characteristic mass (m_0) is used to describe the performance and analytical sensitivity of the measurement. Characteristic mass can be defined as the analyte mass giving an integrated absorbance of 0.0044.[96 pp. 44-46] In the linear range of the integrated absorbance and concentration, the characteristic mass is independent of the concentration, and it can be quantified by measuring the integrated absorbance of a test solution of known concentration using the following equation:

$$m_0 = m_a \cdot 0.0044 s / A_a \tag{5}$$

where m_0 is the characteristic mass of the measured element, m_a is the mass of the element introduced to the furnace (can be calculated from the concentration of the sample), $0.0044s$ is the integrated absorbance in unit s, and A_a is the integrated absorption measured for the test solution. The characteristic mass of the measurement depends on the sample, the sample introduction system, the furnace, the design of the graphite tube, the spectrometer, and the radiation source. GFAAS spectrometer manufacturers often publish expected values for characteristic masses in picograms for different elements and recommended measuring conditions. The measuring system is presumed to work properly if the measured and manufacturer's listed characteristic mass values encounter in a range of ± 20 %.[96 pp. 44-46]

2.4.3 ICP-MS

Inductive coupled plasma mass spectrometry (ICP-MS) is an ultra-trace element analysis technique where analyte ions formed in the plasma are detected by a mass spectrometer. The sample introduction to the plasma occurs the same way as in ICP-OES, but in ICP-MS, plasma is used to generate positively charged ions in contrast to ICP-OES where photons are produced and detected. Generated ions are transferred through the interface region to the mass spectrometer, where ion optics and high a vacuum mass separation device separates analytes ions according to their mass-to-charge ratio before entering the detector. ICP-MS has a wide operation range from the ppm (parts per million, mg L^{-1}) level all the way to ppt (parts per trillion, ng L^{-1}) detection limits, and it can perform rapid multielement analysis.[100 pp. 1-4]

General instrumentation and principle of operation

In the low vacuum (1-2 torr) of the interface region, the ion beam from the argon plasma passes through small orifices of one sampler cone and one to two skimmer cones to maintain ion beam composition and electrical integrity. After the interface region, the ion beam is focused and deflected from the trajectory of other items by ion optics or a quadrupole ion deflector, QID (10^{-3} torr). This enables positive ions from entering the mass separation device while other items are blocked. Next, the focused ion beam enters the high vacuum (10^{-6} torr) mass separation device where ions of the analytes are separated from other interfering ions or ions of the matrix elements usually by quadrupole mass filter. The separation of ions is achieved by quadrupole where the direct current (DC) field and the time-dependent alternating current (AC) of radiofrequency are applied to four stainless steel rods. By selecting an optimum AC/DC combination, ions of a selected mass-to-charge ratio are directed to the detector. The vacuum systems in the ICP-MS are maintained by a low vacuum mechanical pump and high vacuum turbopumps. Most ion detectors with ICP-MS are discrete dynode electron multiplier detectors that are located in a vacuum chamber. A set of dynodes converts the ions into an electrical signal by electron multiplication. The signal is processed by the detection electronics and then sent to the computer.

The magnitude of the signal corresponds to the number of analyte ions in the sample.[100 pp. 1-4]

Modern ICP-MS devices have an additional collision/reaction cell placed most often after ion optics and prior to the analyzer quadrupole that reduces interferences generated by a combination of argon, solvent, and other matrix element ions. Collision/reaction cells multipole system focuses all the ions, which are then collided and/or reacted with molecules of an additional gas (e.g., He, H_2, NH_3, O_2).[100 pp. 73-75]

Most instruments need to be optimized and calibrated daily before starting the analysis. The daily optimization process targets the sample introduction system, the torch, and the cones by performing torch alignment, QID performance check, and/or nebulizer gas flow optimization. By tuning one or more of these parameters, optimal performance can be achieved and validated by a background and sensitivity performance check.

Interferences in ICP-MS

The most common interferences in the ICP-MS technique are spectral, matrix, and physical interferences. Spectral interferences arise from argon used as plasma and nebulizer gas, matrix components of the sample, solvent, and acids or other elements in the sample, which are present at the same atomic mass as the analyte of interest. Spectral interferences are called isobaric when a mass spectrum of an isotope of one element directly overlaps an isotope of another element. Interferences are polyatomic when interfering elements or components generate interfering polyatomic ions that overlap the analyte's isotopes. Doubly charged spectral interferences are generated by doubly charged positive ions that are formed instead of singly charged ions that produce an isotopic peak at half of its mass.[100 pp. 133-143]

Because most elements have more than one naturally occurring isotope, it is often possible to select an isotope without interference. If the interference-free isotope is not available, a popular method for interference correction is the use of a mathematical interference correction equation. It can be applied to isobaric and some polyatomic interferences by measuring the intensity of the interfering species at another mass, free from interferences. When the ratio of the intensity of the interfering species at the analyte mass to the intensity of the interfering species at the mass free from other interferences is known, an analyte's corrected intensity can be calculated. Other means to compensate spectral interferences are the use of a collision/reaction cell, cold plasma technology, and a high-resolution mass analyzer.[100 pp. 133-143]

As with ICP-OES, non-spectral interferences related to the sample transport originates from the physical properties of the sample matrix (viscosity, density, and surface tension). These interferences are the result of the sample matrix effect on the aerosol formation or matrix-induced changes in the ionization conditions in the plasma. The use of the internal standard is the most popular method to compensate for physical interferences in ICP-MS. Like with ICP-OES, the internal standard is added to the samples and calibration solutions prior to the analysis. The suitable internal standard should not be present in the

sample. It should be free from spectral interferences, have similar mass, and possess similar ionization potential as the analyte. Some complex matrices may interfere with the transport of ions through the mass interface, ion optics, and/or mass separation device. These types of space-charge-induced matrix interferences are difficult to overcome but can be reduced by adjusting the voltages of the ion optics.[100 pp. 133-143]

2.4.4 Determination of rubidium

Traditional instrumental methods for the determination of rubidium from a liquid sample are based on flame atomic emission and flame atomic absorption spectrometry. For high-sensitivity measurements, GFAAS is recommended due to its very low detection limits. The downsides of the GFAAS method are its limited analytical working range and slow measurement per element. Multi-elemental ICP-OES and ICP-MS are more popular methods due to their fast analysis, and ICP-MS offers the lowest detection limits in rubidium measurements. Comparison of determination of rubidium by GFAAS, ICP-OES (axial/radial view), and ICP-MS is displayed in table 6.[100 pp. 281-301]

TABLE 6 Detection limits (μg L^{-1}), working ranges, advantages, disadvantages, and equipment costs for four different measuring methods for determination of rubidium announced by different instrument manufacture (Perkin Elmer, Thermo Elemental, EAG laboratories, Agilent).[101,102,100 pp. 281-299]

	LOD (μg L^{-1})	Working range	Advantages	Disadvantages	Equipment cost (€)
GFAAS	0.03-0.06	$x10^2$	inexpensive to operate, low sample consumption, low detection limits	small working range, usually only single element analysis, slow analysis	25,000 - 50,000
ICP-OES axial view	3-5	$x10^5$	fast multi-elemental analysis, moderate detection limits	interfered by EIE	60,000 - 100,000
ICP-OES radial view	35-50	$x10^5$	fast multi-elemental analysis, not prone to interferences	high detection limits	60,000 - 100,000
ICP-MS	0.00001-0.0002	$x10^8$	fast multi-elemental analysis, low detection limits	expensive to operate	140,000 - 250,000

With ICP-OES, rubidium has only one considerable measuring wavelength at 760 nm, which is next to a large argon emission band emerging from plasma gas. Argon band can induce spectral interference to the low emission radial measurement of rubidium, but with axial measurement, interference is minor. Due to this interference, the detection limits of radial rubidium measurements can be rather high. Being an alkali metal, rubidium suffers EIE inter-

ferences in the presence of other alkali metals. This interference is severe with axial measurements. For rubidium, it is also difficult to find an interference-free internal standard that is absent from the samples and has similar behavior during measurement. The multiple linear regression (MLR) method can be applied for the correction of EIE interference in rubidium measurements by ICP-OES.

Due to the very low detection limits of rubidium with the GFAAS technique, after substantial dilution, measurement of rubidium is often interference-free, and no matrix modifier is needed. In many GFAAS devices, dilution of samples is automated up to 100 times, but often manual dilution is still needed. The dilutions and measurements of the samples can be time-consuming, which is a major downfall of the GFAAS technique. Although, GFAAS technique is very sensitive, the precision of the measurements can vary due to the condition of the graphite tube and the difficulties of injecting very small volumes of the sample.

In ICP-MS measurements, rubidium has two suitable isotopes, 85 and 87, with relative abundances of 72.2% and 27.8%. Isotope 85 is interference-free and isotope 87 suffers from isobaric interference induced by isotope 87 of strontium (7% abundance). This interference can be automatically corrected by the software's mathematical interference correction equation. Very low detection limits enable high dilution factors, significantly reducing the matrix interferences, similar to GFAAS.

2.5 Processing analytical results

2.5.1 Calibration

Most instrumental methods used for elemental analysis require an analysis of known standard samples to determine the instrumental response to the changes in analyte concentrations.[28 pp. 85-87] Typically, a blank and one or more standard solutions of known analyte concentrations are analyzed. Then, the instrument software typically constructs a linear equation called a calibration curve to describe the relationship between response and concentrations. After this, unknown concentrations of samples can be determined from their instrumental responses. The calibration line is usually in a form of:

$$y = bx + a, \tag{6}$$

where y stands for instrumental responses, such as emission signal or signal intensity produced by the mass of the analyte, while x is the calibration standard's concentration. Value b is the slope of the calibration line, and a is the intercept of the line with the y-axis. The linear calibration equation that calculates the intercept for the function is often called "simple linear." The linear through zero calibration equation ($a=0$) forces the regression line to go through the origin. Both calibration equations, simple linear and linear through zero, are popular among ICP techniques. The most appropriate way to select the right

calibration equation is to use both and do the significance test to estimate if the value of the origin is significant at a 95% confidence level.

When constructing the calibration curve, the correlation coefficient *r* is often calculated. The correlation coefficient evaluates how well the experimental points fit on the calibration curve, and it can be calculated with equation 7, where $(x_i - \bar{x})$ and $(y_i - \bar{y})$ are the distances of the measured calibration points x_i and y_i to the average of the all calibration values $\bar{x}$ and $\bar{y}$.[103 pp. 114-118]

$$r = \frac{\sum_i\{(x_i-\bar{x})(y_i-\bar{y})\}}{\{[\sum_i(x_i-\bar{x})^2][\sum_i(y_i-\bar{y})^2]\}^{\frac{1}{2}}} \quad (7)$$

r can get values between -1 and +1. When r is ±1, all the calibration points are on the calibration line, and when r = 0, there is no statistical correlation between the points. After constructing the calibration curve, most of the measuring software calculates the correlation coefficient using their own formulas based on the used calibration equation and equation 7. Good calibration fitting often has r ≥ 0.999.

2.5.2 Detection limits

An important part of the method validation is to determine detection limits for the instrument, method, and measurements. The detection limit (*LOD*) is the lowest quantity of the analyte that can be separated from the blank.[28 pp. 100-105] The detection limit of the measurement can be calculated as:

$$LOD = y_B + 3s_B, \quad (8)$$

where y_B is the signal of the blank solution and s_B is the standard deviation of the blanks. *LOD* can also be determined from the calibration data:

$$LOD = \frac{3s_B}{b} \quad (9)$$

In equation 9, s_B is the standard deviation of the blank and *b* is the slope of the calibration equation. The limit of quantification (*LOQ*) gives the lowest signal of the element that can be measured and quantified.

$$LOQ = y_B + 10s_B. \quad (10)$$

The instrumental detection limit (*IDL*) describes the lowest concentration that can be detected with that specific instrument in ideal conditions. According to EPA Methods 200.7 and 200.8, *IDL* is defined as the concentration equivalent to the analyte signal, which is equal to three times the standard deviation of a series of 10 replicate measurements of the calibration blank signal:[105, 106]

$$IDL = 3 \cdot s_{10rep} \quad (11)$$

The method detection limit (*MDL*) is the minimum concentration of the analyte that can be measured, and the concentration of the analyte is greater than zero with a 99% level of confidence. By taking seven replicates of the fortified reagent water and processing and measuring the replicates by the analytical method, *MDL* values can be determined. The reagent water should have analytes concentrations of two to three times the instrumental limit. MDL can be calculated as a multiplication of the Student's *t* value for a 99% confidence level and a standard deviation s of the replicates for $n-1$ degrees of freedom ($t = 3.14$ for seven replicates):[104, 105]

$$MDL = t \cdot s \tag{12}$$

The relative standard deviation (*RSD*) of the seven replicates should be 10% or more to ensure that the concentrations used to determinate the analyte's *MDL* are not too high. With too high concentrations and low deviations, the calculated *MDL* values could be unrealistically low. Often it is beneficial to determine *MDL* values for each analyte from three different fortified reagent waters and use their average to get a more appropriate estimate for *MDL*.[104, 105]

2.5.3 MLR

Multiple linear regression (MLR) is a statistical multivariate regression technique that models the relationship between predictor and response variables.[104 pp. 137-240] The predictor variables are used to predict the outcome of response variables by fitting a linear equation from observed data. In ICP spectrometry, MLR is an appropriate technique when the analyte spectrum is interfered by other elements or molecular species so that analyte concentration cannot be determined without previous chemical separation. Examples of interferences that can be corrected are spectral and EIE interferences.

For example, when determining a concentration of an analyte from a matrix solution, the observed analyte concentration often depends on the concentrations of the matrix elements.[106; C4.2] Dependent response variable y_i represents the corrected concentration of the analyte, and the non-dependent predictor variables x_i are the observed concentrations of the analyte and matrix elements in the sample solutions. Regression equations can be presented by using a reverse calibration model:

$$y_i = b_0 + b_1 x_{1i} + b_2 x_{2i} + \ldots + b_k x_{ki} + e_i\,, \tag{11}$$

where x_i are the measured concentrations of the analyte and matrix elements in the sample solution i, b is the regression coefficient, and e_i is residual for i, an independent random variable with a normal distribution.

Matrix interferences in the ICP-OES measurements can be corrected by the multiple-regression-technique.[22] By analyzing a synthetic mixture of analyte and matrix elements, a multiple regression line for each element can be calculated. The line equation contains terms like intercept (b_0) and elemental components (x_i) that describe the measured analyte concentrations, and the line equa-

tion serves as a correction equation. The feasibility of the correction equation can be tested on synthetic samples or SRM samples. Significance tests, such as the paired *t*-test, can be applied for testing the significance of the differences between the corrected and the added or certified concentrations. The correction equation can be applied for unknown samples if the concentrations of the interfering elements are known and concentrations of the analyte and matrix elements are in the same range with the synthetic samples of the model.

3 OBJECTIVE OF THE STUDY

Rubidium has been labeled as a critical material by the U.S Department of the Interior and the consumption of Rb is expected to rise due to the development of quantum-mechanics-based computing devices where Rb is one of the key components.[1,2] Rubidium can concentrate on fly ash during the combustion process when peat or wood residue is used as a fuel. This makes fly ash a potential raw material for rubidium recovery, which has not been studied before.

In this study, answers to the following research questions are given:

1. Which analytical technique (GFAAS, ICP-OES, or ICP-MS) is most suitable for quantitative analysis of rubidium from fly ash -derived samples?
2. What is the rubidium concentration in different combustion fly ashes?
3. How is rubidium distributed between different size fly ash particles? Is processing by sieving beneficial?
4. How efficiently oxalic acid leaches rubidium from fly ash?
5. What pretreatment is required for the leachate prior to recovery of rubidium by liquid-liquid extraction?
6. Is chlorophene a suitable extraction agent, and what are the optimum parameters for selective recovery of rubidium from fly ash leachates?
7. Can rubidium be selectively recovered from fly ash using a 3D-printed potassium copper(II) hexacyanoferrate sorbent?

4 EXPERIMENTAL

4.1 Samples

Fly ash samples from two Finnish power plants were investigated in this study. Both plants use the fluidized bed as the combustion technique, and fly ash samples were collected with electrostatic precipitators. Different compositions of wood residues (bark, branches, roots, and other parts of the wood) and peat were used as a fuel. Table 7 presents the identifiers, origins, and fuel compositions of the fly ash samples used in this study. In most experiments, fly ash originated from power plant A, from the combustion of 50% wood residue and 50% peat. The fly ashes were collected by electrostatic precipitators.

TABLE 7 Identifiers, origins and fuel compositions of the fly ash samples used in this study.

Sample i.d.	Power plant	Fuel composition
(A) P50:W50	(A)	50% peat and 50% wood residue
(A) P100	(A)	100% peat
(B) P30:W70	(B)	30% peat and 70% wood residue
(B) P50:W50	(B)	50% peat and 50% wood residue
(B) P70:W30	(B)	70% peat and 30% wood residue

Standard reference material SRM1633c (Coal Fly Ash), certified by the National Institute of Standards and Technology, was used to verify the sample pretreatment and analysis procedure.

4.2 Reagents

Ultrapure water of 18.2 MΩ cm resistivity used throughout this study was produced by ELGA PURELAB Ultra Analytic (Buckinghamshire, UK). Chemicals

used and their purities are presented in table 8. All the standard solutions used for calibration solutions were provided by Perkin Elmer and are listed in table 9.

TABLE 8 Chemicals and their suppliers and purities used.

Chemicals	Supplier	Purity/concentration
Ammonium nitrate	Merck	99.0 %
Calcium nitrate tetrahydrate	Merck	98.0 %
Chloroform	VWR International	99.5 %
Chlorophene	Alfa Aesar	96.0 %
Hydrochloric acid	Honeywell Fluka	puriss p.a. ≥37 %
Hydrochloric acid	Analytica	ANALPURE, 34-37 %
Hydrofluoric acid	Merck	40.0 %
Nitric acid	Honeywell Fluka	puriss p.a., ≥65 %
Nitric acid	Analytica	ANALPURE, 67-69 %
Oxalic acid dehydrate	J.T.Baker	99.5-102.5 %
Potassium hexacyanoferrate	Merk	99-102.0%
Rubidium chloride	Cerac	99.9 %
Sodium hydroxide	AnalaR NORMAPUR	99.6 %
Zinc nitrate tetrahydrate	Merck	99.0 %

TABLE 9 Standard solutions supplied by Perkin Elmer.

Standard solutions	Elements
Single element solutions, Pure-purity	
Cesium (1,000 mg L^{-1})	Cs
Potassium (1,000 mg L^{-1})	K
Rubidium (1,000 mg L^{-1})	Rb
Sodium (1,000 mg L^{-1})	Na
Multi-element solutions, PurePlus-purity	
Multi-element standard 3 (10 mg L^{-1})	Al, Ag, As, Ba, Bi, Ca, Cd, Co, Cr, Cs, Cu, Fe, Ga, In, K, Li, Mg, Na, Ni, Pb, Rb, Se, Sr, Tl, U, V, and Zn
Multi-element standards 5 (10 mg L^{-1})	B, Ge, Mo, Nb, P, Re, S, Re, S, Si, Ta, Ti, W, and Zr

4.3 Instrumentation

4.3.1 ICP-OES

The determination of rubidium and major matrix elements (Al, Ca, Cu, Fe, K, Mg, Mn, Na, Si, P, and S) was performed using two different Perkin Elmer ICP-OES models, Optima 8300 and Avio 500 equipped with Perkin Elmer S10 autosamplers.

The Perkin Elmer Optima 8300 with horizontal torch/plasma and FlatPlate™ was used in the earlier studies. The sample was introduced into the plasma via a cyclonic spray chamber and GemCone LowFlow nebulizer or Scott-type double-pass spray chamber with a cross-flow nebulizer. Plasma was generated by a 40 MHz RF power generator into a quartz torch with a 2 mm inner diameter alumina injector. The optics of the Optima 8300 include a polychromator with an echelle grating and a ruling density of 79 lines per mm. The dual detection system with segmented-array charge-coupled-device detectors (SCD) covered a wavelength range from 165 to 782 nm.

The emission of the plasma could be viewed radially and axially. The radial viewing height was set at 15 mm and the measurement points of the radial and axial viewing were aligned by measuring the Mn 257.610 nm emission line. Earlier optimized[21] settings for measurements by the Perkin Elmer Optima 8300 are listed in table 10.

Three calibration solutions in a range of 0.2–10 mg L^{-1} for rubidium and 1–50 mg L^{-1} for matrix elements were diluted from the Perkin Elmer Single-element standard of 1,000 mg L^{-1}. The acid matrix of the standards and samples were adjusted to 15% of HCl (v/v, puriss p.a.) and 5% of HNO_3 (v/v, puriss p.a.). Used calibration equations were simple linear with calculated intercept and had good calibration fitting ($r \geq 0.9997$). Detection limits were calculated from the average signal and the deviation of ten blank solutions with equations 8 and 10. Repeatability (n = 4) and reproducibility (n = 15) for Rb were verified from the relative standard deviation of the measured concentrations of the quality control (QC) samples with a Rb concentration of 5 mg L^{-1}. Repeatability describes deviation in one measurement run, and reproducibility in several runs. Wavelength used for Rb measurements was 780.023 nm. Data for the matrix element measurements by ICP-OES Optima 8300 are in the appendix table A1.

In recent studies, matrix elements were determined by the Perkin Elmer Avio 500. It has a vertical torch/plasma with FlatPlate™, and the sample introduction system included baffled cyclonic spray chamber with a GemCone LowFlow nebulizer. Otherwise, the Avio 500 has a configuration similar to the Optima 8300. The settings used for measurements by the Perkin Elmer Avio 500 are listed in table 10.

The three point calibration was carried out in a range of 0.1–10 mg L^{-1} for the rubidium (1-10 for radial Rb) and matrix elements. Calibration solutions were diluted from the Perkin Elmer Multi-element standard 3 and the Multi-element standard 5 of 10 mg L^{-1}. The acid background of the standards and samples was adjusted to 5% nitric acid (m/v, puriss p.a., ≥65%). In digestion experiments, 15% of HCl (v/v, puriss p.a.) and 5% of HNO_3 (v/v, puriss p.a.) was used as an acid background. Used calibration equations were linear with calculated intercept and had an excellent calibration fitting ($r \geq 0.9999$ for most elements). Detection limits were calculated from the average signal and the deviation of ten blank solutions with equations 8 and 10. Wavelength used for Rb measurements was 780.023 nm. Data for the matrix element measurements by ICP-OES Avio 500 are in the appendix table A2.

TABLE 10 Parameters for the ICP-OES Optima 8300 and ICP-OES Avio 500.

	Optima 8300	Avio500
RF Power (W)	1,500	1,500
Plasma gas flow rate (L min^{-1})	8	8
Carrier gas flow rate (L min^{-1})	0.6	0.7
Auxiliary gas flow rate (L min^{-1})	0.2	0.2
Sample introduction rate (mL min^{-1})	1.5	1.3
Replicates	3	3

4.3.2 GFAAS

Graphite furnace atomic absorption spectrometric determinations of rubidium were performed with the Perkin Elmer AAnalyst 800 atomic absorption spectrometer equipped with the Zeeman effect background correction and AS-800 autosampler. The TGHA graphite tubes with end caps and an integrated L'vov platform supplied by Perkin Elmer were used. A hollow cathode lamp (Rb 780.0 nm) was used for the determination of the rubidium. Argon (AGA, 99.999%) was used as a protective gas during measurements. The sample volume was 20 µL, and no matrix modifiers were used. Parameters for the GFAAS measurements were selected based on the pyrolysis and atomization curves and the shapes of the absorption bands of authentic samples.

The concentrations of the standard solution were 0, 4, 8, 12, 16 and 20 µg L^{-1}. The AS-800 autosampler produced the calibration standards from 20 µg L^{-1} of rubidium solution diluted from the Perkin Elmer Single-element standard (Rb 1,000 mg L^{-1}). The autosampler used 1% nitric acid (v/v, puriss p.a., ≥65%) as a diluent and acid background of the standard, and samples were adjusted to 1% nitric acid. Used calibration equations were linear through zero and had a good calibration fitting ($r \geq 0.999$). Detection limits were calculated from the average signal and three times the deviation of 10 blank solutions with equations 8 and 10. Repeatability ($n = 4$) and reproducibility ($n = 15$) were determined from the relative standard deviation of the measured concentrations of the QC samples with a Rb concentration of 20 µg L^{-1}. The optimal parameters for the determination of rubidium are given in table 11.

TABLE 11 Parameters for GFAAS AAnalyst 800.

Lamp current (mA)	10
Slit (nm)	0.7
Sample volume (µL)	20
Signal quantification	Integrated absorbance
Temperature program (ºC)	
Drying	110–130
Pyrolysis	700
Atomization	1,800
Cleaning	2,400

4.3.3 ICP-MS

The ICP-MS Perkin Elmer NexION 350D was also used for the determination of rubidium (^{85}Rb, ^{87}Rb), cesium (^{113}Cs), lithium (^{7}Li) and potassium (^{38}K). Yttrium (^{89}Y) was selected as an internal standard to correct the instrumental drift, and changes in the analyte sensitivity caused by variation of the sample matrix. The sample was introduced into the plasma via a temperature-controlled (+2 °C) baffled cyclonic glass spray chamber and PFA-ST nebulizer. Plasma was generated by a helical load coil on a quartz torch with a sapphire injector (1.8 mm). The triple cone interface material was nickel, and a triple quadrupole (Quadrupole Ion Defector, Universal Cell Technology and Analyzing Quadrupole) was used for ion separation. A simultaneous dual-mode detector measured both high- and low-level analytes simultaneously. An ESI (Elemental Scientific) prepFAST 4DX autodilution and autosampler system was used for dilutions and sampling. Table 12 shows the used parameters for ICP-MS measurements.

TABLE 12 Parameters for ICP-MS NexION 350D.

RF Power (W)	1,600
Plasma gas flow rate (L min^{-1})	18
Carrier gas flow rate (L min^{-1})	0.93
Auxiliary gas flow rate (L min^{-1})	1.2
Integration time (ms)	2,000
Dwell time (ms)	50
Replicates	3
Spray chamber temperature (°C)	2
Mode of operation	Standard

Tuning of the instrument was conducted daily using the Perkin Elmer NexION set-up solution containing 1 µg L^{-1} Be, Ce, Fe, In, Li, Mg, Pb, and U. The highest sensitivity and lowest variability were achieved by reducing the

production of the ionized oxides and doubly charged ions. Optimizing was performed by torch alignment, nebulizer gas flow rate adjustment, and QID/DRC voltage adjustment. The performance was verified by a Standard Performance Check.

Perkin Elmer single element standards (1,000 mg L^{-1}) for rubidium, cesium, lithium, and potassium were diluted to 100 µg L^{-1} (to 1,000 µg L^{-1} for potassium), and an external calibration from 1 to 10 µg L^{-1} (10 to 100 µg L^{-1} for potassium) was conducted using the ESI prepFAST 4DX autodilution system. The used diluent was 1% (m/v) nitric acid (ANALPURE, 67-69%). An yttrium solution of 30 µg L^{-1} was used as an internal standard, and it was added to the samples and calibration standards via ESI prepFAST 4DX before they entered the spray chamber and went to plasma. Digested ash samples containing yttrium were measured without an internal standard.

Used calibration equations were linear through zero and had excellent calibration fitting ($r \geq 0.9999$ for most elements). Detection limits were calculated from the average signal and three times the deviation of ten blank solutions with equations 8 and 10. By measuring QC samples with Rb concentration of 1 µg L^{-1}, repeatability (n = 4) and reproducibility (n = 15) were determined. Data for Rb, and other alkali metals by ICP-MS NexION 350D are in the appendix table A3.

4.4 Experimental procedures

Fly ash samples from different sites and with different fuel compositions were used in this study. However, most of the rubidium recovery experiments were conducted with fly ash from the combustion of 50% wood residue and 50% peat at power plant A. Total concentrations of rubidium and matrix elements were determined from the fly ash samples by ultrasonic-assisted digestion and microwave-assisted digestion methods.

The oxalic acid leaching procedure used in this thesis is adapted from a patent[108] of a utilizing process of fly ash, and this gave the basis for the recovery studies of rubidium. The development of the oxalic acid leaching procedure of fly ash is presented elsewhere.[22]

4.4.1 Optimization of methods

ICP-OES

The multiple linear regression (MLR) method was applied for creating a correction equation that compensates the increase of the intensities of rubidium measured by axial viewing in ICP-OES. The observed bias was most likely caused by EIE and spectral interferences. The effects of the matrix elements were assumed to be linear. For determining a correction equation, 19 synthetic samples were prepared at five concentration levels mimicking the concentrations of samples originating from rubidium recovery tests. Samples were prepared from 1000 mg L^{-1} elemental stock solutions and the acid matrices were

adjusted to 15% of HCl (v/v, puriss p.a.) and 5% of HNO_3 (v/v, puriss p.a.). Concentrations of rubidium and interfering elements are listed in table 13. The rubidium concentrations of the synthetic samples were measured with the Perkin Elmer Optima 8300 with axial plasma viewing. Microsoft Excel was used to create an MLR model, where the added concentrations of rubidium were used as dependent variables, while measured concentrations of rubidium and added interfering element concentrations were non-dependent variables. Only concentrations of the elements of significance in the 95% significance level were included in the correction equation, which was valid for several months.

The significance of the difference between added and measured as well as added and corrected rubidium concentration was investigated with paired *t*-test at the 95% significance level. The flow sheet of the procedure is displayed in figure 6.

TABLE 13 Concentrations (mg L^{-1}) of rubidium and interfering elements in synthetic samples.

Sample nro	Rb	Na	K	Ca	Fe	Mg
1	5.0	815	0.5	760	1.7	17.5
2	1.0	15	38	1,010	0.2	30
3	4.0	15	13	10	1.2	5
4	3.0	15	13	760	1.2	30
5	4.0	415	38	260	0.7	5
6	1.0	415	0.5	260	0.7	55
7	1.0	1,615	25.5	10	0.7	17.5
8	4.0	415	25.5	1,010	2.2	55
9	1.0	815	50.5	510	1.2	5
10	2.0	1,215	0.5	1,010	1.7	5
11	5.0	815	50.5	510	1.7	42.5
12	5.0	815	25.5	760	0.2	17.5
13	2.0	15	13	10	1.7	42.5
14	2.0	1,215	13	260	2.2	17.5
15	3.0	1,215	38	510	0.2	55
16	4.0	1,615	25.5	10	1.2	42.5
17	3.0	1,615	0.5	510	0.7	42.5
18	3.0	415	50.5	260	2.2	30
19	2.0	1,615	38	760	2.2	30

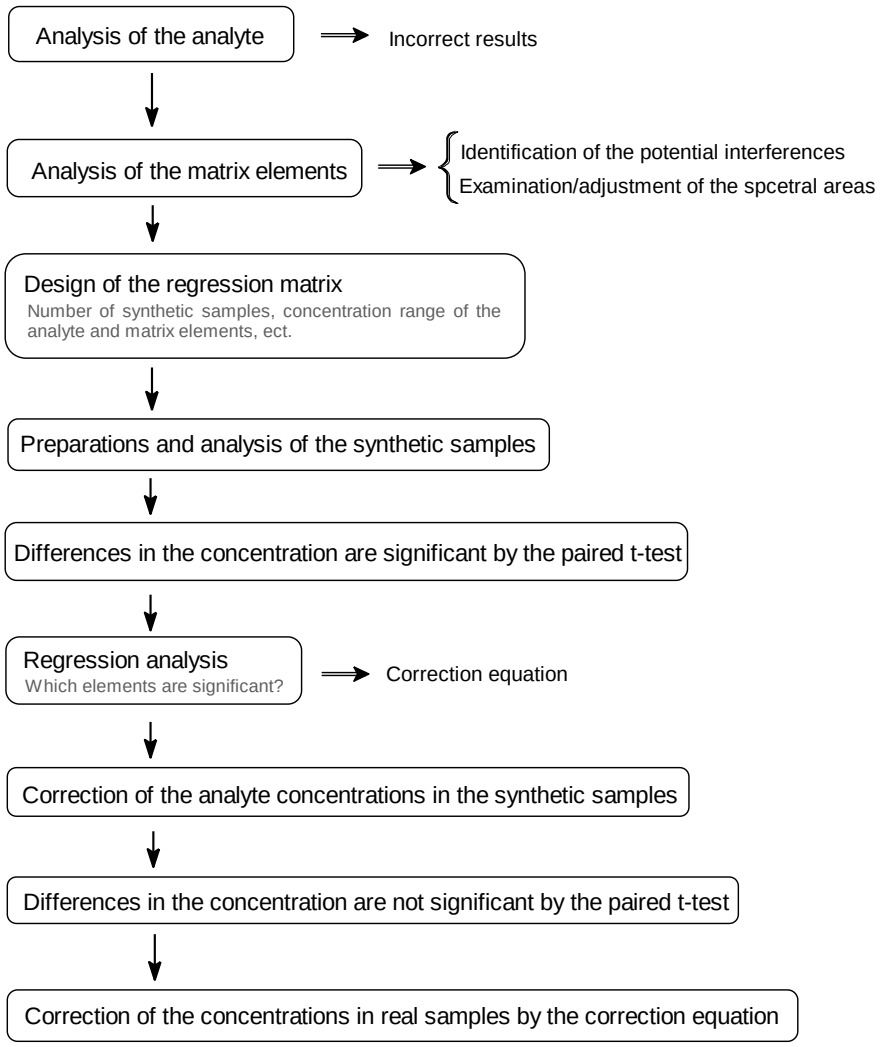

FIGURE 6 Flow chart of the MLR correction procedure for concentration of rubidium measured by ICP-OES axial viewing.

GFAAS

The temperature program was optimized by measuring the absorbance of two test samples with different pyrolysis and atomization temperatures. Cross curves were constructed from the results.

Characteristic mass with end caps was calculated from the absorbance of measured 4 µg L^{-1} Rb standard solutions with equation 5. Data was collected from the calibration data measured during experiments. The sample volume was 20 µL. Rubidium's characteristic mass was calculated from 24 measurements.

4.4.2 Digestion

For the determination of the total concentration of rubidium and matrix elements, two digestion methods were used in this thesis. The ultrasonic (US) assisted digestion method was adapted from Ilander and Väisänen[108] with slight modifications. EPA Method 3052[109] was also modified for digestion of fly, ash

and it was used for comparison of the efficiency of the ultrasonic digestion and oxalic acid leaching.

Ultrasonic-assisted digestion
A fly ash sample of 0.5 g was weighed accurately into a 60 mL plastic centrifuge tube followed by the addition of 6 mL of HNO_3 (puriss p.a. ≥65%), 2 mL of HCl (puriss p.a. ≥37%), and 0.25 mL of hydrofluoric acid (40% m/v). The sample mixture was placed into a 75 °C ultrasonic water bath (Elmasonic P) and treated six times with 3 min sonifications and 3 min standing followed by shaking. After cooling, solutions were filtered (Whatman 42 filter paper) into 50 mL volumetric flasks; the residue was rinsed three times with aliquot of water and diluted to the 50 mL volume with water. The concentrations of rubidium and matrix elements were measured by ICP-MS and ICP-OES after suitable dilutions.

Microwave-assisted digestion
A fly ash sample of 0.25 g was weighed accurately into 110 mL PTFE microwave digestion vessels. 7.0 mL of nitric acid (puriss p.a. ≥65%), 1 mL of hydrochloric acid (puriss p.a. ≥37%), and 1.5 mL of hydrofluoric acid (40% m/v) were added to the vessels and mixed with the samples. After closing, the vessels were placed into a microwave oven (CEM Mars 6 iWave, North-Carolina, U.S.A.), and digestion was conducted in two steps. In the first step, the temperature was ramped to 200 °C in 20 min and held there for 15 min with a microwave power of 290-1800 W. After cooling, a 10 mL of 5% (m/v) boric acid solution was added to the vessels, and they were transferred back into the microwave oven. In the second step, the temperature was ramped to 170 °C in 20 min and held there for 15 min with a microwave power of 290-1800 W. After cooling, the sample solutions were filtered (Whatman 42 filter paper) into 50 mL plastic volumetric flasks, and the vessels and the residue were rinsed three times with a small portion of ultrapure water onto the filter paper. Finally, solutions were diluted to the 50 mL volume with water. After suitable dilutions, the concentrations of rubidium and matrix elements were measured by ICP-MS and ICP-OES.

4.4.3 Sieving

Fly ash samples from different sites and with different fuel compositions were divided into six different size fractions by sieving (Retsch AS 200, the amplitude of 60). Fifty grams of fly ash were sieved through five different size sieves (250, 125, 63, 45, and 32 μm) for 1 hr. After sieving, the fly ash fractions were weighed. A sample of 0.5 g of each fraction was digested with the US digestion procedure described in the previous paragraph. Rubidium was measured with the ICP-MS Nexion 350D and matrix elements were determined with the ICP-OES Optima 8300.

4.4.4 Leaching procedure and pretreatment methods

Rubidium can be leached from fly ash using the previously optimized oxalic acid leaching procedure[22]. After leaching, the oxalic acid can be recovered as

oxalate by precipitation. Rubidium can be recovered from the leachate by liquid-liquid extraction, but the pH of the leachate needs to be adjusted to 12-13 prior to the extraction. Figure 7 shows a schematic presentation of the leaching of fly ash and pretreatment of the leachate.

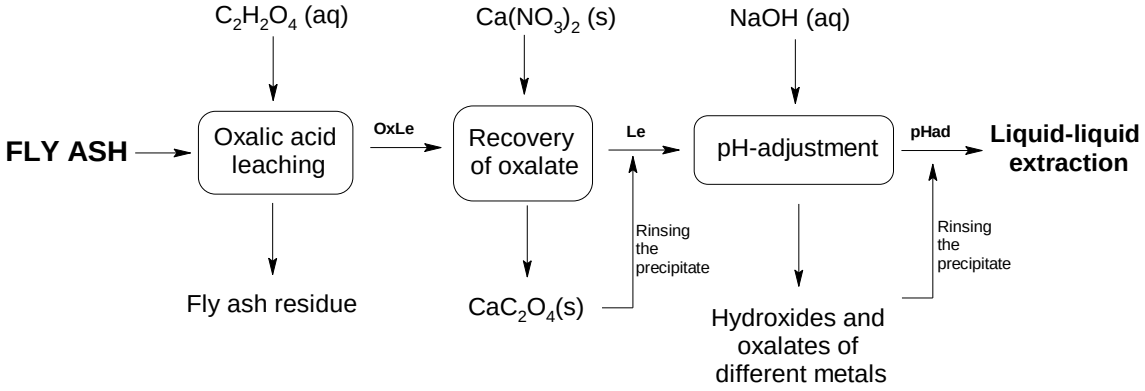

FIGURE 7 Leaching of fly ash and pretreatment of the leachate prior to the liquid-liquid extraction. OxLe = Oxalic acid leachate, Le = Leachate after oxalate precipitation, pHad = pH adjusted leachate.

Oxalic acid leaching

One gram of fly ash was weighed accurately into a 60 mL plastic centrifuge tube and 20 mL of 0.5 mol L^{-1} oxalic acid solution (oxalic acid dehydrate, J.T.Baker, 99.5-102.5%) was added. After sealing the tube and mixing, the sample mixture was placed into a 75 °C ultrasonic water bath (Elmasonic P). The mixture was treated six to eight times with 3 min sonifications and 3 min standing followed by shaking. After cooling, the solutions were centrifuged at 3,500 rcf for 10 min, and the oxalic acid leachate (OxLe) was separated by decanting. For elemental analysis, the OxLe was filtered (Whatman 42 filter paper) into a 50 mL volumetric flask and diluted to volume with ultrapure water and adjusted to 5% nitric acid (puriss p.a. ≥65%). The undiluted OxLe of fly ash (A) P50:W50 had a pH of 0.9, and it was used for the recovery studies of rubidium.

Recovery of oxalate

After oxalic acid leaching, oxalate was recovered by precipitation. Calcium nitrate tetrahydrate and zinc nitrate were tested for precipitation of calcium oxalate and zinc oxalate. The solid reagent was added into the OxLe solution with vigorous mixing. After the dissolution of the nitrate, oxalates started to precipitate, and the solution was left to stand overnight with slow mixing. The next day, the oxalate precipitate was separated by centrifuge (3,500 rcf for 10 min), and the leachate (Le) was transferred for the next treatment. The pH of the Le was 0.5.

pH-adjustment and scrubbing of the precipitate

The pH of the fly ash leachate (Le) was adjusted to pH 12.0–12.8 prior to the liquid-liquid extraction and rubidium recovery. A 1–6 mol L^{-1} sodium hydroxide (NaOH) or ammonium hydroxide (NH_4OH) solution was added into the Le via burette or an Orion 960 titrometer, and pH was measured by a pH meter (WTW inolab pH/cond 720). During pH adjustment, profuse precipitation took place. After a desirable pH was achieved, the solid precipitate was removed by centrifuge (3,500 rcf for 10 min) and the remaining solution (pHad) was used for the liquid-liquid extraction.

The scrubbing of the precipitate (originating from the pH-adjustment of 30 mL of OxLe) was performed three times by adding 5 mL of 0.05 mol L^{-1} of NaOH scrubbing solution on top of the separated precipitate and shaken for 10 min. The solid precipitate was separated from the scrubbing solution by centrifuge (3,500 rcf for 10 min), and elemental analysis was performed for the separated solution.

4.4.5 Liquid-liquid extraction

The organic phase containing 0.5–2.5 mol L^{-1} of chlorophene (Alfa Aesar, 96.0%) in chloroform (VWR International, 99.5%) (CPh/$CHCl_3$) was used for the extraction of rubidium from the pHad. Suitable volumes of aqueous and organic phases with different A:O phase ratios were added in a separating funnel and mechanically shaken for 5 min. After a few minutes, the phases settled, and the heavier loaded organic phase was separated from the aqueous phase by draining it into a new container. The new fresh organic phase was added into the separating funnel and the procedure was repeated 1–6 times. Finally, the organic phases were combined into a new separation funnel.

Rubidium was extracted from the organic phase by adding 0.01–1 mol L^{-1} of a hydrochloric acid solution with different A:O phase rations into the funnel with the loaded organic phase, and the mixture was shaken for 5 min before settling and the separation of the phases. The pH adjustment and the liquid-liquid extraction was repeated until satisfactory pure extract was accomplished.

In a few experiments, there was an additional scrubbing stage of the loaded organic phase. In the scrubbing stage, different aqueous scrubbing solutions were added into the separating funnel with the loaded organic phase with different A:O phase rations. The mixture was shaken for 3–5 min before settling and the separation of the phases. Used scrubbing solutions were 0.01, 0.03, 0.04, and 0.05 mol L^{-1} of sodium hydroxide and 0.1 mol L^{-1} of ammonium hydroxide. After this, rubidium was extracted from the organic phase as described before. Figure 8 shows a schematic presentation of the liquid-liquid procedure with an additional scrubbing stage.

The rubidium and matrix element concentrations in the aqueous phases were measured by ICP-MS and ICP-OES after appropriate dilutions. The rubidium and matrix element concentrations in the organic phase were calculated from the difference between the element concentration in the aqueous phase

before and after extraction. All the experiments were carried out at room temperature (20 ± 2 °C).

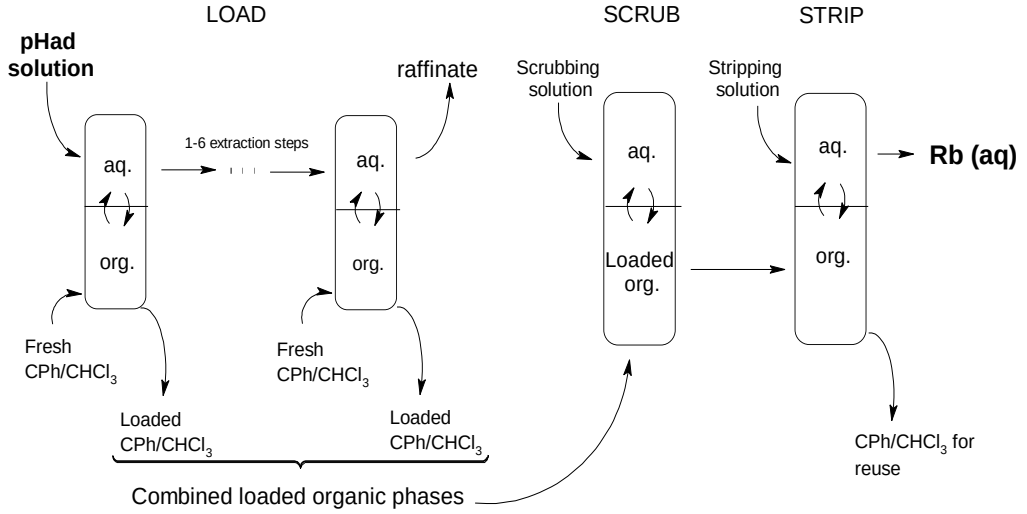

FIGURE 8 Presentation of the liquid-liquid extraction process.

4.4.6 Sorption experiments

In this study, 3D-printed nylon-based potassium copper(II) hexacyanoferrate (KCuFC) functional filters were employed for selective recovery of rubidium from synthetic samples mimicking acid leached fly ash after oxalic acid recovery and pH-adjustment (SynpHad). The elemental concentrations in synpHad are listed in table 14. The sorbent was known to decompose in strongly acidic and basic conditions. The pH of the sample was adjusted to 10 with a 6 mol L^{-1} NaOH solution to precipitate most of the matrix elements from the solution without damaging the sorbent during elution.

TABLE 14 Concentrations (mg L^{-1}) of rubidium and major matrix elements in the synthetic sample, SynpHad.

Element	Concentration (mg L^{-1})
Rb	6.21
Al	44.0
Ca	2.83
Mg	10.9
Na	8.86
Cu	3.54
K	308

The functional filters were prepared in two steps: first, the synthesis of the KCuFC, and second, the printing the functional filters. The schematic presentation of the procedure is shown in figure 9. The KCuFC sorbent was prepared by

adding, slowly and simultaneously, 450 mL 0.5 mg L^{-1} $Cu(NO_3)_2$ and 300 mL 0.5 mg L^{-1} $K_4Fe(CN)_6$ to preheated (55 °C) water of 200 mL. The mixture was left in a beaker overnight at 55 °C with stirring, and after 16 hr, the solid sorbent was separated from the slurry by centrifuge (5 min, 3,000 rcf, washed with water and dried at 55 °C).

The 3D-printing of the functional filters was done by using the Sharebot SnowWhite SLS 3D-printer. Filters were manufactured using a 0.1 mm layer thickness with a temperature of 165 °C and by utilizing 40% laser power (from a maximum of 40 W) at 2,560 mm s^{-1}. The printed filters were squeezed into the bottom of 10 mL syringes before use. The KCuFC content in the filter was 10% and the used matrix was inert nylon.

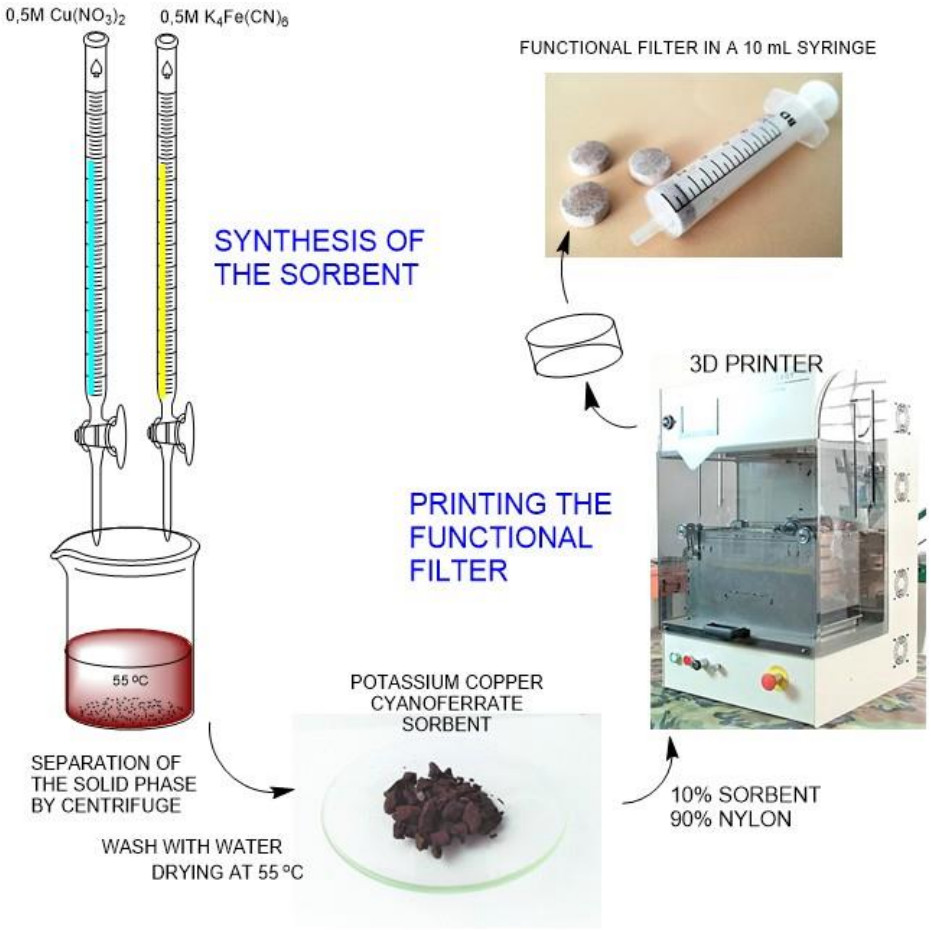

FIGURE 9 Schematic presentation of the preparation of the functional filters.

The loading capacity of the filter (approx. m = 0.6 g, V = 1.1 mL) was tested by passing 500 mL of 100 mg L^{-1} of Rb solution through the filter at a flow rate of 10 mL min^{-1}. The Rb solution was diluted from a 1,000 mg L^{-1} solution manufactured by dissolving 0.7074 g of RbCl(s) (Cerac, 99.9%) to 1 L of ultra-pure water. The same Rb solution was passed through the filter 10 times, and the loaded filter was rinsed with 60 mL of ultra-pure water. The loaded rubidi-

um was extracted from the filter by eluting 10 mL of 1 mol L^{-1} of NH_4NO_3 solution 20 times through the filter.

In the recovery of rubidium from synthetic samples, water was first rinsed through the functional filter a few times before use. It was observed in earlier experiments that the best Rb recovery was gained by using a diluted sample. Therefore, the filter was loaded by passing 10 mL of a tenfold diluted synthetic sample through the filter. The same 10 mL sample was passed through the filter five times at a speed of 10 mL min^{-1}. After loading, the filter was rinsed again with 30 mL of ultra-pure water to diminish the content of matrix elements in the final eluent. Finally, rubidium was eluted from the filter by a 1 mol L^{-1} NH_4Cl solution.

Rubidium and matrix element concentrations in the aqueous phases were measured by the ICP-MS PerkinElmer NexIon 350D and ICP-OES PerkinElmer Avio 500 after suitable dilutions. Rubidium and matrix element concentrations in the solid sorbent were calculated from the difference between the element concentration in the aqueous phase before and after extraction and elution. Extraction efficiency was calculated with equation 2. All the experiments were carried out at room temperature (20 ± 2 °C).

5 RESULTS AND DISCUSSION

5.1 Development of the analysis methods

5.1.1 MLR method for ICP-OES

Measurement of low concentration of rubidium by ICP-OES in the presence of other alkali and earth alkali metals is challenging due to the ionization interferences. Rubidium has only two noteworthy analytical wavelengths at 780.023 and 420.185 nm, from which the first one is mostly used due to the poor sensitivity of the latter. Radial plasma viewing is not prone to ionization interferences but cannot detect low concentrations of rubidium. In addition, the effect of the interference of argon emission on radial measurements is severe as can be seen in figure 10. Axial plasma viewing is very sensitive but suffers interferences caused by EIE elements. When measuring a low concentration of rubidium from samples where the Na/Rb concentration ratio can be over 1,500, axial measurement is the only option to reach the required sensitivity, but the ionization interferences must be corrected.

The multiple linear regression (MLR) method was applied for creating a correction equation that compensates for the increase of the intensities measured by axial plasma viewing. In 19 synthetic samples, the measured rubidium concentrations were 127-277% compared to the added rubidium concentrations. From the suspected interference elements (Na, K, Ca, Mg, and Fe), only sodium and calcium had a significant effect on the measured concentrations of rubidium. The concentration ranges where the equation can be applied were 1-5 mg L^{-1} for Rb, 15-1,615 mg L^{-1} for Na, and 10-1,010 mg L^{-1} for Ca. The correction equation was:

$$y = 0.401[Rb] - 0.0007[Na] - 0.00058[Ca] + 1.11$$

Symbols *[Rb]*, *[Na]*, and *[Ca]* represent measured concentrations of elements Rb, Na, and Ca. Correction equation was assumed to be valid for rubidium deter-

minations by ICP-OES Optima 8300 with the same method for longer period, and update before each measurement sequence was not needed.

The effect of the correction of the synthetic samples can be seen in figure 11. After correction, the measured rubidium concentrations were 78-155% compared to the added rubidium concentrations, and they had no significant difference at a 95% level of confidence according to Student's paired *t*-test.

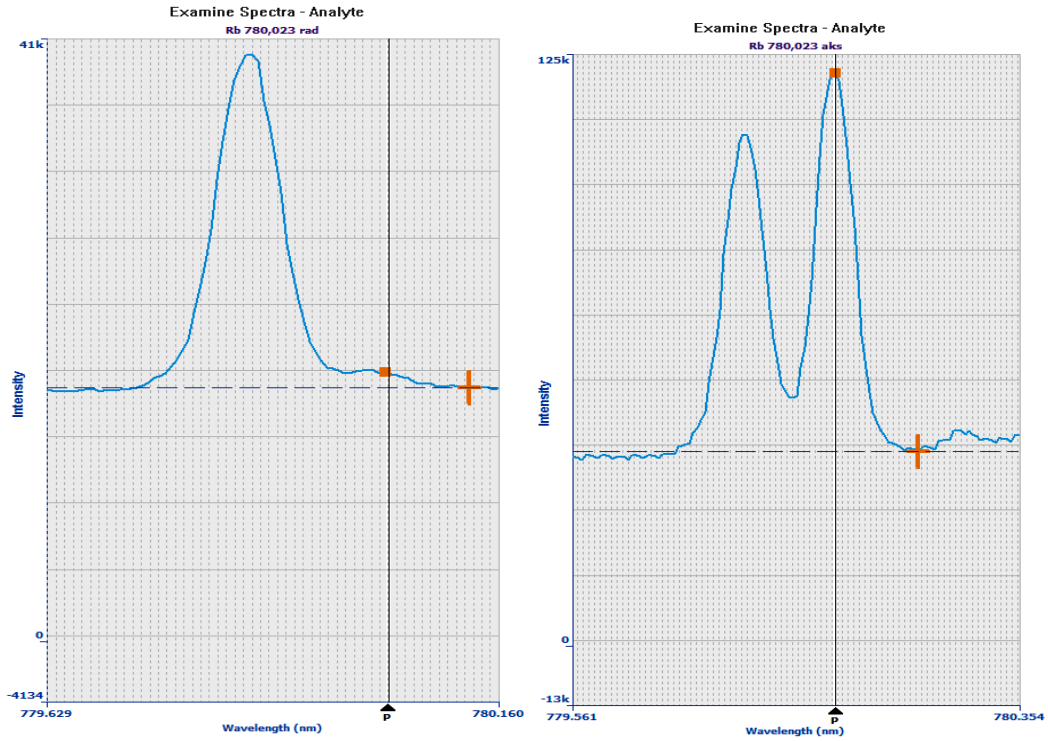

FIGURE 10 Effect of the interference of argon emission on the radial (left) and axial (right) measurements of 5 mg L^{-1} of rubidium. The vertical line represents the rubidium's emission wavelength of 780.023 nm.

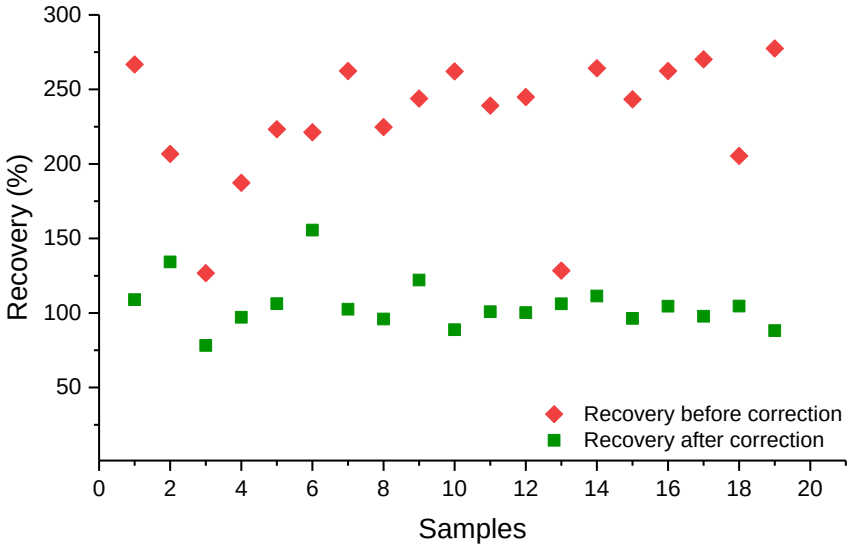

FIGURE 11 Recoveries of rubidium before and after MLR correction with 19 synthetic samples.

The correction equation was tested on three synthetic oxalic acid leachate (samples 1-3) and two real samples originating from rubidium recovery tests (samples 4 and 5). The real samples were from rubidium recovery tests where sample treatment often leads to high sodium concentrations (table 15). Samples 1-3 had moderate Na concentrations, and high other EIE concentrations. Sample 4 had a very high Na concentration and lower concentrations of other EIEs. Sample 5 had low concentrations of Na and Ca but high concentrations of other matrix elements. Samples were diluted so that the concentrations of MLR model samples would cover concentrations of rubidium and most of the matrix elements in the samples. In samples 3 and 5, the Na concentration was lower than the concentration area in the MLR model, and in sample 4 the Na concentration was over the area. Samples 4 and 5 also had very low Ca concentrations.

The results of MLR correction on samples 1-5 measured by the ICP-OES Optima 8300 are presented in table 16. Corrected values were compared to rubidium values of the added Rb concentrations (samples 1-3) and to the values determined by the accurate GFAAS method (samples 4 and 5). The reliability of the GFAAS method is verified in chapter 5.1.2. With real samples, recoveries of rubidium were 68–322% before correction and 96-114% after correction. The correction equation was very useful at the concentration ranges of the synthetic MLR samples, resulting in recoveries of 97-107%, and even when the Na concentration was under or over the MLR area, the correction gave satisfactory recoveries for rubidium. The feasibility of the correction equation on low rubidium concentration (< 1 mg L^{-1}) were also tested, but the MLR model gave excessively low values for rubidium.

TABLE 15 Concentration of rubidium and interfering elements (mg L^{-1}) in 3 synthetic samples (1-3) and 2 real samples (4-5) (Rb concentrations in real samples measured by GFAAS). Concentrations in *italics* are the matrix element values resulting outside the MLR concentration area.

	Rb	Na	Ca
Sample 1	3.20	20	700
Sample 2	3.70	20	700
Sample 3	2.60	*10*[1]	350
Sample 4	2.75	*2,190*[2]	*0.21*[1]
Sample 5	1.62	*2.41*[1]	*0.53*[1]

(1) Concentration under MLR area, (2) concentration over MLR area

TABLE 16 Recoveries of rubidium from 3 synthetic samples and 2 real samples before and after MLR correction. Recoveries are calculated by comparing ICP-OES results to added Rb concentrations (samples 1-3) and to concentrations obtained by GFAAS measurements (samples 4 and 5).

	Before correction		After correction	
	Conc. ($mg\ L^{-1}$)	Recovery (%)	Conc. ($mg\ L^{-1}$)	Recovery (%)
Sample 1	6.31	197	3.22	101
Sample 2	7.26	196	3.60	97
Sample 3	4.67	180	2.77	107
Sample 4	8.87	322	3.13	114
Sample 5	1.10	68	1.55	96

5.1.2 GFAAS method

Optimization of the temperature program

Careful optimization of the temperature program is needed to ensure reliable results in GFAAS measurements when a new measuring method is created. The aim is to produce smooth and symmetric absorption signals with adequate peak height. Absorption of rubidium was measured after different pyrolysis and atomization temperatures from two test samples from liquid-liquid extraction experiments. Sample 1 was the raffinate of the pHad solution after extraction of Rb, and sample 2 was the stripping solution (1 mol L^{-1} HCl) after stripping Rb from the organic phase (1 mol L^{-1} chlorophene in $CHCl_3$). Samples were diluted 700–2,000 times, and the acid background was adjusted to 1% nitric acid (m/v, puriss p.a., ≥65%) before measurements.

The optimal pyrolysis temperature was determined by varying the pyrolysis temperature from 600 to 1,000 °C, while the atomization temperature was constant at 1,800 °C. In the optimization of atomization, the pyrolysis temperature was kept at 700 °C, while the atomization temperature variated from 1,600 to 1900 °C. Pyrolysis and atomization curves for the two samples were constructed from the result (figure 12).

A pyrolysis temperature of 700 °C and atomization temperature of 1,800 °C produced the maximum integrated absorbance with the desirable absorption band shapes with both samples. Table 11, on page 45 shows the selected parameters for GFAAS measurements.

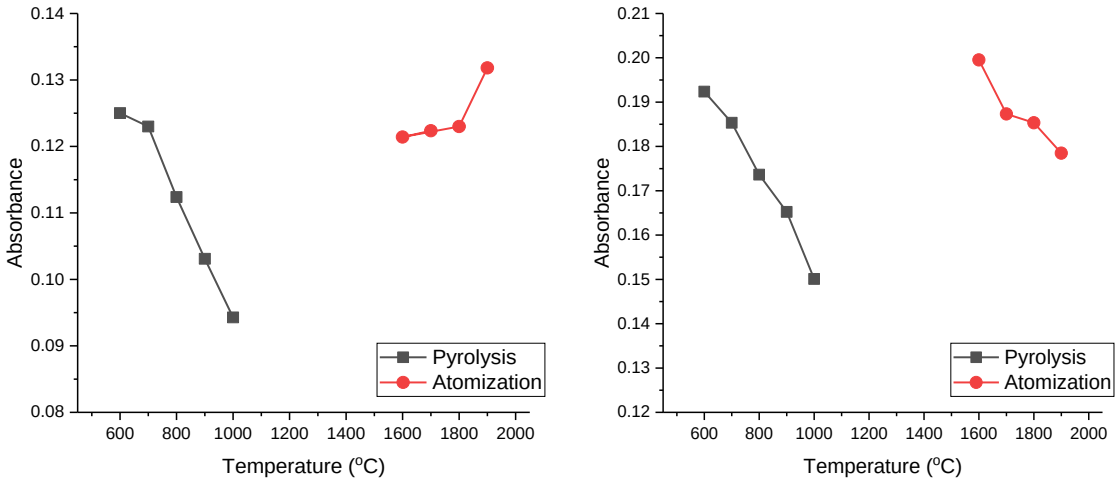

FIGURE 12 Pyrolysis and atomization curves of sample 1 (right) and sample 2 (left) by GFAAS. Integrated absorbances of rubidium are displayed as a function of temperature by changing pyrolysis and atomization temperatures.

The optimized GFAAS method was tested on three synthetic samples, whose rubidium concentrations were known. In sample 1, the added Rb concentration was 20 µg L^{-1}. Sample 2 had 5 µg L^{-1} of Rb with 10 mg L^{-1} of Na. Sample 2 expresses the concentration ratio of Rb and Na (1:2,000) in the pHad solution. Sample 3 was diluted from a synthetic sample mimicking the oxalic acid leachate in a way that the Rb concentration was 8 µg L^{-1}. Two replicates were manufactured from every sample and the average and relative standard deviation are shown in Table 17. The deviations of the measurements were under 5%, and recoveries of rubidium were between 90–101%. Therefore, the optimized GFAAS method can be considered as suitable for Rb analysis in fly ash derived samples with good accuracy.

TABLE 17 Added concentrations of Rb and some matrix elements of three synthetic samples and values of rubidium measured by GFAAS. Concentrations diluted to the calibration area are shown. The measured concentrations are reported as average and standard deviation of two replicates. In addition, recoveries in percent are shown.

	Added Rb (µg L^{-1})	Other elements (mg L^{-1})	Measured Rb (µg L^{-1})	Recovery (%)
Sample 1	20	-	20.2 ± 0.3	101
Sample 2	5	Na 10	4.935 ± 0.007	99
Sample 3	8	Ca 1.75; K 0.15; Mg 0.15; Al 0.6; Fe 0.85	7.2 ± 0.3	90

Characteristic mass of rubidium

THGA tubes with end caps increase sensitivities and improve detection limits compared to THGA tubes without end caps.[100] There are table values for characteristic masses with THGA tubes with end caps for some elements, but no information about the characteristic mass of rubidium with end caps is available. Characteristic mass with end caps for rubidium was determined during this study.

The characteristic mass was calculated from absorbance of measured 4 µg L^{-1} Rb standard solutions with equation 5. Data was collected from the calibration data measured during experiments. The sample volume was 20 µL. Table value for rubidium's characteristic mass with TGHA and EDL-lamp reported by PerkinElmer was 10.0 pg. Unfortunately, there are no reported values available for characteristic mass for TGHA with end caps. Rubidium's characteristic mass was calculated from 24 individual measurements. All the values were within 11% of the average value of 4.2 pg. End caps on the TGHA tubes improve sensitivity about 2–3 -fold. For other elements (Ag, Al, As, Au, Be, Bi, Cd, Co, Cr, Cu, Fe, Ga, Ge, In, Ir, Mg, Mn, Ni, P, Pb, Pd, Pt, Rh, Sb, Se, Si, Sn, Te, Tl, and V), a decrease on the characteristic masses from 0 to 55% has been reported earlier,[100] and in this study, a 58% decrease on characteristic mass of rubidium was determined.

5.1.3 Comparison of the analysis methods

Three different measuring methods were used for the determination of rubidium. In the preliminary experiments, rubidium content was determined by ICP-OES, but high concentrations of other EIE elements interfered with accurate measurements. During experiments, lower and lower concentrations of rubidium needed to be measured accurately from samples with high matrix content, and the detection limits of ICP-OES methods were not satisfactory enough. Next, GFAAS was used for the determination of rubidium, and it turned out to be a very sensitive method with an MDL value over 100 times lower than with axial ICP-OES. Unfortunately, the GFAAS technique was slow and problems in reproducibility were observed, especially during summer months and higher humidity, so when ICP-MS came available for use, it was selected as the method for determination of rubidium. Table 18 shows correlation coefficients, different detection limits (mg L^{-1}), and RSD (%) ranges for rubidium with three different measuring methods: ICP-OES, GFAAS, and ICP-MS. From the table, it can be seen, that the GFAAS technique has the lowest detection limits, but ICP-MS has the best calibration correlation coefficients and reproducibility.

Accuracy of the ICP-OES method with the MLR model was verified by comparing measured Rb concentrations of synthetic and real samples on the concentrations obtained by GFAAS (table 15). Recoveries of Rb were 96–114% even outside the concentration area of the matrix elements in the MLR model. By determining rubidium concentration from synthetic samples with different matrices imitating real samples from rubidium's recovery experiments, the accuracy of the GFAAS method was verified (table 17). Recoveries were between

90 and 101%. Accuracy of the ICP-MS method was established by determining Rb concentration from standard reference material, SRM1633c with 99% recovery (table 19). The relative standard deviation of four replicates was 4%.

TABLE 18 Wavelengths and isotopes used in three different measuring methods for determination of rubidium as well as correlation coefficients (r) of external calibrations, limits of detection (µg L^{-1}), limits of quantifications (µg L^{-1}), instrumental detection limits (µg L^{-1}), method detection limits (µg L^{-1}), and RSD values (%) for short- and long-term reproducibility of the measurements.

ICP-OES Optima 8300								
Plasma viewing	Wavelength nm	r	LOD µg L^{-1}	LOQ µg L^{-1}	IDL µg L^{-1}	MDL µg L^{-1}	RSD_S[(1)] (%)	RSD_L[(2)] (%)
Radial	780.023	0.9999	570	1,680	410	550	3.02	3.66
Axial	780.023	0.9998	65	88	11	52	1.77	2.99
GFAAS AAnalyst 800								
	Wavelength nm	r	LOD µg L^{-1}	LOQ µg L^{-1}	IDL µg L^{-1}	MDL µg L^{-1}	RSD_S[(1)] (%)	RSD_L[(2)] (%)
	780.023	0.9990	0.094	0.30	0.090	0.093	2.91	4.29
ICP-MS NexION 350D								
Isotope	Abundance (%)	r	LOD µg L^{-1}	LOQ µg L^{-1}	IDL µg L^{-1}	MDL µg L^{-1}	RSD_S[(1)] (%)	RSD_L[(2)] (%)
85	72.17	0.99999	0.47	1.30	0.36	6.59	1.03	1.41
87	27.83	0.99999	0.80	2.39	0.68	12.7	0.72	1.68

(1) Short-term relative standard deviation, n = 4
(2) Long-term relative standard deviation, n = 15

5.2 Comparison of digestion and leaching methods for fly ash

Two digestion methods, ultrasonic-assisted digestion (modified from Ilander and Väisänen[109]) and microwave-assisted digestion (modified from EPA method 3052[110]), were applied for the determination of rubidium from fly ash. The microwave-assisted digestion method was verified by standard reference material SRM 1663c coal fly ash and applied for real fly ash with fuel content of 50% of peat and 50% of wood residue. The microwave digestion method was compared to the ultrasonic-assisted digestion and oxalic acid leaching of the real fly ash. The rubidium, potassium, and cesium concentrations of the digested and leached samples were determined by ICP-MS NexION 350D and other elements by ICP-OES Avio 500.

The concentrations of rubidium and major matrix elements after microwave digestion are shown in table 19. The digestion method worked well with 90-102% recoveries for certified elements apart from Ti, which had a recovery of 86%. Recoveries of elements of informational values deviated more from the

table values with recoveries of 81-103%. Recovery of sulfur was exceptionally high in the MW digested samples (recovery of 198%), which can originate from contamination of the samples. The recovery of rubidium was at a desirable level, 99%. The same digestion method was applied for digestion of real fly ash from power plant A with 50% peat and 50% wood residue as a fuel. Real fly ash differs from certified coal fly ash with its lower concentration of heavy metals and higher concentration of some alkali and alkaline earth metals as seen in table 19. Real fly ash has a rubidium concentration similar to certified coal fly ash.

TABLE 19 Comparison of the elemental concentration of SRM 1663c coal fly ash and real fly ash from power plant A with fuel content of 50% of peat and 50% of wood residue using microwave (MW) digestion method. The measured concentrations are reported as average concentrations and ± standard deviation (s.d.) of four replicates. ICP-MS NexION 350D and ICP-OES Avio 500 were used for the elemental analysis.

	SRM 1663c			Real fly ash
Element	Determined conc.	Certified conc.	Recovery	Determined conc.
	mg kg^{-1}	mg kg^{-1}	(%)	mg kg^{-1}
Rb	**115.7 ± 3.8**	**117.42**	**99**	**114 ± 3**
	m(%)	m(%)	(%)	m(%)
Al	12.8 ± 0.3	13.28	97	6.6 ± 0.1
Ba	0.1045 ± 0.0015	0.113	93	0.12 ± 0.04
Ca	1.30 ± 0.02	1.365	96	11.1 ± 0.2
Fe	10.3 ± 0.3	10.49	99	6.36 ± 0.09
K	1.66 ± 0.03	1.773	93	2.6 ± 0.1
Mg	0.448 ± 0.006	0.498	90	1.39 ± 0.04
Na	0.174 ± 0.004	0.171	102	1.22 ± 0.04
S	0.218 ± 0.005	0.11*	198	1.435 ± 0.015
Si	20.4 ± 1.1	21.3*	96	6 ± 3
Ti	0.6212 ± 0.0014	0.724	86	0.215 ± 0.007
P	0.186 ± 0.005	0.192*	97	1.097 ± 0.008
	mg kg^{-1}	mg kg^{-1}	(%)	mg kg^{-1}
Cr	209 ± 7	258*	81	65.6 ± 0.2
Cu	158 ± 8	173.7	91	93.4 ± 0.2
Mn	221 ± 5	240.2	92	3,617 ± 7
Sr	906 ± 7	901	101	737.9 ± 1.3
Zn	235 ± 9	235*	100	522.0 ± 1.1
Cs	9.70 ± 0.13	9.39*	103	2.53 ± 0.07

*Reference values, not certified

The first step in the recovery process of rubidium is to perform oxalic acid leaching of the fly ash to liberate most of the valuable elements of the ash. The development of oxalic acid leaching has been described earlier and was not a part of this study. Elemental content and recoveries of microwave (MW) digested, ultrasonic (US) digested, and oxalic acid leached fly ash with a fuel content of 50% of peat and 50% of wood residue are presented in table 20.

TABLE 20 Elemental content of real fly ash from power plant A with a fuel content of 50% of peat and 50% of wood residue using the microwave (MW) digestion method, ultrasonic (US) digestion method, and oxalic acid leaching. The measured concentrations are reported as average and ± standard deviation (s.d.) of four replicates. Recoveries of the US digestion method and the oxalic acid leaching are calculated from MW digestion results. ICP-MS NexION 350D and ICP-OES Avio 500 were used for the elemental analysis.

	MW digestion	US digestion		Oxalic acid leaching	
Element	Conc.	Conc.	Recovery	Conc.	Recovery
		mg kg^{-1}	(%)	mg kg^{-1}	(%)
Rb	**114 ± 3**	**84.9 ± 1.5**	**75**	**60.7 ± 0.9**	**53**
	m(%)	m(%)		m(%)	
Al	6.6 ± 0.1	4.06 ± 0.03	62	2.84 ± 0.04	43
Ba	0.12 ± 0.04	0.059 ± 0.001	48	0.0038 ± 0.0001	3
Ca	11.1 ± 0.2	10.78 ± 0.07	98	0.31 ± 0.02	3
Fe	6.36 ± 0.09	6.6 ± 0.2	104	5.23 ± 0.08	82
K	2.6 ± 0.1	1.7 ± 0.2	62	1.00 ± 0.03	38
Mg	1.39 ± 0.04	1.38 ± 0.01	100	1.04 ± 0.02	75
Na	1.22 ± 0.04	0.48 ± 0.01	39	0.27 ± 0.01	22
S	1.435 ± 0.015	1.65 ± 0.03	115	1.486 ± 0.012	104
Si	6 ± 3	2.01 ± 0.09	30	2.46 ± 0.02	42
Ti	0.215 ± 0.007	0.1302 ± 0.0015	60	0.0672 ± 0.008	27
P	1.097 ± 0.008	1.221 ± 0.015	111	1.078 ± 0.010	112
	mg kg^{-1}	mg kg^{-1}	(%)	mg kg^{-1}	(%)
Cr	65.6 ± 0.2	86 ± 4	130	29.1 ± 0.5	44
Cu	93.4 ± 0.2	114.6 ± 1.3	123	54 ± 4	58
Mn	3,617 ± 7	4,220 ± 40	117	2,800 ± 90	79
Sr	737.9 ± 1.3	690 ± 7	93	183 ± 7	25
Zn	522.0 ± 1.1	538 ± 7	103	299 ± 11	57
B	-	153 ± 5	-	114.8 ± 1.3	-
Cs	2.53 ± 0.07	1.86 ± 0.03	73	1.260 ± 0.012	50

Results obtained with US-assisted digestion were comparable to MW-assisted digestion for several elements (Rb, Cs, Ca, Fe, Mg, S, P, Cr, Cu, Mn, Zn) with recoveries of 73-130%. For some elements (Al, Ba, K, Na, Si, Ti) US-assisted digestion was not as efficient, with recoveries approximately half compared to MW-assisted digestion. One reason for this is the higher concentration of hydrofluoric acid used in MW-assisted digestion, enabling effective digestion of silicates.

Oxalic acid leaching recovered 53% of rubidium from real fly ash samples. Recoveries of most matrix elements were between 22–76%, but sulfur and phosphorous had higher recoveries. Barium and calcium had very low recoveries due to the possible precipitation of barium and calcium oxalate. Due to the addition of boric acid into the samples during microwave digestion, the boron concentration in those samples is not determined, and in table 20, the recoveries for boron cannot be calculated.

5.3 Rubidium in fly ash

Five different fly ash samples of different fuel contents of peat and wood residue were evaluated by their elemental content and particle size. US-assisted digestion was used for sample digestion since MW-assisted digestion was not available at this time. Fly ash samples originate from two different Finnish energy power plants (plant A and plant B), and their fuel composition varied from 30–100% of peat and 30–70% of woody biomaterial. Concentrations of rubidium and major matrix elements are shown in table 21.

Rubidium concentrations in fly ash varied from 27 to 94 mg kg^{-1} when peat or wood residue is used as a fuel (table 21). The highest rubidium concentrations were in ashes originating from 50% of peat and 50% of wood residue, and the lowest concentration of rubidium was produced when only peat was used as a fuel. However, the fly ash sample originating from the highest wood residue content (B) P30:W70 had only 63% of the rubidium content compared to the fly ash from (B) P50:W50 fuel content. The rubidium concentration in MW-assisted digested (A) P50:W50 ashes (114 mg kg^{-1}) was 27% higher than in Earth's crust (90 mg kg^{-1}). This shows that rubidium is slightly concentrated in fly ash (A) P50:W50, and when rubidium recovery is combined with recovery of other elements, such as REEs and PGMs, fly ash has potential as alternative rubidium source. Additionally, fly ash needs less pretreatment than ores in hydrometallurgical recovery process.

TABLE 21 Concentrations of rubidium (mg kg^{-1}) and major matrix elements (m%) in fly ash samples with different fuel compositions from two different power plants (plant A and plant B). The concentration of rubidium was determined by ICP-MS NexIon 350D and matrix elements by ICP-OES Avio 500 after US-assisted digestion.

Element	(A) P50:W50	(A) P100	(B) P30:W70	(B) P50:W50	(B) P70:W30
Rb	87.2	26.9	58.7	93.6	40.0
Na	0.63	0.30	0.48	0.57	0.37
K	1.76	0.50	1.03	1.54	0.55
Mg	1.29	1.30	0.61	1.28	0.61
Ca	8.53	16.40	3.26	9.63	3.75
Fe	5.79	6.76	2.42	4.74	4.03
Al	4.50	4.02	2.82	4.58	3.65
Si	2.64	3.20	3.86	3.30	1.59
P	1.17	0.71	0.35	1.21	2.17
S	1.41	1.61	0.10	0.56	1.92

Major matrix elements were quite evenly distributed, except for the fly ash of 100% peat (P100%), which had lower concentrations of alkali metals and a significantly higher concentration of calcium compared to the ashes originating from other fuel contents. Carbon content was above the detection limit only in

samples originating from power plant B, suggesting differences in the burning processes in the two power plants. Due to the too low concentration of HF in the digestion solution, silicon was dissolved only partially.

To investigate rubidium's distribution on different sized ash particles, five different ash samples were sieved into six fractions by their size. Figure 13 presents ash fractions of five fractionated fly ash samples. Distribution of different fly ash samples by their particle size on different mass fractions depends highly on the type of the electric precipitator of the power plant and the material used as fuel. In two samples originating from power plant A, the particle size distribution of fly ash is very similar even though the fuel composition is quite different. Most of the fly ash particles have a diameter of 32–45 µm, and 64–76% of the particles are smaller than 45 µm. Only 0.06% or less of the plant A fly ash particles were larger than 250 µm.

The particle size distribution of fly ash samples from power plant B differ considerably from each other. Fly ash samples with fuel compositions of P30:W70 and P70:W30 were quite evenly distributed into different size fractions. Over half of the fly ash particles were larger than 63 µm. The particle size distribution of fly ash sample P50:W50 differed considerably from other ashes from the same power plant. Nearly half of the particles were smaller than 32 µm. In addition, the samples with the same fuel composition originating from different power plants differed remarkably. It can be seen from the results that both, the type of the burning process and the type of the biomaterial used as fuel, have an effect on the particle size of the fly ash.

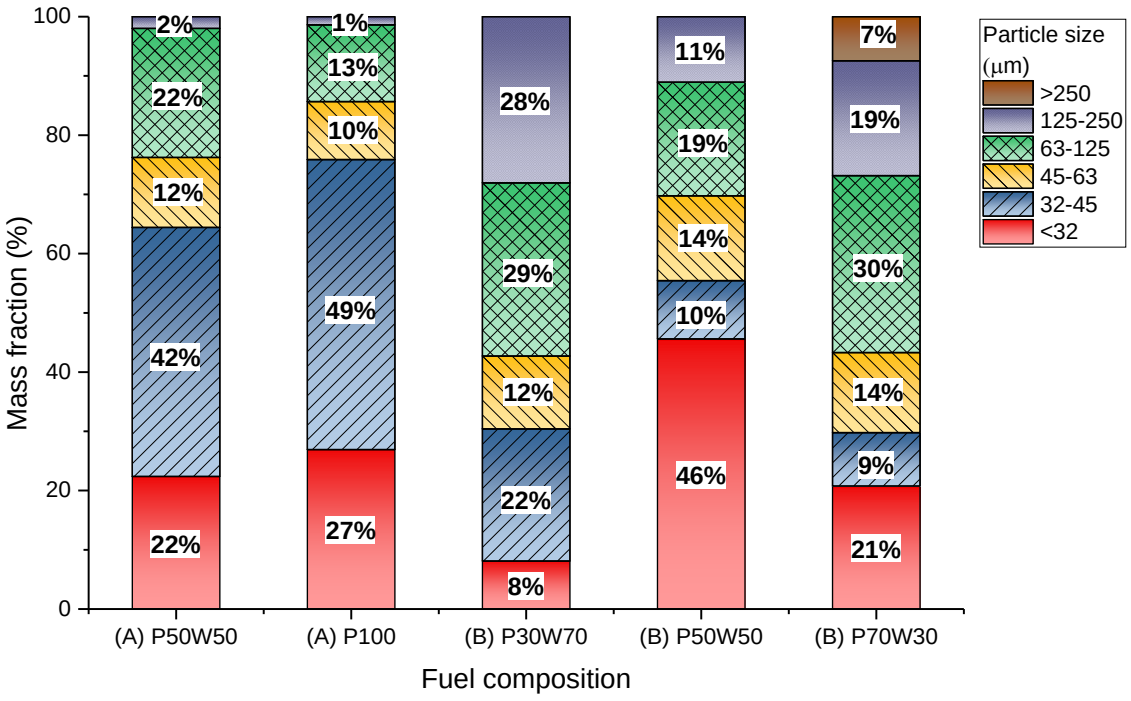

FIGURE 13 Mass fractions of five fractionated fly ash samples from the power plant (A) and power plant (B).

Fractioned fly ash samples were digested with the US-assisted digestion procedure, and the distribution of rubidium and matrix elements into different sized particles was determined. Concentrations of rubidium (mg kg^{-1}) in different particle size fly ash fractions are shown in table 22.

Highest rubidium concentrations were found in the largest fly ash particles in sample P50:W50 from power plant A, but in samples from power plant B, the highest rubidium content was in the smallest particles. By utilizing only the smallest particles (< 32 μm) of the fly ash from power plant B, the concentration of rubidium can be elevated 113-154% compared to the non-sieved ashes. This fraction covers 8-46% of the total mass of the fly ash and 12-51% of the total rubidium content. On the contrary, in a fly ash sample originating from power plant A using 50% peat and 50% wood residue as fuel, 126 % of rubidium was concentrated into the large-size ash particles (63-250 μm). This fraction was 24% of the total mass of the fly ash and it had 30 % of the total rubidium content. Distribution of rubidium into different particle size fractions was rather even with fly ash originating from 100% peat.

TABLE 22 Concentrations of rubidium (mg kg^{-1}) in different particle size fractions in different fly ash samples from power plant (A) and power plant (B). Concentrations in **bold** are above-average concentrations before sieving and indicate when rubidium becomes concentrated.

Size fraction (μm)	(A) P50:W50	(A) P100	(B) P30:W70	(B) P50:W50	(B) P70:W30
250 <	-	-	-	-	41.0
125-250	**122.0**	**26.5**	45.9	80.3	31.2
63-125	**105.9**	20.7	48.9	77.3	32.6
45-63	86.0	25.0	**65.4**	88.6	42.7
32-45	84.6	**29.2**	**71.8**	90.1	38.0
< 32	71.5	26.3	**91.7**	**106.1**	**57.5**
Before sieving	87.2	26.9	58.7	93.6	40.0

Table 23 presents the concentration of matrix elements in different particle size fractions with fly ash sample (A) P50:B50. The distribution of alkali metals other than rubidium is quite even between different sized fly ash particles. Nevertheless Ca, Mg, Fe, P, and S are mostly concentrated into small particles.

Quite even distribution of rubidium occurs between different sized ash particles and heterogeneity of the materials used as a fuel reduces the benefit of sieving. If the peat and wood residue is always collected from the same source and the fuel material stays consistent, it is possible to define the size fraction where rubidium could concentrate. Unfortunately, this is rarely the case when peat or wood are harvested.

TABLE 23 Concentrations of major matrix elements (m%) in fly ash sample (A) P50:W50 after and before sieving. Concentrations in **bold** are above-average concentrations before sieving and indicate when matrix elements become concentrated.

Size fraction (µm)	Na	K	Mg	Ca	Fe	Al	Si	P	S
125 <	0.47	**1.98**	0.94	1.98	2.78	3.40	2.35	0.43	0.21
125-63	**0.67**	**2.02**	0.94	2.02	3.35	4.00	2.38	0.48	0.57
45-63	**0.80**	**1.87**	1.10	1.87	5.06	**4.72**	2.64	0.67	0.68
32-45	0.60	1.73	**1.46**	**11.55**	**7.00**	**4.83**	**2.94**	**1.36**	**1.70**
< 32	0.57	1.50	**1.45**	**13.30**	**6.53**	4.33	2.35	**1.78**	**2.17**
Before sieving	0.63	1.76	1.29	8.53	5.79	4.50	2.64	1.16	1.41

5.4 Leaching of fly ash and pretreatment of the leachate

A significant amount of rubidium can be leached from fly ash by oxalic acid solution. Furthermore, the oxalic acid can be recovered as an oxalate after the leaching. The leached rubidium can be separated from other elements by liquid-liquid extraction, but first, it is necessary to adjust the pH of the solution to an appropriate level.

5.4.1 Oxalic acid leaching and recovery of oxalate

The oxalic acid leaching procedure is part of a patented method for processing fly ash, and the method has been optimized for rare earth elements (REEs) and platinum group metals (PGMs).[108] Rubidium is also leached from the fly ash during oxalic acid leaching with a 54% recovery and can be recovered from the leachate after recovery of REEs and PGMs. This was the basis for this study, and recovery of rubidium from the oxalic acid leachate was the aim.

After oxalic acid leaching of the fly ash, it is possible to recover oxalic acid from the leachate. Oxalic acid can be recovered as calcium oxalate and precipitated by adding an excess of calcium nitrate to the leachate. This leads to an increase in the calcium concentration in the solution after extraction of the precipitated calcium oxalate. It was discovered in the early experiments that an excess of calcium in the leachate interfered with the pH-adjustment, and most of it stayed with rubidium during liquid-liquid extraction all the way to the final product. By adding a suitable amount of calcium nitrate into the leachate, some of the oxalate can be recovered as calcium oxalate without increasing calcium concentration in the solution. With this method, 10% of the total oxalate in the solution can be recovered as calcium oxalates, but further development of the method would be needed to reach higher oxalate recoveries. This was outside the scope of this thesis.

In the following experiments, 3 g of $Ca(NO_3)_2 \cdot 4H_2O$ in 100 mL of oxalic acid leachate (OxLe) was used to precipitate calcium oxalate before pH-adjustment. After separating the solid oxalate from the leachate (Le), the precipitate was scrubbed a few times with 1–5 mL of ultra-pure water, and the scrubbing solution was added to the Le. The loss of rubidium was not more than few percent after precipitation and scrubbing of the oxalate.

5.4.2 pH-adjustment of the oxalic acid leachate

It is known from the literature that the extraction efficiency of substituent phenols is best at high pH values. Due to this, the pH of the aqueous Le needs to be adjusted to pH 12–13 before liquid-liquid extraction with CPh in chloroform. pH-adjustment was performed by adding sodium hydroxide solution into the Le solution with vigorous stirring until the desired pH was achieved. During pH-adjustment, strong precipitation took place and some of the rubidium co-precipitated out from the sample solution. The effect of the concentration of the NaOH solution on the co-precipitation of rubidium was investigated with six different NaOH solutions in a concentration range of 1–6 mol L^{-1}. Recoveries of rubidium and major matrix elements after pH adjustment and separation of the precipitate are shown in table 24. Recoveries are determined as percentages of the elements after and before of the precipitations in the samples.

TABLE 24 Recoveries (%) of rubidium and major matrix elements from Le after pH-adjustment and separation of the precipitate. 1–6 mol L^{-1} NaOH solution was used for pH-adjustment.

NaOH concentration of the pH-adjusting solution (mol L^{-1})	1	2	3	4	5	6
Increase in the sample volume (%)	64	30	21	15	12	10
Recoveries (%)						
Rb	74.6	69.9	65.6	64.8	64.1	62.2
Al	54.2	46.8	36.1	35.2	35.2	33.6
Ca	0.37	0.42	0.46	0.47	0.81	0.14
Fe	0.09	0.20	0.25	0.16	0.20	0.12
K	96.4	86.1	85.2	77.2	77.3	75.0
Li	82.2	75.7	73.2	69.0	61.7	57.9
Mg	0.01	0.05	0.15	0.12	0.15	0.09
B	105	97.2	92.1	89.9	84.5	88.3
S	94.9	89.2	86.3	86.2	84.2	83.2
Si	0.43	1.15	2.14	2.16	1.74	1.89
P	72.1	73.3	78.0	76.3	72.1	73.9
All matrix elements	40.8	37.5	35.0	33.8	33.2	32.6

There was a slight increase in the recoveries of rubidium after pH-adjustment and removal of a precipitate when a more diluted NaOH solution was used. Recoveries of rubidium varied from 61% to 76%, but the volume of

the sample solution increases dramatically when diluted NaOH solutions were used for pH-adjustment. In addition, the final Na content in the pHad samples was the smallest when concentrated NaOH solution was used. During experiments, it was discovered that the speed and volume in which the NaOH solution was added to the sample had more significant effect on the co-precipitation of rubidium than the concentration of the NaOH solution. In addition, additional scrubbing steps could improve the recovery of rubidium. As a result, six molar NaOH solution was selected for pH adjustment of the oxalic acid leachate of fly ash, and the adjustment was made very slowly with small volumes at the time.

During pH adjustment, most of the matrix elements originating from the fly ash precipitate out of the sample presumably as oxalates or hydroxides. Only the most soluble elements, like rubidium, and other alkali metals, sulfur, phosphorus, boron, and some of the aluminium, stayed in the solution at high pH.

5.4.3 Scrubbing the precipitate

After the pH-adjustment, the selective recovery of rubidium could be improved by scrubbing the precipitate formed during pH-adjustment. Preliminary experiments showed that the scrubbing solution should have a similar pH with the pH-adjusted sample, and a 0.05 mol L^{-1} NaOH (pH 12.7) solution was selected for this purpose. The scrubbing was performed in three steps to the precipitates formed in the previous experiment during pH-adjustment with six different concentrations of NaOH solutions. Recovery of rubidium after pH adjustment and scrubbing of the precipitate are shown in figure 14.

The recovery of rubidium is increased from 62% to 79% after three scrubbing steps when a 6 mol L^{-1} NaOH solution was used for pH-adjustment. When a 1 mol L^{-1} NaOH solution was used, recovery of rubidium was 75% before scrubbing and 84% after three scrubbing steps. After pH-adjustment and combining scrubbing solutions with sample solutions, the volumes of the samples increased to 190-249%. In addition, sodium concentration in the samples increased due to the NaOH content of the scrubbing solutions.

Because there is no significant increase in the rubidium recoveries after the second scrubbing step, the volume and the NaOH content of the sample can be diminished by performing only two scrubbing steps or using smaller volumes of the scrubbing solution. Also, a scrubbing solution of lower pH and NaOH concentrations can be used (0.01-0.04 mol L^{-1} NaOH solution, pH 12.3-12.6).

Figure 15 shows three pretreatments for fly ash prior to liquid-liquid extraction. After oxalic acid leaching, 56% of rubidium is recovered, and during recovery of oxalate, most of the rubidium stays in the solution. During the pH-adjustment, a great amount of rubidium can be lost due to the co-precipitation. A very slow addition of a NaOH solution, vigorous stirring of the solution, and the use of a diluted NaOH solution diminished the co-precipitation. In addition, some of the co-precipitated rubidium can be recovered by scrubbing the precipitate. Depending on the conditions of the pH-adjustment and the number of the

scrubbing stages, 62–84% of rubidium can be recovered from the OxLe after the pH-adjustment.

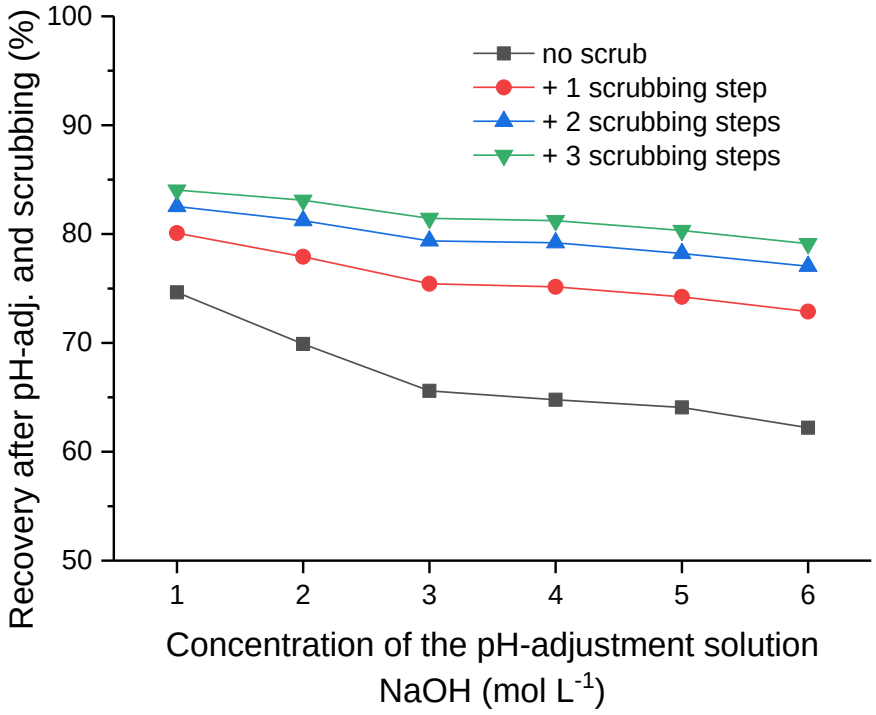

FIGURE 14 Recovery of rubidium in the aqueous phase after pH-adjustment and scrubbing of the precipitate by a 0.05 mol L^{-1} NaOH (pH 12.7) solution. pH-adjustment was performed with six different concentrations of NaOH solutions.

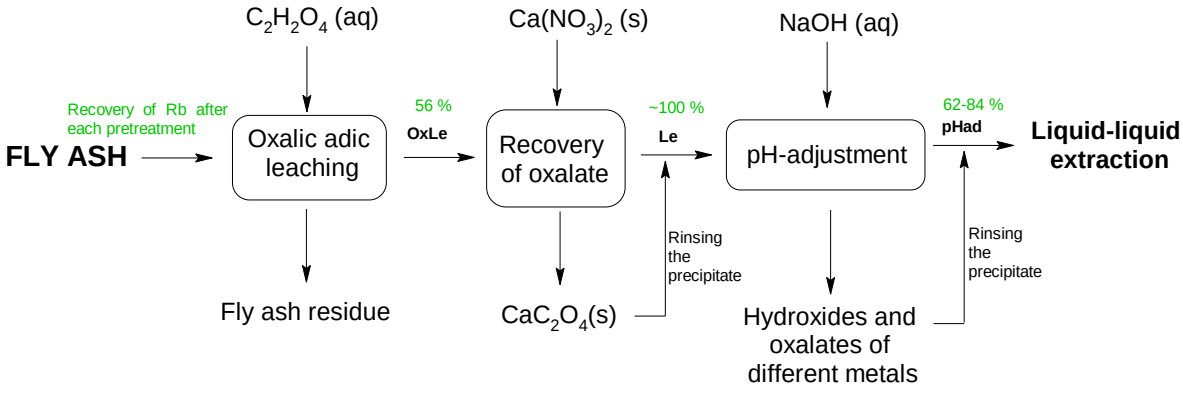

FIGURE 15 Schematic presentation of three pretreatments for fly ash prior to liquid-liquid extraction. Recoveries of rubidium after each treatment are displayed in green. The total recovery or Rb from fly ash after three pretreatments is 41–47%.

5.5 Liquid-liquid extraction

Substituted phenols are known to have high selectivity towards heavy alkali metals.[30 p. 96] Although a lot of promising research has been done about the extraction of rubidium and cesium by BAMBP compounds[3-7,31], high price and poor availability makes these extracting agents less attractive. Chlorophene (CPh) has properties similar to BAMBP compounds and is less expensive, which makes it a good alternative for the extraction of rubidium. Due to this, CPh was selected as the extracting agent.

In initial experiments, it was discovered that CPh was moderately soluble in kerosene and hexane, easily soluble in toluene and xylene, and highly soluble in chloroform. Chloroform was selected as the solvent for chlorophene.

5.5.1 Loading the organic phase

Effect of the initial pH of the sample on the extraction efficiency
The effect of pH on extraction of rubidium from the oxalic acid leachate was studied by performing liquid-liquid extraction experiments in five different pH values of the aqueous phase in a range of pH 12.03-12.80. Concentrations of Rb, K, Na, and Cs in the pHad samples are displayed in table 25. In the liquid-liquid extraction, the A:O phase ratio was 1:1, the concentration of the CPh in $CHCl_3$ was 1 mol L^{-1}, and the contact time was 5 min. The percentage extraction of rubidium, potassium, sodium, and cesium into the organic phase are shown in figure 16 on the left, and separation factors are displayed on right.

TABLE 25 Concentrations (mg L^{-1}) of Rb, K, Na, and Cs in the pHad samples after pH-adjustment to five different pH values.

initial pH	Rb	K	Na	Cs
pH 12.0	2.05	446	17,700	0.035
pH 12.4	2.06	459	18,000	0.035
pH 12.6	2.05	455	18,300	0.036
pH 12.7	2.02	440	18,400	0.035
pH 12.8	2.05	440	19,400	0.036

It can be seen from the results that the extraction of rubidium increases when the initial pH of the sample increases. The same trend can be observed with cesium, but recoveries of potassium and sodium are minor compared to their initial concentrations. Despite the pH of the sample solution, the separation factors of Rb/Cs remained between 0.2 and 0.8. This indicates that the separation of rubidium and cesium is minor after loading the organic phase. Potassium and sodium clearly separate from rubidium and cesium, but the calculated separation factors of sodium were negative and are not shown here. When determining small concentration differences between two samples by measuring concentrations that are rather high, the result can get lost in the variation of

the measured values. This can lead to negative percentage extraction and separation factor values that are not real.

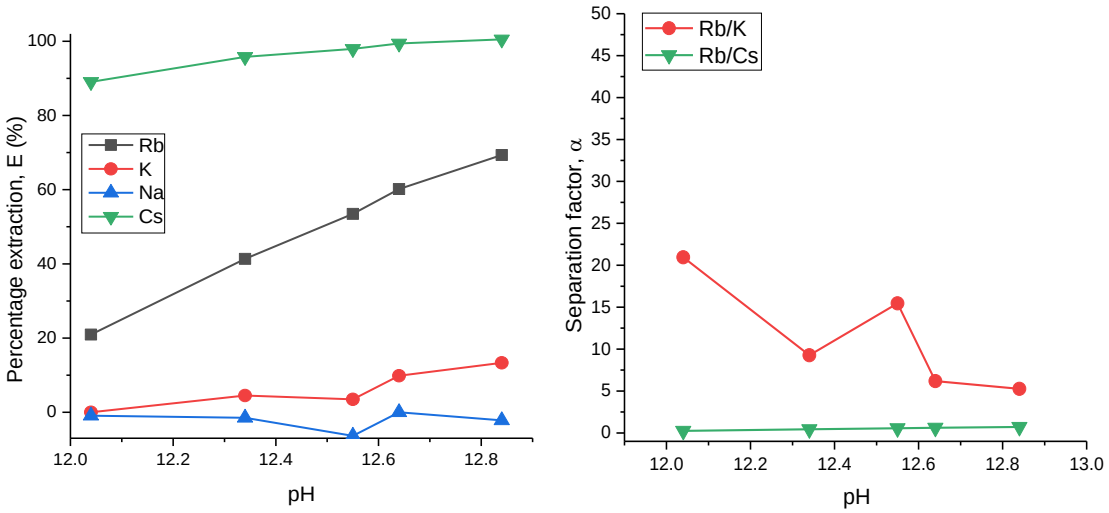

FIGURE 16 Effect of the initial pH of the aqueous phase on the extraction efficiency (left) and on the separation factor, α (right).

At high alkalinity above pH 12.7, the organic phase began to dissolve in to the aqueous phase. In figure 17, this can be seen as change in the color of the aqueous phase (on top) when the pH is too high. For this reason, the pH of the oxalic acid leachate was adjusted to 12.6-12.7 before liquid-liquid extraction.

FIGURE 17 In the separating funnels on the top are aqueous phases and on the bottom are organic phases (1 mol L^{-1} CPh in $CHCl_3$). Initial pH values of the aqueous phases from the left are: (1) 12.0, (2) 12.3, (3) 12.5, (4) 12.6, and (5) 12.8.

Effect of the concentration of the extractant in the organic phase on the extraction efficiency

Five different concentrations of CPh in the organic phase were applied in the liquid-liquid extraction experiments. The A:O phase ratio was 1:1, the pH of the aqueous phase was 12.7, the contact time was 5 min, and the concentration of the chlorophene in chloroform was between 0.5 and 2.5 mol L^{-1}. Percentage extractions of rubidium, potassium, sodium, and cesium into the organic phase are shown in figure 18, left. The extraction of rubidium was most efficient with a chlorophene concentration of 2.5 mol L^{-1}. In addition, the separation of rubidium from sodium and potassium increased when the concentration of CPh in the organic phase increased (figure 18, right). However, when using a high concentration of CPh in the organic phase, the CPh easily precipitated on the wall of the separating funnel. Due to the usability of the organic phase, 1 mol $L^{-1}$of CPh was selected as its concentration.

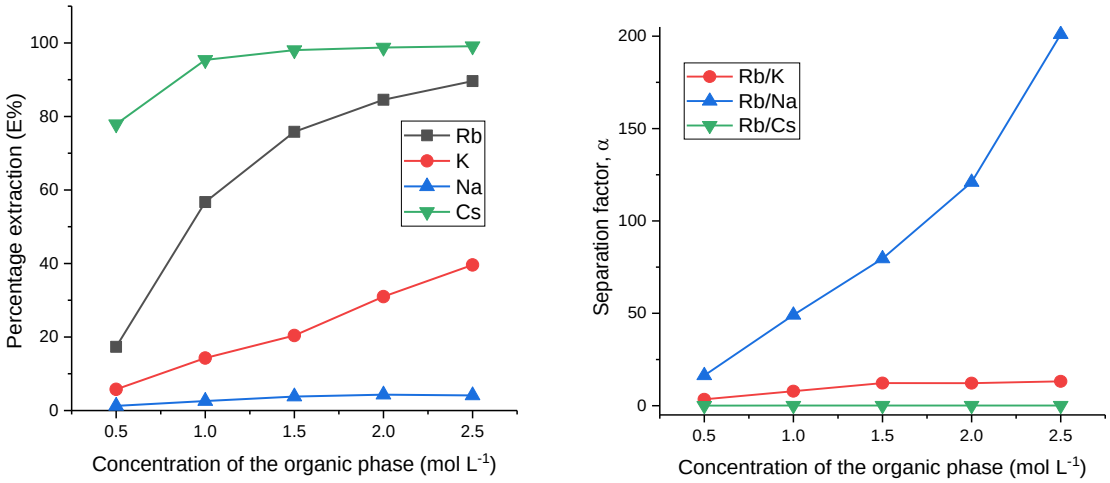

FIGURE 18 Left: Effect of the chlorophene concentration of the organic phase on the extraction efficiency of Rb, K, Na, and Cs. Right: Separation factors of Rb/K, Rb/Na, and Rb/Cs.

Effect of the A:O phase ratio on the extraction efficiency

The effect of the aqueous to organic phase ratio on the extraction of rubidium into the organic phase was investigated by performing six experiments with A:O ratios from 10:1 to 1:5. The used aqueous phase was pHad at pH 12.7 and the organic phase was 1 mol L^{-1} chlorophene in chloroform. Figure 19 shows how the extraction efficiency of rubidium improves when the volume of the organic phase increases compared to the volume of the aqueous phase. However, even when using the A:O ratio of 1:5, the extraction efficiency is under 70%. This indicates that multiple steps of extractions are needed for good recovery of rubidium.

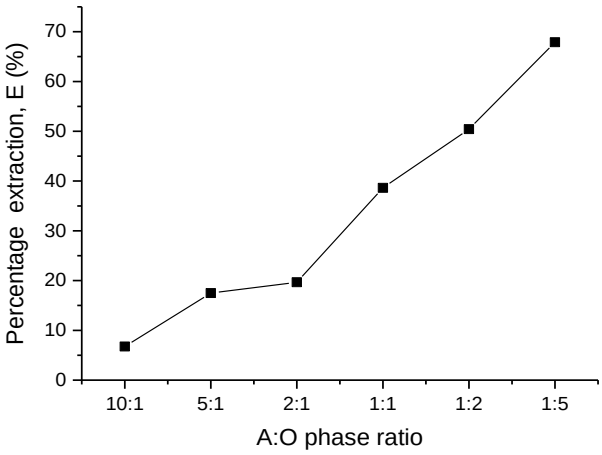

FIGURE 19 Effect of the A:O phase ratio on the extraction efficiency in the loading of the organic phase.

Effect of the number of extraction steps on the extraction efficiency

The extraction efficiency of rubidium was investigated by performing six experiments with a different number of extraction steps. The used aqueous phase was pHad at pH 12.6. The A:O phase ratio was 1:1, and the organic phase was 1 mol L^{-1} chlorophene in chloroform. Figure 20, left, shows how the extraction efficiency of rubidium improves when the number of extractions increases. After the first extraction, 47% of rubidium was loaded into the organic phase, and the pH of the aqueous phase dropped to 12.1. After four extractions, 94 % of rubidium was loaded into the organic phase and the extraction efficiency did not improve significantly with five or six extractions. The pH of the aqueous phases was stabile after the first extraction. The extraction efficiency of cesium was high from the first load (92%), but the extraction of other alkali metals was significantly lower even after six loading steps (figure 20, left). The extraction efficiency of the other major matrix elements (Al, Ca, Fe, Mg, B, S, Si, and P) was lower than 1.2%.

Separation factors for ion pairs Rb/K, Rb/Cs, and Rb/Na are shown in figure 20, right. The separation of Rb from Na and K clearly increases, while Rb and Cs are hardly separated. The amount of loaded Na is estimated from the concentration of the stripping solution rather than calculated from the concentrations of the original sample and the raffinate.

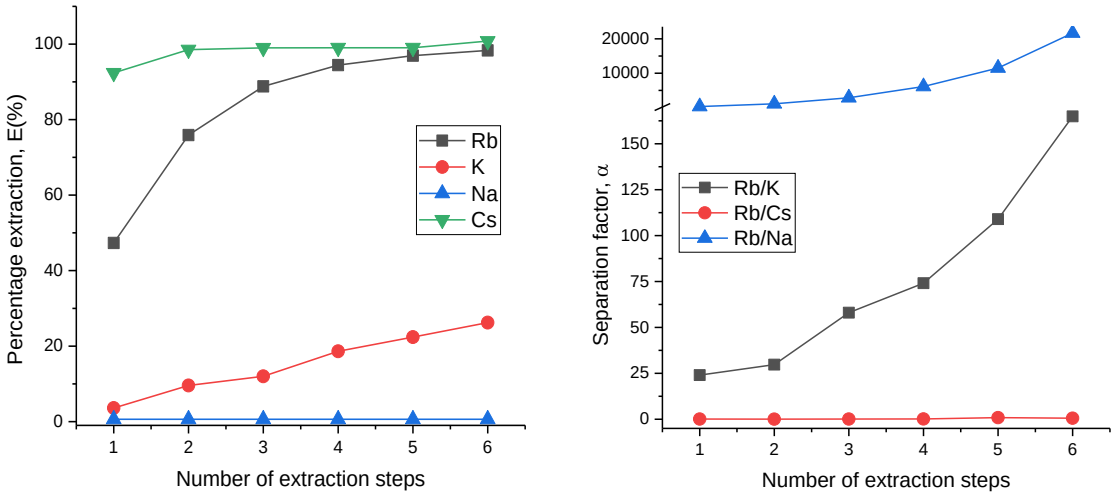

FIGURE 20 Left: Effect of extraction steps on the extraction efficiency of Rb, K, Na, and Cs. Right: Separation factors of Rb/K, Rb/Na, and Rb/Cs.

5.5.2 Scrubbing of the loaded organic phase

The efficiency of scrubbing the loaded organic phase before stripping was investigated with five different scrubbing solutions. The goal was to diminish the matrix element content in the final product solutions without great loss in rubidium content. Scrubbing solutions were 0.05, 0.04, 0.03, and 0.01 mol L^{-1} of NaOH solutions and 0.10 mol L^{-1} of the NH_3(aq) solution. The A:O phase ratio was 1:4, and the contact time was 3 min. After scrubbing, rubidium was stripped from the organic phase by 1 mol L^{-1} HCl with an A:O phase ratio of 1:4 and contact time of 5 min. The concentrations and pH values of the scrubbing solutions are displayed in table 26, and the schematic presentation of the extraction procedure is presented in figure 21.

TABLE 26 Concentrations and pH values of the scrubbing solutions.

	Solution	Conc. (mol L^{-1})	pH
1	NaOH	0.05	12.7
2	NaOH	0.04	12.6
3	NaOH	0.03	12.5
4	NaOH	0.01	12.3
5	NH_3 (aq)	0.10	11.0

Figure 15 shows three pretreatments for fly ash prior to liquid-liquid extraction. After oxalic acid leaching, 56% of rubidium is recovered, and during recovery of oxalate, most of the rubidium stays in the solution. During the pH-adjustment, a great amount of rubidium can be lost due to the co-precipitation. A very slow addition of a NaOH solution, vigorous stirring of the solution, and the use of a diluted NaOH solution diminished the co-precipitation. In addition, some of the co-precipitated rubidium can be recovered by scrubbing the precipitate. Depending on the conditions of the pH-adjustment and the number of the

scrubbing stages, 62–84% of rubidium can be recovered from the OxLe after the pH-adjustment.

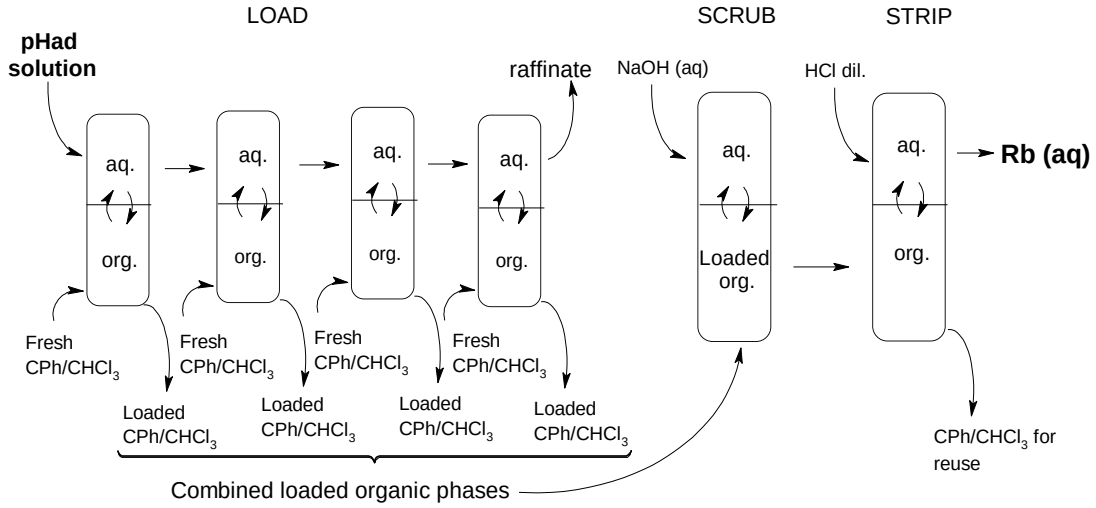

FIGURE 21 Schematic presentation of extraction of rubidium.

Figure 22 (left) shows the extraction efficiency of Rb, K, Na, and Cs from the organic phase with five different scrubbing solutions. Sodium contents of the scrubbing solutions before scrubbing have been extracted from the results. 77–92% of sodium and potassium can be extracted with the scrubbing stage, but also 20–62% of Rb can be lost. When a more diluted NaOH solution was used for scrubbing, more alkali metals transferred into the scrubbing solutions. An ammonia solution extracted most rubidium and some cesium due to the low pH. When scrubbing with NaOH solutions, cesium stayed firmly in the organic phase.

The separation of rubidium from sodium and potassium is most efficient in a 0.05 mol L^{-1} NaOH solution, while the separation of Rb and Cs is almost constant with different NaOH scrubbing solutions. With an ammonia scrubbing solution, separation of Rb from other alkali ions is less efficient. Separation factors of Rb, K, and Cs are displayed in figure 22 on the right.

Table 27 shows the amounts of major matrix elements (Al, Ca, Fe, K, Mg, Mn, Na, S, P) and rubidium that are transferred from the loaded organic phase into the stripping solutions after different scrubbing stages. The scrubbing of potassium and sodium is quite efficient with all scrubbing solutions, but most of the Ca, Fe, S, and P transfers into the stripping solution. Also, 20–50% of Al, Mg, and Mn get into the stripping solutions. The transfer of Al, Fe, and Na is least efficient with a 0.05 mol L^{-1} NaOH solution and vice versa with K and Mg. The transfer of Mn is the same with all scrubbing solutions, and the transfer of Mg varies irregularly from 13 to 40%. The lowest percentage transfer of all the matrix elements occured after scrubbing the loaded organic phase with a 0.03 mol L^{-1} NaOH solution.

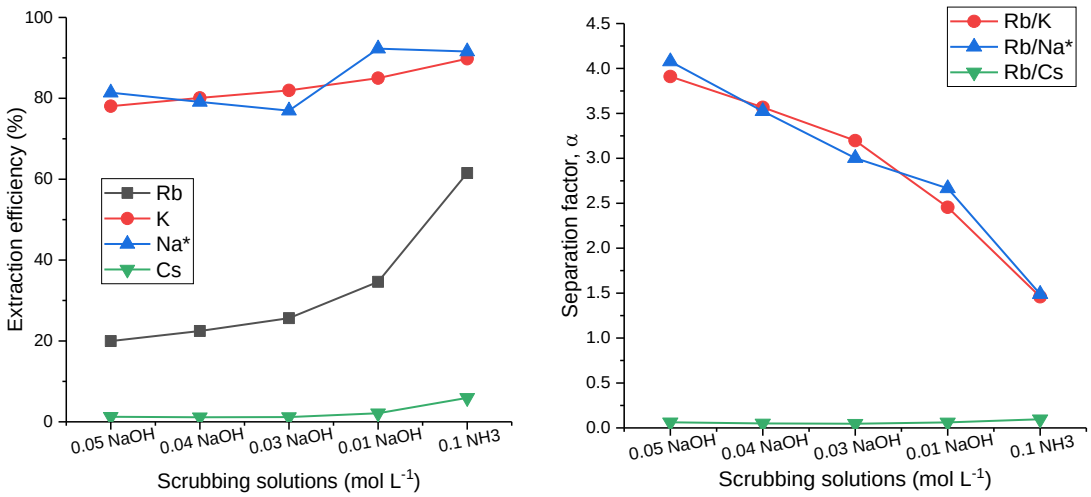

FIGURE 22 Extraction efficiencies, E(%) of the scrubbing solutions (left) and separation factors α of different ions (right) after scrubbing. (*) notifies that Na concentrations of the unused scrubbing solutions are extracted from the results.

TABLE 27 Percentage (%) transfer of Rb and the matrix elements from the loaded organic phase into the stripping solution after scrubbing with solutions 1-5.

Scrubbing solution	Rb	Al	Ca	Fe	K	Mg	Mn	Na	S	P	Total
0.05 mol L^{-1} NaOH	80	38	100	88	23	40	19	3.2	100	100	5.3
0.04 mol L^{-1} NaOH	78	47	100	93	11	13	19	3.7	100	n.d.	5.2
0.03 mol L^{-1} NaOH	74	41	n.d.	90	18	20	19	3.8	100	n.d.	6.2
0.01 mol L^{-1} NaOH	65	51	100	92	16	26	19	4.4	100	100	7.6
0.1 mol L^{-1} NH_3 (aq)	39	26	100	90	18	37	20	8.4	100	100	17

n.d. = not detected; < LOD

Concentrations of major matrix elements in the stripping solutions, after scrubbing the organic phase with different solutions, are shown in table 28. After scrubbing and stripping, there are still quite high concentrations of sodium, potassium, and iron in the final extractant with all the scrubbing solutions. The highest rubidium, sodium, and potassium concentrations in the stripping solutions resulted when a 0.05 mol L^{-1} NaOH solution was used for scrubbing. Concentrations of other matrix elements are minor regardless of the stripping solution.

The highest recovery of rubidium after scrubbing and stripping is achieved with a 0.05 mol L^{-1} NaOH scrubbing solution, but 20% of rubidium is lost with a scrubbing solution, and the concentration of matrix elements is still

almost 50 times higher than rubidium's concentration. The ratio of rubidium to the matrix elements in the stripping solution was the highest with 0.01 mol L^{-1} NaOH scrubbing solution, but 35% of Rb is scrubbed away. These results indicate that an efficient scrubbing stage is difficult to execute.

TABLE 28 Matrix element concentrations (mg L^{-1}) in the stripping solution after scrubbing stages with solutions 1-5.

Scrubbing solution	Rb	Al	Ca	Fe	K	Mg	Mn	Na	S	P	Total
0.05 mol L^{-1} NaOH	1.69	0.37	0.85	5.35	29.0	0.13	0.05	39.4	0.45	4.67	80.4
0.04 mol L^{-1} NaOH	1.63	0.51	0.14	7.45	24.9	0.06	0.05	36.7	0.36	n.d.	70.1
0.03 mol L^{-1} NaOH	1.57	0.36	n.d.	6.61	24.2	0.05	0.05	27.9	0.29	n.d.	59.4
0.01 mol L^{-1} NaOH	1.38	0.40	0.17	6.41	19.9	0.07	0.05	20.8	0.41	0.20	48.4
0.1 mol L^{-1} NH_3 (aq)	0.83	0.29	0.74	7.51	24.2	0.12	0.05	9.8	0.44	1.84	45.0

n.d. = not detected; < LOD

5.5.3 Stripping the loaded organic phase

Effect of the A:O phase ratio on the stripping efficiency

The A:O phase ratio in stripping of the loaded organic phase was studied by performing four experiments with different A:O phase ratios from 1:1 to 1:20. Rubidium was stripped from the loaded organic phase by 1 mol L^{-1} HCl and contact time of 5 min.

Percentage recoveries of rubidium were near 100% with all A:O phase ratios indicating that during stripping, rubidium can be concentrated into a 20 times smaller volume than the loaded phase. The effect of the A:O phase ratio on the extraction efficiency in the stripping of the loaded organic phase is presented in figure 23.

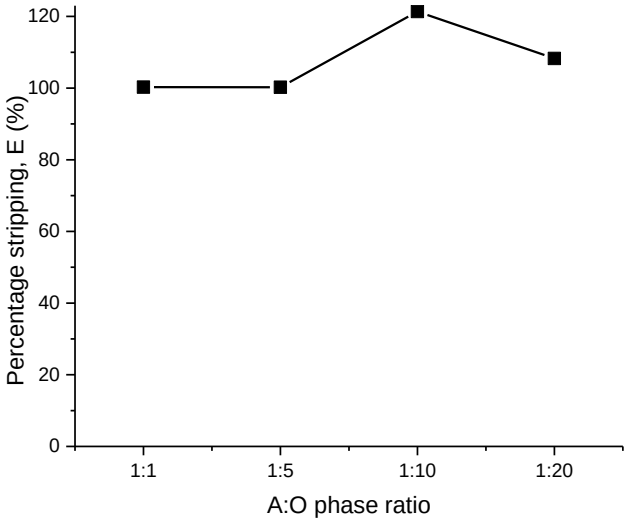

FIGURE 23 Effect of the A:O phase ratio on the extraction efficiency in stripping of the loaded organic phase.

Concentration of the stripping agent

The efficiency of stripping of the loaded organic phase was investigated with four different stripping solutions: 1.0, 0.1, and 0.01 mol L^{-1} of HCl solution and ultra-pure water. The A:O phase ratio was 1:4 and the contact time was 5 min. The effect of the concentration of the aqueous stripping solution on the extraction efficiency of rubidium, potassium, sodium, and cesium is shown in figure 24.

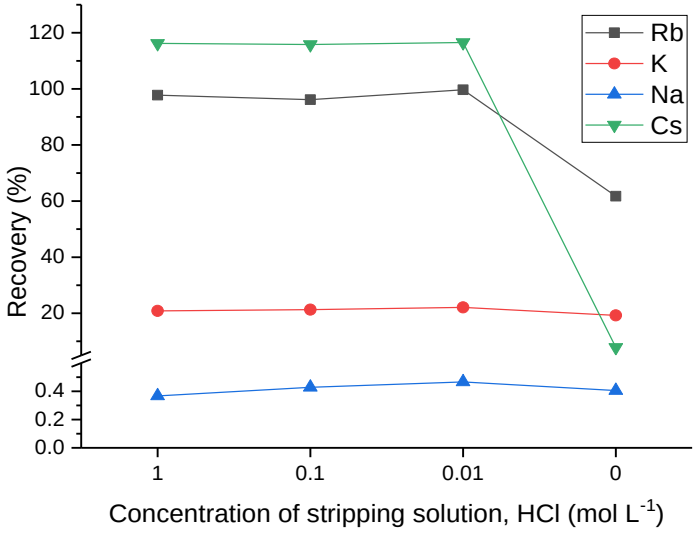

FIGURE 24 Effect of the HCl concentration of the aqueous stripping solution on the extraction efficiency of rubidium, potassium, sodium, and cesium.

Recovery of rubidium from the pH-adjusted leachate was over 96% with all acidic stripping solutions, but the highest recovery of 99.7% was gained when stripping with 0.01 mol L^{-1} HCl. Stripping rubidium with water produced only 62% recovery. Recovery of cesium was also high with all HCl stripping

solutions, but recovery decreased dramatically when water was used for stripping. Recoveries of potassium and sodium were very low, but still some matrix elements transferred into the stripping solution.

Table 29 shows the effect of the concentration of the aqueous stripping solution on the concentration of Al, Ca, Fe, K, Na, S, and Rb. Less than 1% of the initial amount of the major matrix elements transfers all the way to the final stripping solutions regardless of the stripping solution. All the alkali metals behave similarly, and most of the loaded elements are stripped even after one stripping stage. The highest recoveries are with a 0.01 mol L^{-1} HCl solution, and the lowest recoveries are with water. Also, with other elements, the recoveries are lowest with water, but recoveries grow when a more concentrated HCl solution is used. The highest recovery of rubidium and lowest recoveries of matrix elements are achieved by stripping with a 0.01 mol L^{-1} HCl solution.

TABLE 29 Concentration (mg L^{-1}) of the major matrix elements and Rb in the pHad solution before liquid-liquid extractions and in stripping solutions after loading the organic phase and stripping with different solutions.

	Al	Ca	Fe	K	Na	P	S	Rb
Before liquid-liquid extraction	620	2.31	14.2	479	18143	342	608	2.02
Stripping with 1 mol L^{-1} HCl	0.44	n.d.	6.03	100	67	0.26	0.43	1.97
Stripping with 0.1 mol L^{-1} HCl	0.51	0.23	5.75	102	78	0.28	0.43	1.94
Stripping with 0.01 mol L^{-1} HCl	0.46	n.d.	2.47	106	85	0.18	0.41	2.01
Stripping with water	0.24	0.25	n.d.	92	74	0.22	0.42	1.25

n.d. = not detected

5.5.4 Number of extraction cycles

The matrix element content in the final extractant could be decreased by repeating the liquid-liquid extraction cycle. This was examined by performing three liquid-liquid extraction cycles for the same sample. First, rubidium was extracted from the pHad sample by three extraction steps with an organic phase of 1 mol L^{-1} CPh in chloroform. The A:O phase ratio was 1:1, and the contact time was 5 min. After combining the organic phases, rubidium was extracted with one extraction step of an A:O ratio of 1:3, stripping solution of 0.01 mol L^{-1} HCl, and contact time of 5 min. After stripping, the pH of the extractant was again adjusted to 12.6 with 6 and 1 mol L^{-1} NaOH solutions, and the liquid-liquid extraction was repeated. The pH-adjustment and liquid-liquid extraction were performed altogether three times, and samples for elemental analysis were collected after every liquid-liquid extraction cycle. The schematic presentation of the extraction cycles is shown in figure 25.

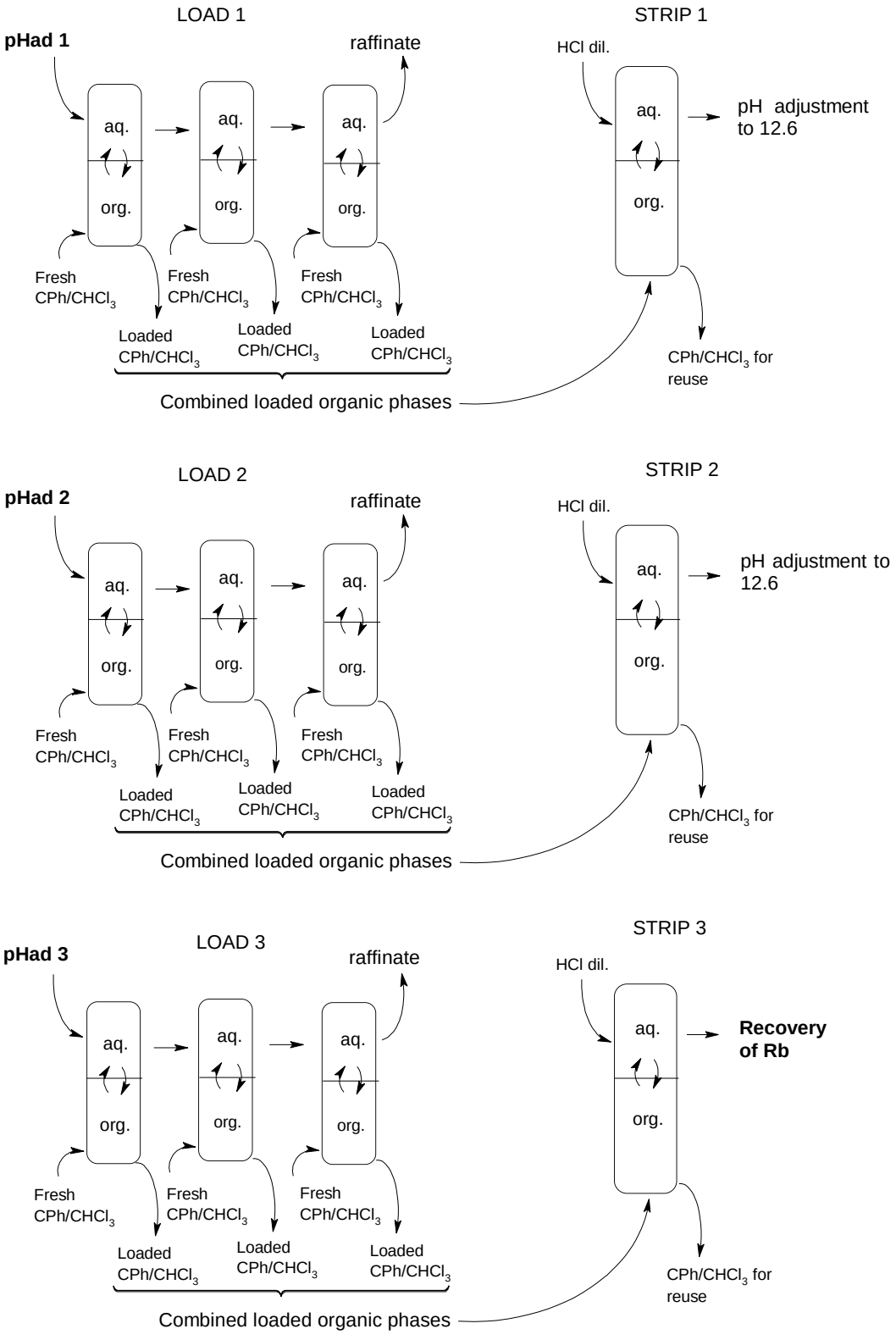

FIGURE 25 Schematic presentation of three extraction cycles.

Concentrations and recoveries of rubidium in different phases after three extraction cycles are shown in table 30. When loading the organic phase, the

recoveries of rubidium reduces 5 to 6% after every cycle. Overall, the recoveries are low due to the low number of extraction steps. Here, the extraction step with the organic phase was performed only three times instead of the optimized four steps. Nevertheless, the recoveries of rubidium from the organic phase during stripping were over 91% after every extraction cycle.

TABLE 30 Concentrations of rubidium in different phases after three liquid-liquid extraction cycles and recoveries (%) after stripping the loaded organic phase. Concentrations of the loaded phases are normalized to aqueous phases by multiplying the concentrations of Rb in the organic phases by three.

	Sample	Concentration	Recovery from the aqueous phase	Recovery from the organic phase
		mg L^{-1}	%	%
	pHad	2.24		
Cycle 1	*Load 1*	*1.89*	84.4	
	Strip 1	1.84		97.4
Cycle 2	*Load 2*	*1.46*	79.3	
	Strip 2	1.33		91.4
Cycle 3	*Load 3*	*0.98*	73.7	
	Strip 3	0.93		94.8

Concentrations of major matrix elements in the pHad and stripping solutions after three extraction cycles are shown in table 31. Most of the matrix elements are extracted from rubidium during the first extraction cycle when the total matrix content of the sample is diminished 100 times. Only Na (116 mg L^{-1}) and K (82.4 mg L^{-1}) occur in medium-high concentrations in the first stripping solution. The iron concentration increases after the first stripping, indicating contamination in the sample. After the second extraction cycle, the matrix content still decreases 10 times. Sodium concentration falls to 5.7 mg L^{-1} and potassium to 12.8 mg L^{-1}. The third extraction cycle still reduces the total matrix element concentration to half in the stripping solution, but sodium concentration starts to increase.

By performing several extraction cycles, the matrix content in the sample can be diminished considerably compared to the concentration of rubidium. By increasing extraction steps in the loading phase to 4 or 5, nearly 100% of rubidium can be extracted, and by decreasing the volume of the stripping solutions, rubidium can be concentrated four times in every extraction cycle.

TABLE 31 Concentrations (mg L^{-1}) of major matrix elements in pHad solution before liquid-liquid extraction and stripping solutions after one to three liquid-liquid extraction cycles.

	pHad	Strip Cycle1	Strip Cycle2	Strip Cycle3
Al	762	2.46	n.d.	n.d.
Ca	2.76	0.58	0.10	0.11
Fe	1.12	8.55	0.61	0.32
K	512	82.4	12.8	3.45
Mg	0.27	0.15	n.d.	n.d.
Na	19,800	116	5.69	7.43
S	690	1.81	0.71	0.76
P	359	0.97	0.29	0.32
Total	22,100	213	20	12

n.d. = not detected, < LOD

5.5.5 Re-circulation of the organic phase

After stripping, the organic phase of 1 mol L^{-1} of CPh in $CHCl_3$ can be reused for recovery of rubidium. After one liquid-liquid extraction with a fresh organic phase of an A:O phase ratio of 1:1, the recovery of Rb was 44.7%. The recovery decreased 8.2% units in the first reuse and 2.6% units more in the second reuse. After three extraction cycles, the extraction efficiency diminished for a total of 11.8% units compared to one extraction cycle with the fresh organic phase. By additional optimization or addition of the fresh organic phase into the used one, the organic phase can be reused at least three times.

5.6 3D-printed potassium copper hexacyanoferrate functional filters

3D-printed nylon-based potassium copper(II) hexacyanoferrate (KCuFC) functional filters were employed for selective recovery of rubidium from synthetic samples mimicking acid leached fly ash after pH-adjustment (SynpHad). KCuFC sorbent was stabile only in near neutral-conditions, so the pH of the sample was adjusted to 10.

The loading capacity of the functional filter (m = 0.6 g, V = 1.1 mL) was tested by passing synthetic sample containing 50 mg of Rb in 500 mL of aqueous solution through the filter. The pH of this sample was not adjusted and was determined as 5. After loading, 6.6% of rubidium was transferred into the filter,

and after elution with water, 6.4% of rubidium still stayed in the filter. The loading capacity was determined as 5.06 mg g^{-1} by equation 4.

Rubidium was eluted from the fully loaded filter by 20 elution steps with 10 mL of 1 mol L^{-1} of NH_4NO_3 solution. The goal was to replace Rb^+ ion by a similar size NH_4^+ ion in the filter. Recoveries of rubidium after every elution step are displayed in figure 26. After eluting the loaded functional filter, 80% of rubidium was recovered after 8 elution steps of 10 mL, and after 20 steps, the recovery was 88%. This indicates that more elution steps are needed for near 100% recovery of rubidium from the fully loaded functional filter.

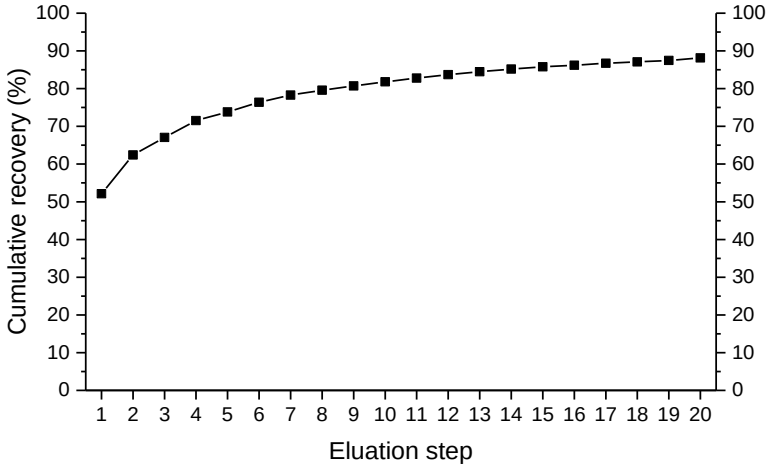

FIGURE 26 Total (cumulative) recovery (%) of rubidium from the loaded functional filter after 1-20 elution steps of 10 mL of 1 mol L^{-1} of NH_4 NO_3 solution.

The elution of rubidium was also tested with different concentration KCl solutions, but this led to a final product with high concentrations of K and a low concentration of Rb. Eluting the loaded filter with ammonium ions diminished the potassium content on the final product, and therefore, NH_4NO_3 and NH_4Cl solutions were used for elution of rubidium.

Preliminary experiments with SynpHad samples showed that in the presence of other matrix elements, the rubidium loading capacity of the functional filter was much lower. Good recoveries from SynpHad were gained only when diluting the sample by a factor of 10 with water before recovery. Rubidium and matrix element (Al, Ca, Fe, Mg, and Na) contents in the SynpHad sample after dilution, in the raffinate and filter after loading, in the washing solution, and in the eluent after 10 extraction steps, are presented in table 32. The pH of the SynpHad sample after dilution was 10.

After 10 loading runs, 94 % of the rubidium transferred from the synthetic sample into the functional filter, while 98% of the matrix elements stayed in the raffinate. Copper and potassium leached from the functional filters during loading and elution, and their distribution in different phases during extraction are shown in table 33. A very high amount of potassium (1390 µg) was released from the filter during loading. This can be a consequence of the slightly alkaline

nature of the original sample. After 100 mL elution using a 1 mol L^{-1} of NH_4Cl solution, 68% of the loaded rubidium was recovered.

TABLE 32 Rb and matrix element contents (µg) in the synthetic sample (SynpHad) after dilution, in the raffinate and filter after loading, in the washing solution and eluent after extraction. Recoveries (%) of Rb and matrix elements are also shown.

	SynpHad	Raffinate	Sorbed to filter	Extracted by wash	Extracted by elution
Rb	6.21	0.36	5.85	0.01	4.00
Rb (%)	100	5.8	94	0.16	64
Al	42.2	25.0	17.2	n.d.	0.41
Ca	2830	2680	154	4.07	183
Fe	n.d.	4.17	n.d.	1.43	0.06
Mg	10.0	6.70	3.31	n.d.	0.58
Na	8,860	8,800	64.2	364	76.1
Matrix	11,700	11,500	239	370	260
Matrix (%)	100	98	2.0	3.2	2.2

n.d. = not detected

TABLE 33 Cu and K contents (µg) in the synthetic sample (SynpHad) after dilution, in the raffinate and filter after loading, in the scrubbing solution and eluent after extraction.

	SynpHad	Raffinate	Desorbed from filter	Extracted by wash	Extracted by elution
Cu	1.95	197	195	28.6	553
K	213	1600	1390	353	1130

n.d. = not detected

For lowering the potassium content in the final product, ion exchange from potassium to ammonium ion could be done to the sorbent before rubidium loading. In addition, it is possible to diminish the matrix content in the final product by adding washing steps with diluted NH_4Cl solutions. After more development to the elution process, the 3D-printed potassium copper hexasyanoferrate functional filters can be a useful tool for extracting rubidium from leached fly ash.

6 CONCLUSIONS

This study presents an optimized method for recovery of rubidium as part of a utilization process, where most of the valuable elements are recovered from industrial fly ash. The properties of fly ash originating from different fuel content and their rubidium content were also investigated, and different methods to determinate low concentrations of rubidium from difficult matrices were studied.

Three spectroscopic methods, ICP-OES, GFAAS, and ICP-MS, were employed for determining low concentrations of rubidium from samples of high matrix element content, and their features were compared. High concentrations of other easily ionized elements (EIE) interfered with accurate measurements of rubidium by ICP-OES, but the multiple linear regression (MLR) method can be used for the correction of spectral interferences in Rb measurements induced by high concentrations of Na and Ca. The GFAAS was a very sensitive method in rubidium determination, but the measurements were very slow. ICP-MS was fast and simple to use due to the auto-dilution system, and it provided accurate and reproducible results. In GFAAS and ICP-MS, interferences induced by matrix elements in the samples were negligible due to the high dilution factor used for the samples, while due to the wide linear range and tolerance of high concentrations of matrix elements, in ICP-OES techniques, high dilution factors were not needed. Nevertheless, some dilutions were still required due to the very high matrix content in samples derived from fly ash. This can lead to rubidium concentration under the detection limits of ICP-OES. Therefore, GFAAS and ICP-MS are most suitable methods for quantitative analysis of rubidium or small groups of elements. For multi-elemental analysis of many elements simultaneously, ICP-OES is a fast and reliable measuring method.

The properties of five different fly ash samples of different fuel contents of peat and wood residue were evaluated by their elemental content and particle size. Sieved and un-sieved ash samples were digested by the ultrasonic (US) digestion method and elemental analysis was performed by ICP-OES and ICP-MS. The concentration of rubidium varied from 27 mg kg^{-1} to 94 mg kg^{-1}, depending on the fuel compositions and origin of the fly ashes. The highest rubidium concentrations were in fly ashes of 50% peat and 50% wood residue as fuel, and the lowest Rb concentration originated from fly ash from combustion of 100% of peat.

In ashes originating from 50% peat and 50% wood residue, the Rb concentration was over 26% higher than in the Earth´s crust. This indicates that the recovery of rubidium from fly ash can be profitable, especially combined with the recovery of other valuable elements. Sieving of the fly ash into fractions by different particle sizes before recovery of rubidium did not offer any real benefit, because the concentrations were similar in each size fraction.

The method for the recovery of rubidium was developed as part of the wide utilization process of power plant fly ash. The basis for the recovery studies was an earlier-developed oxalic acid leaching procedure for fly ash. This procedure leached 56% of the total Rb from the studied fly ash. Rubidium was recovered from the oxalic acid leachate by liquid-liquid extraction. Prior to liquid-liquid extraction, the oxalic acid was recovered from the leachate as oxalate, and the pH of the solution was adjusted to a suitable level for liquid-liquid extraction. pH-adjustment was studied to reduce the co-precipitation of rubidium. The concentration of the NaOH solution used for pH-adjustment had a minor effect on the rubidium content in the solution, but rinsing of the precipitate was needed to ensure high recovery.

Liquid-liquid extraction of rubidium from a pHad solution was studied by optimizing the A:O phase ratios of aqueous and organic phases and the number of extraction steps in the loading and stripping stages. The effect of the CPh concentration in $CHCl_3$ on the extraction efficiency and the benefit of additional scrubbing of the loaded organic phase were also studied. The influence of a stripping solution of different HCl concentrations on the recovery of Rb was investigated, and the advantage of the repetition of the complete extraction cycle was examined.

Using the optimized conditions, the organic phase of 1 mol L^{-1} CPh in $CHCl_3$, with an A:O phase ratio of 1 and four extraction steps, 94% recovery of rubidium was achieved. Scrubbing of the loaded organic phase was tested to diminish the matrix content in the final product, but was not found beneficial. During the stripping stage, rubidium was completely recovered by 1 mol L^{-1} HCl and can be concentrated to at least 4 times the smaller volume than the original sample. In addition, a stripping solution of 0.01-1 mol L^{-1} HCl can be applied with only a small effect on the recovery of rubidium. To diminish the matrix element content of the sample, the extraction cycle can be repeated 2-3 times. By performing the stripping into a smaller volume, after three extraction cycles, rubidium can be concentrated up to 12 times from the concentration of the original sample. This results in a product of 30 mg L^{-1} Rb with very low matrix concentration. To ensure high rubidium recovery, the number of liquid-liquid extraction steps in the loading phase can be elevated from four to six and the number of extraction cycles can be increased. Recycling of the used organic phase is possible, and by mixing a used organic phase with a fresh one, good recoveries are ensured. The schematic presentation of the total process of the three pretreatments of fly ash and one extraction cycle with four loading steps is presented in figure 27. The overall recovery of rubidium from the oxalic acid leachate after one liquid-liquid extraction cycle is 58-79% depending on the conditions of the pH-adjustment and the number of the rinsing stages of the precipitate.

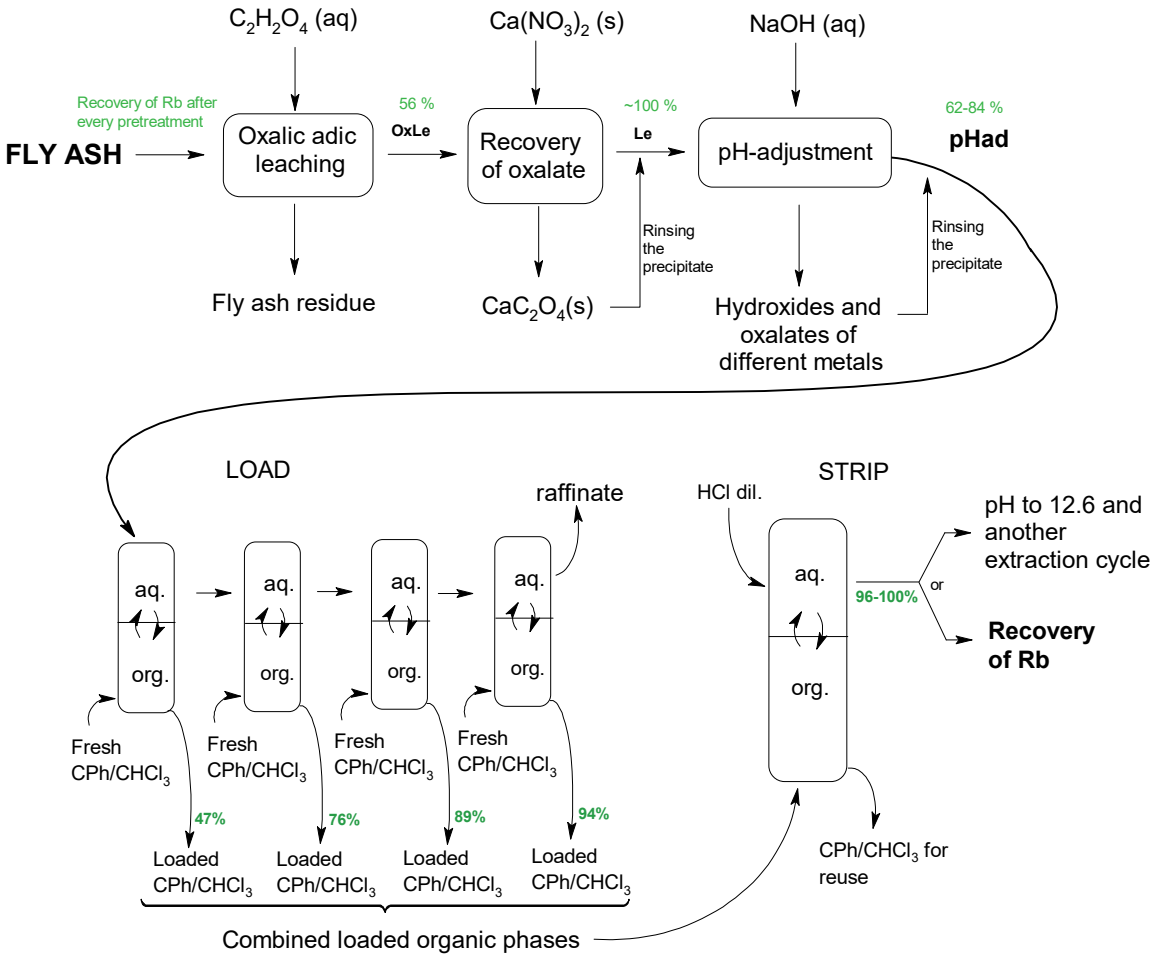

FIGURE 27 Schematic presentation of the three pretreatments for fly ash prior to liquid-liquid extraction and one extraction cycle with four loading steps. Recovery of rubidium after every treatment steps is displayed in green.

An additional test for recovery of rubidium was performed with an inorganic sorbent called potassium copper(II) hexacyanoferrate (KCuFC). KCuFC was printed in a nylon-based functional filter by a 3D-printer to ease the handling of the KCuFC powder. The functional filters were employed for the recovery of rubidium from synthetic samples mimicking acid-leached fly ash. The recovery of rubidium was very effective (94%), but the extraction of rubidium from the filter was only 60% by a 1 mol L^{-1} NH_4Cl solution after 10 extraction steps. The benefit of the method compared to liquid-liquid extraction was the reduction in the pretreatments needed prior to rubidium recovery, during which some of the rubidium can be lost. However, the sample needed to be diluted tenfold to reach a high recovery of rubidium, and additionally, copper and potassium were leached from the filter during experiments. Hence, rubidium recovery using a KCuFC sorbent needs further development to work successfully for fly ash leachates.

REFERENCES

1. Final List of Critical Minerals 2018, Department of Interior, Office of the Secretary, Federal Information & News Dispatch, Inc., Washington, United States, Washington, 2018, Federal Register *83*(97), 23295-23296, https://www.govinfo.gov/app/details/FR-2018-05-18/2018-10667/summary, (16.5.2019)

2. Zinke, R. K. and Werkheiser, W. H., U.S. Geological Survey, Mineral commodity summaries 2019, Rubidium, U.S. Department of the Interior, U.S. Geological Survey, Reston, Va, 2019, 136-137.

3. B.Z. Egan, R.A. Zingaro and B.M. Benjamin, Extraction of alkali metals by 4-*sec*-butyl-2-(α-methylbenzyl)phenol (BAMBP), *Inorg. Chem.*, **1965**, *4*(7), 1055-1061.

4. Z. Li, Y. Pranolo, Z. Zhu and C.Y. Cheng, Solvent extraction of cesium and rubidium from brine solutions using 4-*tert*-butyl-2-(α-methylbenzyl)-phenol, *Hydrometallurgy*, **2017**, *171*, 1-7.

5. S. Liu, H. Liu, Y. Huang and W. Yang, Solvent extraction of rubidium and cesium from salt lake brine with *t*-BAMBP–kerosene solution, *Trans. Nonferrous Met. Soc. China*, **2015**, *25*, 329-334.

6. W.J. Ross and J.C. White, Determination of cesium and rubidium after extraction with 4-*sec*-butyl-2(α-methylbenzyl)phenol, *Anal. Chem.*, **1964**, *36*(10), 1998-2000.

7. J. Wang, D. Che and W. Qin, Extraction of rubidium by *t*-BAMBP in cyclohexane, *Chin. J. Chem. Eng.*, **2015**, *23*, 1110-1113.

8. J. Bryan, L. Delmau, B. Hay, J. Nicholas, L. Rogers, R. Rogers and B. Moyer, Cesium recognition by supramolecular assemblies of 2-benzylphenol and 2-benzylphenolate, *Struct. Chem.*, **1999**, *10*(3), 187-203.

9. G. Naidu, T. Nur, P. Loganathan, J. Kandasamy and S. Vigneswaran, Selective sorption of rubidium by potassium cobalt hexacyanoferrate, *Sep. Purif. Technol.*, **2016**, *163*, 238-246.

10. J. Moon, E. Lee and H. Kim, Ion exchange of Cs ion in acid solution with potassium cobalt hexacyanoferrate, *Korean J. Chem. Eng*, **2004**, *21*(5), 1026-1031.

11. G. Naidu, P. Loganathan, S. Jeong, M.A.H. Johir, V.H.P. To, J. Kandasamy and S. Vigneswaran, Rubidium extraction using an organic polymer encapsulated potassium copper hexacyanoferrate sorbent, *Chem. Eng. J.*, **2016**, *306*, 31-42.

12. F.S. Wagner, *Rubidium and Rubidium Compounds in Kirk-Othmer Encyclopedia of Chemical technology*, John Wiley and Sons, Inc., 2013, 591-600.

13. W. Lenk, H. Prinz and A. Steinmetz, *Rubidium and Rubidium Compounds in Ullmann's Encyclopedia of Industrial Chemistry*, Wiley Online Library ,Wiley-VCH Verlag GmbH & Co. KGaA, Weinheim, 2012, 123-126.

14. W.M. Haynes and D.R. Lide, *CRC handbook of chemistry and physics : a ready-reference book of chemical and physical data*, 91st ed., CRC Press, Boca Raton, 2010.

15. R. Salminen, Geochemical atlas of Europe. Part 1, Background information, methodology and maps, R. Salminen ed., Geological Survey of Finland, Espoo, 2005.

16. W.D. Vos and T. Tarvainen, Geochemical atlas of Europe. Part 2, Interpretation of geochemical maps, additional tables, figures, maps and related publications, Geological Survey of Finland, Espoo, 2006.

17. Prices of rubidium compounds by Alfa Aesar by Thermo Fisher Scientific, https://www.alfa.com/en/search/?q=Rubidium, (25.3.2019).

18. Gold Price. Where the Word Checks the Gold Price, https://goldprice.org/, (25.3.2019).

19. Z.T. Yao, X.S. Ji, P.K. Sarker, J.H. Tang, L.Q. Ge, M.S. Xia, and Y.Q.A. Xi, Comprehensive review on the applications of coal fly ash, *Earth-Sci. Rev.*, **2015**, *141*, 105-121.

20. S.V. Vassilev, D. Baxter, L.K. Andersen and C.G. Vassileva, An overview of the composition and application of biomass ash. Part 1. Phase–mineral and chemical composition and classification, *Fuel*, **2013**, *105*, 40-76.

21. S. Perämäki, *Method development for determination and recovery of rare earth elements from industrial fly ash*, PhD-thesis, University of Jyväskylä, Finland, 2014.

22. V. Soikkeli, *Hydrometallurgical recovery and leaching studies for selected valuable metals from fly ash samples by ultrasound-assisted extraction followed by ICP-OES determination*, PhD-thesis, University of Jyväskylä, Finland, 2016.

23. S.E. Perämäki, A.J. Tiihonen and A.O. Väisänen, Occurrence and recovery potential of rare earth elements in Finnish peat and biomass combustion fly ash, *J. Geochem. Explor.*, **2019**, *201*, 71-78.

24. M.P. Ketris and Y.E. Yudovich, Estimations of Clarkes for Carbonaceous biolithes: World averages for trace element contents in black shales and coals, *Int. J. Coal Geol.*, **2009**, *78*, 135-148.

25. S.V. Vassilev, C.G. Vassileva and V.S. Vassilev, Advantages and disadvantages of composition and properties of biomass in comparison with coal: An overview, *Fuel*, **2015**, *158*, 330-350.

26. ecoba, European Coal Combustion Products Association, http://www.ecoba.com/ecobaccpprod.html (1.10.2018).

27. S. Wang, Application of solid ash based catalysts in heterogeneous catalysis, *Environ. Sci. Technol.*, **2008**, *42*(19), 7055-7063.

28. D.C. Harris, *Quantitative chemical analysis*, 8th ed. Internat., Freeman, New York, 2010.

29. T. Braun and G. Ghersini, *Extraction Chromatography*, Elsevier Scientific Publishing Company, 1975.

30. A.G. Volkov, S. Paula and D.W. Deamer, Two mechanisms of permeation of small neutral molecules and hydrated ions across phospholipid bilayers, *Bioelectrochem. Bioenerg.*, **1997**, *42*, 153-160.

31. P. Xing, G. Wang, C. Wang, B. Ma and Y. Chen, Separation of rubidium from potassium in rubidium ore liquor by solvent extraction with *t*-BAMBP, *Miner. Eng.*, **2018**, *121*, 158-163.

32. D.E. Horne, K.B. Brown, D.J. Crouse and B. Weaver, Recovery of fission products from waste solutions by solvent extraction, ORNL report 3518, Oak Ridge National Laboratories, U.S. Atomic Energy Commission, United States, 1963, 19-27.

33. K.B. Brown, Chemical Technology Division, Chemical Development Section C, Progress report on separations chemistry and separations process research for January-June 1963, Oak Ridge National Laboratories, U.S. Atomic Energy Commission, United States, 1963, 10-15.

34. E. Weber, *Crown Ethers in Ullmann's Encyclopedia of Industrial Chemistry*, Wiley-VCH Verlag GmbH & Co. KGaA, Weinheim, 2012, 471-480.

35. S. Maleknia and J. Brodbelt, Cavity-size-dependent dissociation of crown ether/ ammonium ion complexes in the gas phase, *J. Am. Chem. Soc.*, **1993**, *115*(7), 2837-2843.

36. C.J. Pedersen, Cyclic polyethers and their complexes with metal salts, *J. Am. Chem. Soc.*, **1967**, *89*(26), 7017-7036.

37. W. Xiaolin, L. Yinong and F. Yibei, Solvent extraction separation of rubidium with a crown ether for neutron activation analysis in rock samples, *J. Radioanal. Nucl.*, **1995**, *189*(1), 127-132.

38. C.M. Goff, M.A. Matchette, N. Shabestary and S. Khazaeli, Complexation of Ceasium and Rubidium cations with crown ethers in *N,N*-dimethylformamide, Polyhedron, **1996**, *15*(21), 3897-3903.

39. G.G. Talanova, N.S.A. Elkarim, R.E.J. Hanes and H. Hwang, Extraction selectivities of crown ethers for alkali metal cations: Differences between single-species and competitive solvent extractions, *Anal. Chem.*, **1999**, *71*(3), 672-677.

40. D. Huang, H. Zheng, Z. Liu, A. Bao and B. Li, Extraction of rubidium and cesium from brine solutions using a room temperature ionic liquid system containing 18-crown-6, *Pol. J. Chem. Tech.*, **2018**, *20*(2), 40-46.

41. B. Ertan and Y. Erdoğan, Separation of rubidium from boron containing clay wastes using solvent extraction, *Powder Technology*, **2016**, *295*, 254-260.

42. K. Dorfner, ed., *Ion exhangers*, Walter de Gruyter & Co., Berlin, 1991.

43. M.M. Nasef and Z. Ujang, Introduction to Ion Exchange Processes, In: Inamuddin and M. Luqman (eds.), *Ion Exchange Technology I: Theory and Materials,* Springer Netherlands, Dordrecht, 2012, 1-39.

44. M. Qureshi and K.G. Varshney, *Inorganic ion exchangers in chemical analysis*, CRC Press, Boca Raton, Florida, 1991.

45. S. Ayrault, C. Loos-Neskovic, M. Fedoroff, E. Garnier and D.J. Jones, Compositions and structures of copper hexacyanoferrates(II) and (III): Experimental results, *Talanta*, **1995**, *42*(11), 1581-1593.

46. S. Ayrault, B. Jimenez, E. Garnier, M. Fedoro, D.J. Jones and C. Loos-Neskovic, Hexacyanoferrates and their relation to the crystalline structure, *Journal of Solid State Chemistry*, **1998**, *141*, 475-485.

47. A. Widmann, H. Kahlert, I. Petrovic-Prelevic, H. Wulff, J.V. Yakhmi, N. Bagkar and F. Scholz, Structure, insertion electrochemistry, and magnetic properties of a new type of substitutional solid solutions of copper, nickel, and iron hexacyanoferrates/hexacyanocobaltates, *Inorg. Chem.*, **2002**, *41*(22), 5706-5715.

48. C. Loos-Neskovic, S. Ayrault, V. Badillo, B. Jimenez, E. Garnier, M. Fedoroff, D.J. Jones and B. Merinov, Structure of copper-potassium hexacyanoferrate (II) and sorption mechanisms of cesium, *J. Solid State Chem.*, **2004**, *177*(6), 1817-1828.

49. T.P. Valsala, A. Joseph, J.G. Shah, K. Raj and V. Venugopal, Synthesis and characterization of cobalt ferrocyanides loaded on organic anion exchanger, *J. Nucl. Mater.*, **2009**, *384*(2), 146-152.

50. N.R. de Tacconi, K. Rajeshwar and R.O. Lezna, Metal hexacyanoferrates: Electrosynthesis, in situ characterization, and applications, *Chem. Mater.*, **2003**, *15*(16), 3046-3062.

51. J. Lehto, S. Haukka, R. Harjula and M. Blomberg, Mechanism of caesium ion exchange on potassium cobalt hexacyanoferrates(II), *J. Chem. Soc., Dalton Trans.*, **1990**, (3), 1007-1011.

52. M. Ramaswamy, Sorption of cesium by hexacyanoferrate composites from neutral and acidic media, *Solvent Extr. Ion Exch.*, **1997**, *15*(6), 1119-1131.

53. J. Orechovská and P. Rajec, Sorption of cesium on composite sorbents based on nickel ferrocyanide, *J. Radioanal. Nucl. Chem.*, **1999**, *242*(2), 387-390.

54. A. Nilchi, A. Khanchi, H. Atashi, A. Bagheri and L. Nematollahi, The application and properties of composite sorbents of inorganic ion exchangers and polyacrylonitrile binding matrix, *J. Hazard. Mater.*, **2006**, *137*(3), 1271-1276.

55. A.M. El-Kamash, Evaluation of zeolite A for the sorptive removal of Cs^{+} and Sr^{2+} ions from aqueous solutions using batch and fixed bed column operations, *J. Hazard. Mater*, **2008**, *151*(2), 432-445.

56. T.P. Valsala, S.C. Roy, J.G. Shah, J. Gabriel, K. Raj and V. Venugopal, Removal of radioactive caesium from low level radioactive waste (LLW) streams using cobalt ferrocyanide impregnated organic anion exchanger, *J. Hazard. Mater.*, **2009**, *166*(2-3), 1148-1153.

57. S. Taj, D. Muhammad, M. Chaudhry and M. Mazhar, Lithium, rubidium and cesium ion removal using potassium iron(III) hexacyanoferrate(II) supported on polymethylmethacrylate, *J. Radioanal. Nucl. Chem.*, **2011**, *288*(1), 79-88.

58. Z. Du, M. Jia and X. Wang, Cesium removal from solution using PAN-based potassium nickel hexacyanoferrate (II) composite spheres, *J. Radioanal. Nucl. Chem.*, **2013**, *298*(1), 167-177.

59. F. Han, G. Zhang and P. Gu, Adsorption kinetics and equilibrium modeling of cesium on copper ferrocyanide, *J. Radioanal. Nucl. Chem.*, **2013**, *295*(1), 369-377.

60. Y. Qing, J. Li, B. Kang, S. Chang, Y. Dai, Q. Long and C. Yuan, Selective sorption mechanism of Cs^{+} on potassium nickel hexacyanoferrate(II) compounds, *J. Radioanal. Nucl. Chem.*, **2015**, *304*(2), 527-533.

61. J. Lehto and R. Harjula, Selective Separation of Radionuclides from Nuclear Waste Solutions with Inorganic Ion Exchangers, *Radiochim. Acta*, **1999**, *86*, 65.

62. E. Tusa, Use of highly selective ion exchangers for minimization of waste volumes, *WM'01 Conf.*, Tucson, USA, 25.3.2001, Fortum Engineering Ltd, 2001, 1-9.

63. J, Lehto, R. Paajanen and R. Harjula, Selectivity of potassium cobalt hexacyanoferrate (II) for alkali and alkaline earth metal ions, *J. Radioanal. Nucl. Chem. Lett.*, **1992**, *164*(1), 39-46.

64. R. Harjula, J. Lehto, A. Paajanen, L. Brodkin and E. Tusa, Removal of radioactive cesium from nuclear waste solutions with the transition metal hexacyanoferrate ion exchanger CsTreat, *Nucl. Sci. Eng.*, **2001**, *137*(2), 206-214.

65. O., Gilbert, C. Valderrama, M. Peterkóva and J.L. Cortina, Evaluation of selective sorbents for the extraction of valuable metal ions (Cs, Rb, Li, U) from reverse osmosis rejected brine, *Solvent Extr. Ion Exch.*, **2010**, *28*(4), 543-562.

66. M. Petersková, C. Valderrama, O. Gibert and J.L. Cortina, Extraction of valuable metal ions (Cs, Rb, Li, U) from reverse osmosis concentrate using selective sorbents, *Desalination*, **2012**, *286*, 316-323.

67. J. Le Dirach, S. Nisan and C. Poletiko, Extraction of strategic materials from the concentrated brine rejected by integrated nuclear desalination systems, *Desalination*, **2005**, *182*, 449-460.

68. T. Nur, G. Naidu, P. Loganathan, J. Kandasamy and S. Vigneswaran, Rubidium recovery using potassium cobalt hexacyanoferrate sorbent, *Desalin. Water Treat.*, **2016**, *57*(55), 26577-26585.

69. R.W. Broach, D-Y. Jan, D.A. Lesch, S. Kulprathipanja, E. Roland and P. Kleinschmit, *Zeolites in Ullmann's Encyclopedia of Industrial Chemistry*, Wiley Online Library, Wiley-VCH Verlag GmbH & Co. KGaA, Weinheim, 2012, 1-35.

70. P. Rajec and K. Domianová, Cesium exchange reaction on natural and modified clinoptilolite zeolites, *J. Radioanal. Nucl. Chem.*, **2008**, *275*(3), 503-508.

71. E. Johan, T. Yamada, M.W. Munthali, P. Kabwadza-Corner, H. Aono and N. Matsue, Natural Zeolites as Potential Materials for Decontamination of Radioactive Cesium, *Procedia Environ. Sci.*, **2015**, *28*, 52-56.

72. M.W. Munthali, E. Johan, H. Aono and N. Matsue, Cs^{+} and Sr^{2+} adsorption selectivity of zeolites in relation to radioactive decontamination, *Journal of Asian Ceramic Societies*, **2015**, *3*(3), 245-250.

73. X. Fang, F. Fang, C. Lu and L. Zheng, Removal of Cs^{+}, Sr^{2+}, and Co^{2+} Ions from the Mixture of Organics and Suspended Solids Aqueous Solutions by Zeolites, *Nucl. Eng. Technol*, **2017**, *49*, 556-561.

74. J.V.R. Smit, Ammonium salts of the heteropolyacids as cation exchangers, *Nature*, **1958**, *181*, 1530.

75. F. Šebesta and V. Štefula, Composite ion exchanger with ammonium molybdophosphate and its properties, *J. Radioanal. Nucl. Chem.*, **1990**, *140*(1), 15-21.

76. C.J. Miller, A.L. Olson and C.K. Johnson, Cesium absorption from acidic solutions using ammonium molybdophosphate on a polyacrylonitrile support (AMP-PAN), *Sep. Sci. Technol.*, **1997**, *32*(1-4), 37.

77. D. Ding, Z. Zhang, R. Chen and T. Cai, Selective removal of cesium by ammonium molybdophosphate – polyacrylonitrile bead and membrane, *J. Hazard. Mater.*, **2017**, *324*, 753-761.

78. Y. Park, Y. Lee, W.S. Shin and S. Choi, Removal of cobalt, strontium and cesium from radioactive laundry wastewater by ammonium molybdophosphate–polyacrylonitrile (AMP–PAN), *Chem. Eng. J.*, **2010**, *162*, 685-695.

79. A. Bao, H. Zheng, Z. Liu, D. Huang, S. Wang and B. Li, Preconcentration and separation of rubidium from salt lake brine by ammonium phosphomolybdate – polyacrylonitrile (AMP-PAN) composite adsorbent, *ChemistrySelect*, **2017**, *2*(25), 7741-7750.

80. C. Luca, *Ion Exchange/Organic Ion Exchangers in Encyclopedia of Separation Science*, Academic Press, 2000, 1647-1632.

81. M.A. Ebra and R.M. Wallace, Phenolic cation exchange resin material for recovery of cesium and strontium, *U.S. Pat*. 4,423,159, 27.12.1983.

82. J.P. Bibler and R.M. Wallace, Cesium-specific phenolic ion exchange resin, *U.S. Pat.*, 5,441,991, 15.8.1995.

83. F.G. Smith, Modeling of Ion-Exchange for Cesium Removal from Dissolved Saltcake in SRS Tanks 1-3, 37 and 41, Report prepared for the U.S. Department of Energy , Savannah River National Laboratory, United States, 2007.

84. A. Favre-Réguillon, B. Dunjic, M. Lemaire and R. Chomel, Synthesis and evaluation of resorcinol-based ion-exchange resins for the selective removal of cesium, *Solvent Extr. Ion Exch.*, **2001**, *19*(1), 181-191.

85. N.M. Hassan and K. Adu-Wusu, Cesium Removal from Hanford Tank Waste Solution Using Resorcinol-Formaldehyde Resin, *Solvent Extr. Ion Exch.*, **2005**, *23*(3), 375-389.

86. S.K. Fiskum, D.L. Blanchard, M.J. Steele, K.K. Thomas, T. Trang-Le and M.R. Thorson, Spherical Resorcinol-Formaldehyde Resin Testing for Cesium Removal from Hanford Tank Waste Simulant, *Sep. Sci. Technol.*, **2006**, 41(11), 2461.

87. S.K. Fiskum, S.T. Arm, M.J. Steele and M.R. Thorson, Spherical Resorcinol-Formaldehyde Performance Testing with Hanford Tank Waste, *Solvent Extr. Ion Exch*, **2008**, 26(4), 435-452.

88. K.P. Brooks, B.S. Augspurger, D.L. Blanchard, J.M. Cuta, S.K. Fiskum and M.R. Thorson, Hydraulic Testing of Ion Exchange Resins for Cesium Removal from Hanford Tank Waste, *Sep. Sci. Technol.*, **2006**, 41(11), 2391.

89. M. Duignan and C. Nash, Removal of Cesium from Savannah River Site Waste with Spherical Resorcinol Formaldehyde Ion Exchange Resin: Experimental Tests, *Sep. Sci. Technol.*, **2010**, *45*, 1828-1840.

90. D. Banerjee, M.A. Rao and P.K. Wattal, Separation and Recovery of Cs from High Active Waste Simulant using Resorcinol Formaldehyde Polycondensate Resin: Batch and Column Studies, *Sep. Sci. Technol*, **2013**, *48*(1), 133-139.

91. C.A. Nash and S.T. Isom, Characterization of Spherical Resorcinol-Formaldehyde Resin Cesium Adsorption with Batch Contact Tests, *Sep. Sci. Technol*, **2010**, *45*(12-13), 1822-1827.

92. L. Shelkovnikova, S. Kargov, O. Gavlina, V. Ivanov and G. Al'tshuler, Selectivity of ion exchangers in extracting cesium and rubidium from alkaline solutions, *Russ. J. Phys. Chem*. A, **2013**, *87*(1), 125-128.

93. J. Nölte, *ICP Emission Spectrometry: A Practical Guide*, Wiely-VCH Verlag GmbH & Co. KGaA, Weinheim, 2003.

94. J. Todoli and J. Mermet, *Liquid Sample Introduction in ICP Spectrometry: A Practical Guide*, Elsevier, Amsterdam, The Netherlands, 2008.

95. J.M. Mermet, Use of magnesium as a test element for inductively coupled plasma atomic emission spectrometry diagnostics, *Anal. Chim. Acta*, **1991**, *250*, 85-94.

96. G. Schlemmer and R. Bernard, *Analytical Graphite Furnace Atomic Absorption Spectrometry: A Laboratory Guide*, Birkhäuser Verlag, Basel, Switzerland, 1999.

97. *The TGHA Graphite Furnace: Techniques and Recommended Conditions by Perkin-Elmer*, Bodenseewerk Perkin-Elmer GmbH, Ueberlingen, Germany, 1995.

98. B.V. L'vov, L.A. Pelieva and A.I. Sharnopol'skii, Reduction of the effect of the main component in the atomic-absorption analysis of solutions in tube furnaces by evaporation of the samples from a graphite support, *J. Appl. Spectrosc.*, **1977**, *27*(3), 1104-1107.

99. G. Schlemmer, Graphite furnace AAS for complex samples: Detection limits, precision, long-term stability, *Atom. Spec.*, **1996**, *17*, 15-21.

100. R. Thomas, *Practical Guide to ICP-MS: A Tutorial for Beginners*, 3th ed., CRC Press, Taylor & Francis Group, Boca Raton, USA, 2013.

101. AAS, GFAAS, ICP or ICP-MS? Which technique should I use? An elementary overview of elemental analysis, Thermo Elemental, booklet S002B Rev 02/01, USA, 2001.

102. https://www.eag.com/resources/appnotes/icp-oes-and-icp-ms-detection-limit-guidance/, (20.6.2019)

103. J.N. Miller and J.C. Miller, *Statistics and Chemometrics for Analytical Chemistry*, 6th ed., Pearson Educated Limited, Harlow, U.K., 2010.

104. EPA Method 200.7, Determination of metals and trace elements in waters and wastes by inductive coupled plasma –atomic emission spectrometry, 1996.

105. EPA Method 200.8, Determination of trace elements in waters and wastes by inductive coupled plasma –mass spectrometry, Methods for the Determination of Metals and Inorganic Chemicals in Environmental Samples, 1996.

106. S. Laudau and B. Everitt, *A Handbook of Statistical Analyses using SPSS*, Chapman & Hall/CRC Press LLC, Boca Raton, Florida, 2004.

107. A. Väisänen, J. Valkonen, S. Perämäki, V. Soikkeli and R. Ryymin, Method for processing ash, particularly fly ash, *WIPO PCT*, Patent WO 2013079804 A1, 6.6.2013.

108. A. Ilander and A. Väisänen, An ultrasound-assisted digestion method for the determination of toxic element concentrations in ash samples by inductively coupled plasma optical emission spectrometry, *Anal. Chim. Acta*, **2007**, *602*(2), 195-201.

109. EPA-Method 3052, Microwave assisted acid digestion of siliceous and organically based matrices, 1996.

APPENDIX

TABLE A1 Matrix element wavelengths used in the elemental analysis by ICP-OES Optima 8300 as well as calibration areas, correlation coefficients of external calibrations, limits of detection (µg L^{-1}), limit of quantifications (µg L^{-1}), and RSD (%) ranges of three replicates.

	ICP-OES Optima 8300						
	Plasma viewing	Wave-length	Calibration range	r	LOD	LOQ	RSD
		nm	mg L^{-1}		µg L^{-1}	µg L^{-1}	(%)
Al	Radial	396.153	1 - 50	0.99999	267	891	0.11 - 3.03
Ca	Radial	317.933	4 - 200	0.99999	938	3128	0.21 - 3.76
Cu	Axial	327.393	0.02 - 1	0.99991	15	48	0.05 - 3.00
Fe	Radial	238.204	1 - 50	0.99996	498	1659	0.26 - 1.46
K	Radial	766.490	1 - 50	1.00000	54	179	0.09 - 2.61
Mg	Radial	285.213	1 - 50	0.99997	400	1332	0.18 - 1.23
Mn	Radial	257.610	2 - 10	0.99988	171	571	0.16 - 1.89
Na	Radial	589.592	1 - 50	0.99999	243	809	0.11 - 1.60
Si	Radial	251.611	1 - 50	0.99970	1334	4445	0.22 - 3.15
P	Axial	178.221	1 - 50	0.99996	503	1675	0.24 - 3.76
S	Axial	181.975	1 - 50	0.99998	267	890	0.09 - 2.19

TABLE A2 Matrix element wavelengths used in elemental analysis by ICP-OES Avio 500 as well as calibration areas, correlation coefficients of external calibrations, limits of detection (µg L^{-1}), limit of quantifications (µg L^{-1}), and RSD (%) ranges of three replicates.

	ICP-OES Avio 500						
	Plasma viewing	Wave-length	Calibration range	r	LOD	LOQ	RSD
		nm	mg L^{-1}		µg L^{-1}	µg L^{-1}	(%)
Al	Radial	396.153	0.1 - 10	0.99999	113	366	0.2 - 3.5
Ba	Axial	233.527	0.1 - 10	1.00000	9.90	11.4	0.2 - 2.1
Ca	Radial	317.933	0.1 - 10	0.99990	85.0	137	0.2 – 4.1
Cr	Axial	267.716	0.1 - 10	0.99999	12.0	14.7	0.1 – 2.6
Cu	Axial	327.393	0.1 - 10	1.00000	20.7	49.3	0.3 – 2.3
Fe	Radial	238.204	0.1 - 10	1.00000	221	662	0.2 – 4.1
K	Radial	766.490	0.1 - 10	0.99997	365	1010	0.2 – 4.1
Li	Radial	670.784	0.1 - 10	0.99999	10.2	24.2	0.3 – 2.7
Mg	Radial	285.213	0.1 - 10	1.00000	43.2	135	0.2 – 1.5
Mn	Radial	257.610	0.1 - 10	1.00000	17.9	49.0	0.3 – 2.6
Na	Radial	589.592	0.1 - 10	0.99999	227	610	0.1 – 5.4
Zn	Axial	206.200	0.1 - 10	0.99999	16.5	21.6	0.2 – 2.0
B	Axial	249.677	0.1 - 10	0.99985	69.9	131.4	0.2 – 3.9
S	Axial	181.975	0.1 - 10	0.99988	281	703	0.2 – 2.1
Si	Radial	251.611	0.1 - 10	0.99826	1650	1910	0.4 – 4.1
Ti	Axial	334.940	0.1 - 10	0.99999	18.2	25.0	0.2 – 2.3
P	Axial	178.221	0.1 - 10	0.99994	204	525	0.2 – 2.4
Rb	Axial	780.023	0.1 - 10	0.99966	110	147	0.1 – 4.1
Rb	Radial	780.023	1 - 10	0.99991	559	1,670	5.1 – 18.5

TABLE A3 Isotopes of alkali metals used in elemental analysis by ICP-MS NexION 350D as well as abundances, calibration areas, correlation coefficients of external calibrations, limits of detection (µg L^{-1}), limit of quantifications (µg L^{-1}), and RSD (%) ranges of three replicates.

	ICP-MS NexION 350D						
	Isotope	Abundance	Calibration range	r	LOD	LOQ	RSD
		(%)	mg L-1		µg L-1	µg L-1	(%)
Li	7	92.5	1 - 10	0.99991	0.0105	0.024	0.05 - 6.6
K	39	93.3	10 - 100	0.99983	3.08	8.38	0.08 - 22
Rb	85	72.2	1 - 10	0.99995	0.0043	0.013	0.05 – 4.1
Rb	87	27.8	1 - 10	0.99998	0.0040	0.012	0.12 – 7.3
Cs	133	100	1 - 10	0.99995	0.0050	0.014	0.03 – 4.1

DEPARTMENT OF CHEMISTRY, UNIVERSITY OF JYVÄSKYLÄ
RESEARCH REPORT SERIES

1. Vuolle, Mikko: Electron paramagnetic resonance and molecular orbital study of radical ions generated from (2.2)metacyclophane, pyrene and its hydrogenated compounds by alkali metal reduction and by thallium(III)trifluoroacetate oxidation. (99 pp.) 1976
2. Pasanen, Kaija: Electron paramagnetic resonance study of cation radical generated from various chlorinated biphenyls. (66 pp.) 1977
3. Carbon-13 Workshop, September 6-8, 1977. (91 pp.) 1977
4. Laihia, Katri: On the structure determination of norbornane polyols by NMR spectroscopy. (111 pp.) 1979
5. Nyrönen, Timo: On the EPR, ENDOR and visible absorption spectra of some nitrogen containing heterocyclic compounds in liquid ammonia. (76 pp.) 1978
6. Talvitie, Antti: Structure determination of some sesquiterpenoids by shift reagent NMR. (54 pp.) 1979
7. Häkli, Harri: Structure analysis and molecular dynamics of cyclic compounds by shift reagent NMR. (48 pp.) 1979
8. Pitkänen, Ilkka: Thermodynamics of complexation of 1,2,4-triazole with divalent manganese, cobalt, nickel, copper, zinc, cadmium and lead ions in aqueous sodium perchlorate solutions. (89 pp.) 1980
9. Asunta, Tuula: Preparation and characterization of new organometallic compounds synthesized by using metal vapours. (91 pp.) 1980
10. Sattar, Mohammad Abdus: Analyses of MCPA and its metabolites in soil. (57 pp.) 1980
11. Bibliography 1980. (31 pp.) 1981
12. Knuuttila, Pekka: X-Ray structural studies on some divalent 3d metal compounds of picolinic and isonicotinic acid N-oxides. (77 pp.) 1981
13. Bibliography 1981. (33 pp.) 1982
14. 6^{th} National NMR Symposium, September 9-10, 1982, Abstracts. (49 pp.) 1982
15. Bibliography 1982. (38 pp.) 1983
16. Knuuttila, Hilkka: X-Ray structural studies on some Cu(II), Co(II) and Ni(II) complexes with nicotinic and isonicotinic acid N-oxides. (54 pp.) 1983
17. Symposium on inorganic and analytical chemistry May 18, 1984, Program and Abstracts. (100 pp.) 1984
18. Knuutinen, Juha: On the synthesis, structure verification and gas chromatographic determination of chlorinated catechols and guaiacols occuring in spent bleach liquors of kraft pulp mill. (30 pp.) 1984
19. Bibliography 1983. (47 pp.) 1984
20. Pitkänen, Maija: Addition of BrCl, B_2 and Cl_2 to methyl esters of propenoic and 2-butenoic acid derivatives and ^{13}C NMR studies on methyl esters of saturated aliphatic mono- and dichlorocarboxylic acids. (56 pp.) 1985
21. Bibliography 1984. (39 pp.) 1985
22. Salo, Esa: EPR, ENDOR and TRIPLE spectroscopy of some nitrogen heteroaromatics in liquid ammonia. (111 pp.) 1985

23. Humppi, Tarmo: Synthesis, identification and analysis of dimeric impurities of chlorophenols. (39 pp.) 1985
24. Aho, Martti: The ion exchange and adsorption properties of sphagnum peat under acid conditions. (90 pp.) 1985
25. Bibliography 1985 (61 pp.) 1986
26. Bibliography 1986. (23 pp.) 1987
27. Bibliography 1987. (26 pp.) 1988
28. Paasivirta, Jaakko (Ed.): Structures of organic environmental chemicals. (67 pp.) 1988
29. Paasivirta, Jaakko (Ed.): Chemistry and ecology of organo-element compounds. (93 pp.) 1989
30. Sinkkonen, Seija: Determination of crude oil alkylated dibenzothiophenes in environment. (35 pp.) 1989
31. Kolehmainen, Erkki (Ed.): XII National NMR Symposium Program and Abstracts. (75 pp.) 1989
32. Kuokkanen, Tauno: Chlorocymenes and Chlorocymenenes: Persistent chlorocompounds in spent bleach liquors of kraft pulp mills. (40 pp.) 1989
33. Mäkelä, Reijo: ESR, ENDOR and TRIPLE resonance study on substituted 9,10-anthraquinone radicals in solution. (35 pp.) 1990
34. Veijanen, Anja: An integrated sensory and analytical method for identification of off-flavour compounds. (70 pp.) 1990
35. Kasa, Seppo: EPR, ENDOR and TRIPLE resonance and molecular orbital studies on a substitution reaction of anthracene induced by thallium(III) in two fluorinated carboxylic acids. (114 pp.) 1990
36. Herve, Sirpa: Mussel incubation method for monitoring organochlorine compounds in freshwater recipients of pulp and paper industry. (145 pp.) 1991
37. Pohjola, Pekka: The electron paramagnetic resonance method for characterization of Finnish peat types and iron (III) complexes in the process of peat decomposition. (77 pp.) 1991
38. Paasivirta, Jaakko (Ed.): Organochlorines from pulp mills and other sources. Research methodology studies 1988-91. (120 pp.) 1992
39. Veijanen, Anja (Ed.): VI National Symposium on Mass Spectrometry, May 13-15, 1992, Abstracts. (55 pp.) 1992
40. Rissanen, Kari (Ed.): The 7. National Symposium on Inorganic and Analytical Chemistry, May 22, 1992, Abstracts and Program. (153 pp.) 1992
41. Paasivirta, Jaakko (Ed.): CEOEC'92, Second Finnish-Russian Seminar: Chemistry and Ecology of Organo-Element Compounds. (93 pp.) 1992
42. Koistinen, Jaana: Persistent polychloroaromatic compounds in the environment: structure-specific analyses. (50 pp.) 1993
43. Virkki, Liisa: Structural characterization of chlorolignins by spectroscopic and liquid chromatographic methods and a comparison with humic substances. (62 pp.) 1993
44. Helenius, Vesa: Electronic and vibrational excitations in some

biologically relevant molecules. (30 pp.) 1993

45. Leppä-aho, Jaakko: Thermal behaviour, infrared spectra and x-ray structures of some new rare earth chromates(VI). (64 pp.) 1994
46. Kotila, Sirpa: Synthesis, structure and thermal behavior of solid copper(II) complexes of 2-amino-2- hydroxymethyl-1,3-propanediol. (111 pp.) 1994
47. Mikkonen, Anneli: Retention of molybdenum(VI), vanadium(V) and tungsten(VI) by kaolin and three Finnish mineral soils. (90 pp.) 1995
48. Suontamo, Reijo: Molecular orbital studies of small molecules containing sulfur and selenium. (42 pp.) 1995
49. Hämäläinen, Jouni: Effect of fuel composition on the conversion of fuel-N to nitrogen oxides in the combustion of small single particles. (50 pp.) 1995
50. Nevalainen, Tapio: Polychlorinated diphenyl ethers: synthesis, NMR spectroscopy, structural properties, and estimated toxicity. (76 pp.) 1995
51. Aittola, Jussi-Pekka: Organochloro compounds in the stack emission. (35 pp.) 1995
52. Harju, Timo: Ultrafast polar molecular photophysics of (dibenzylmethine)borondifluoride and 4-aminophthalimide in solution. (61 pp.) 1995
53. Maatela, Paula: Determination of organically bound chlorine in industrial and environmental samples. (83 pp.) 1995
54. Paasivirta, Jaakko (Ed.): CEOEC'95, Third Finnish-Russian Seminar: Chemistry and Ecology of Organo-Element Compounds. (109 pp.) 1995
55. Huuskonen, Juhani: Synthesis and structural studies of some supramolecular compounds. (54 pp.) 1995
56. Palm, Helena: Fate of chlorophenols and their derivatives in sawmill soil and pulp mill recipient environments. (52 pp.) 1995
57. Rantio, Tiina: Chlorohydrocarbons in pulp mill effluents and their fate in the environment. (89 pp.) 1997
58. Ratilainen, Jari: Covalent and non-covalent interactions in molecular recognition. (37 pp.) 1997
59. Kolehmainen, Erkki (Ed.): XIX National NMR Symposium, June 4-6, 1997, Abstracts. (89 pp.) 1997
60. Matilainen, Rose: Development of methods for fertilizer analysis by inductively coupled plasma atomic emission spectrometry. (41 pp.) 1997
61. Koistinen, Jari (Ed.): Spring Meeting on the Division of Synthetic Chemistry, May 15-16, 1997, Program and Abstracts. (36 pp.) 1997
62. Lappalainen, Kari: Monomeric and cyclic bile acid derivatives: syntheses, NMR spectroscopy and molecular recognition properties. (50 pp.) 1997
63. Laitinen, Eira: Molecular dynamics of cyanine dyes and phthalimides in solution: picosecond laser studies. (62 pp.) 1997
64. Eloranta, Jussi: Experimental and theoretical studies on some

quinone and quinol radicals. (40 pp.) 1997

65. Oksanen, Jari: Spectroscopic characterization of some monomeric and aggregated chlorophylls. (43 pp.) 1998
66. Häkkänen, Heikki: Development of a method based on laser-induced plasma spectrometry for rapid spatial analysis of material distributions in paper coatings. (60 pp.) 1998
67. Virtapohja, Janne: Fate of chelating agents used in the pulp and paper industries. (58 pp.) 1998
68. Airola, Karri: X-ray structural studies of supramolecular and organic compounds. (39 pp.) 1998
69. Hyötyläinen, Juha: Transport of lignin–type compounds in the receiving waters of pulp mills. (40 pp.) 1999
70. Ristolainen, Matti: Analysis of the organic material dissolved during totally chlorine-free bleaching. (40 pp.) 1999
71. Eklin, Tero: Development of analytical procedures with industrial samples for atomic emission and atomic absorption spectrometry. (43 pp.) 1999
72. Välisaari, Jouni: Hygiene properties of resol-type phenolic resin laminates. (129 pp.) 1999
73. Hu, Jiwei: Persistent polyhalogenated diphenyl ethers: model compounds syntheses, characterization and molecular orbital studies. (59 pp.) 1999
74. Malkavaara, Petteri: Chemometric adaptations in wood processing chemistry. (56 pp.) 2000
75. Kujala Elena, Laihia Katri, Nieminen Kari (Eds.): NBC 2000, Symposium on Nuclear, Biological and Chemical Threats in the 21st Century. (299 pp.) 2000
76. Rantalainen, Anna-Lea: Semipermeable membrane devices in monitoring persistent organic pollutants in the environment. (58 pp.) 2000
77. Lahtinen, Manu: *In situ* X-ray powder diffraction studies of Pt/C, CuCl/C and Cu_2O/C catalysts at elevated temperatures in various reaction conditions. (92 pp.) 2000
78. Tamminen, Jari: Syntheses, empirical and theoretical characterization, and metal cation complexation of bile acid-based monomers and open/closed dimers. (54 pp.) 2000
79. Vatanen, Virpi: Experimental studies by EPR and theoretical studies by DFT calculations of α-amino-9,10-anthraquinone radical anions and cations in solution. (37 pp.) 2000
80. Kotilainen, Risto: Chemical changes in wood during heating at 150-260 °C. (57 pp.) 2000
81. Nissinen, Maija: X-ray structural studies on weak, non-covalent interactions in supramolecular compounds. (69 pp.) 2001
82. Wegelius, Elina: X-ray structural studies on self-assembled hydrogen-bonded networks and metallosupramolecular complexes. (84 pp.) 2001
83. Paasivirta, Jaakko (Ed.): CEOEC'2001, Fifth Finnish-Russian Seminar: Chemistry and Ecology of Organo-Element Compounds. (163 pp.) 2001
84. Kiljunen, Toni: Theoretical studies on spectroscopy and

atomic dynamics in rare gas solids. (56 pp.) 2001

85. Du, Jin: Derivatives of dextran: synthesis and applications in oncology. (48 pp.) 2001
86. Koivisto, Jari: Structural analysis of selected polychlorinated persistent organic pollutants (POPs) and related compounds. (88 pp.) 2001
87. Feng, Zhinan: Alkaline pulping of non-wood feedstocks and characterization of black liquors. (54 pp.) 2001
88. Halonen, Markku: Lahon havupuun käyttö sulfaattiprosessin raaka-aineena sekä havupuun lahontorjunta. (90 pp.) 2002
89. Falábu, Dezsö: Synthesis, conformational analysis and complexation studies of resorcarene derivatives. (212 pp.) 2001
90. Lehtovuori, Pekka: EMR spectroscopic studies on radicals of ubiquinones Q-*n*, vitamin K_3 and vitamine E in liquid solution. (40 pp.) 2002
91. Perkkalainen, Paula: Polymorphism of sugar alcohols and effect of grinding on thermal behavior on binary sugar alcohol mixtures. (53 pp.) 2002
92. Ihalainen, Janne: Spectroscopic studies on light-harvesting complexes of green plants and purple bacteria. (42 pp.) 2002
93. Kunttu, Henrik, Kiljunen, Toni (Eds.): 4th International Conference on Low Temperature Chemistry. (159 pp.) 2002
94. Väisänen, Ari: Development of methods for toxic element analysis in samples with environmental concern by ICP-AES and ETAAS. (54 pp.) 2002
95. Luostarinen, Minna: Synthesis and characterisation of novel resorcarene derivatives. (200 pp.) 2002
96. Louhelainen, Jarmo: Changes in the chemical composition and physical properties of wood and nonwood black liquors during heating. (68 pp.) 2003
97. Lahtinen, Tanja: Concave hydrocarbon cyclophane π-prismands. (65 pp.) 2003
98. Laihia, Katri (Ed.): NBC 2003, Symposium on Nuclear, Biological and Chemical Threats – A Crisis Management Challenge. (245 pp.) 2003
99. Oasmaa, Anja: Fuel oil quality properties of wood-based pyrolysis liquids. (32 pp.) 2003
100. Virtanen, Elina: Syntheses, structural characterisation, and cation/anion recognition properties of nano-sized bile acid-based host molecules and their precursors. (123 pp.) 2003
101. Nättinen, Kalle: Synthesis and X-ray structural studies of organic and metallo-organic supramolecular systems. (79 pp.) 2003
102. Lampiselkä, Jarkko: Demonstraatio lukion kemian opetuksessa. (285 pp.) 2003
103. Kallioinen, Jani: Photoinduced dynamics of $Ru(dcbpy)_2(NCS)_2$ – in solution and on nanocrystalline titanium dioxide thin films. (47 pp.) 2004
104. Valkonen, Arto (Ed.): VII Synthetic Chemistry Meeting and XXVI Finnish NMR Symposium. (103 pp.) 2004

105. Vaskonen, Kari: Spectroscopic studies on atoms and small molecules isolated in low temperature rare gas matrices. (65 pp.) 2004
106. Lehtovuori, Viivi: Ultrafast light induced dissociation of $Ru(dcbpy)(CO)_2I_2$ in solution. (49 pp.) 2004
107. Saarenketo, Pauli: Structural studies of metal complexing Schiff bases, Schiff base derived *N*-glycosides and cyclophane π-prismands. (95 pp.) 2004
108. Paasivirta, Jaakko (Ed.): CEOEC'2004, Sixth Finnish-Russian Seminar: Chemistry and Ecology of Organo-Element Compounds. (147 pp.) 2004
109. Suontamo, Tuula: Development of a test method for evaluating the cleaning efficiency of hard-surface cleaning agents. (96 pp.) 2004
110. Güneş, Minna: Studies of thiocyanates of silver for nonlinear optics. (48 pp.) 2004
111. Ropponen, Jarmo: Aliphatic polyester dendrimers and dendrons. (81 pp.) 2004
112. Vu, Mân Thi Hong: Alkaline pulping and the subsequent elemental chlorine-free bleaching of bamboo (*Bambusa procera*). (69 pp.) 2004
113. Mansikkamäki, Heidi: Self-assembly of resorcinarenes. (77 pp.) 2006
114. Tuononen, Heikki M.: EPR spectroscopic and quantum chemical studies of some inorganic main group radicals. (79 pp.) 2005
115. Kaski, Saara: Development of methods and applications of laser-induced plasma spectroscopy in vacuum ultraviolet. (44 pp.) 2005
116. Mäkinen, Riika-Mari: Synthesis, crystal structure and thermal decomposition of certain metal thiocyanates and organic thiocyanates. (119 pp.) 2006
117. Ahokas, Jussi: Spectroscopic studies of atoms and small molecules isolated in rare gas solids: photodissociation and thermal reactions. (53 pp.) 2006
118. Busi, Sara: Synthesis, characterization and thermal properties of new quaternary ammonium compounds: new materials for electrolytes, ionic liquids and complexation studies. (102 pp.) 2006
119. Mäntykoski, Keijo: PCBs in processes, products and environment of paper mills using wastepaper as their raw material. (73 pp.) 2006
120. Laamanen, Pirkko-Leena: Simultaneous determination of industrially and environmentally relevant aminopolycarboxylic and hydroxycarboxylic acids by capillary zone electrophoresis. (54 pp.) 2007
121. Salmela, Maria: Description of oxygen-alkali delignification of kraft pulp using analysis of dissolved material. (71 pp.) 2007
122. Lehtovaara, Lauri: Theoretical studies of atomic scale impurities in superfluid ^{4}He. (87 pp.) 2007
123. Rautiainen, J. Mikko: Quantum chemical calculations of structures, bonding, and spectroscopic properties of some sulphur and selenium iodine cations. (71 pp.) 2007
124. Nummelin, Sami: Synthesis, characterization, structural and

retrostructural analysis of self-assembling pore forming dendrimers. (286 pp.) 2008

125. Sopo, Harri: Uranyl(VI) ion complexes of some organic aminobisphenolate ligands: syntheses, structures and extraction studies. (57 pp.) 2008
126. Valkonen, Arto: Structural characteristics and properties of substituted cholanoates and *N*-substituted cholanamides. (80 pp.) 2008
127. Lähde, Anna: Production and surface modification of pharmaceutical nano- and microparticles with the aerosol flow reactor. (43 pp.) 2008
128. Beyeh, Ngong Kodiah: Resorcinarenes and their derivatives: synthesis, characterization and complexation in gas phase and in solution. (75 pp.) 2008
129. Välisaari, Jouni, Lundell, Jan (Eds.): Kemian opetuksen päivät 2008: uusia oppimisympäristöjä ja ongelmalähtöistä opetusta. (118 pp.) 2008
130. Myllyperkiö, Pasi: Ultrafast electron transfer from potential organic and metal containing solar cell sensitizers. (69 pp.) 2009
131. Käkölä, Jaana: Fast chromatographic methods for determining aliphatic carboxylic acids in black liquors. (82 pp.) 2009
132. Koivukorpi, Juha: Bile acid-arene conjugates: from photoswitchability to cancer cell detection. (67 pp.) 2009
133. Tuuttila, Tero: Functional dendritic polyester compounds: synthesis and characterization of small bifunctional dendrimers and dyes. (74 pp.) 2009
134. Salorinne, Kirsi: Tetramethoxy resorcinarene based cation and anion receptors: synthesis, characterization and binding properties. (79 pp.) 2009
135. Rautiainen, Riikka: The use of first-thinning Scots pine (*Pinus sylvestris*) as fiber raw material for the kraft pulp and paper industry. (73 pp.) 2010
136. Ilander, Laura: Uranyl salophens: synthesis and use as ditopic receptors. (199 pp.) 2010
137. Kiviniemi, Tiina: Vibrational dynamics of iodine molecule and its complexes in solid krypton - Towards coherent control of bimolecular reactions? (73 pp.) 2010
138. Ikonen, Satu: Synthesis, characterization and structural properties of various covalent and non-covalent bile acid derivatives of N/O-heterocycles and their precursors. (105 pp.) 2010
139. Siitonen, Anni: Spectroscopic studies of semiconducting single-walled carbon nanotubes. (56 pp.) 2010
140. Raatikainen, Kari: Synthesis and structural studies of piperazine cyclophanes – Supramolecular systems through Halogen and Hydrogen bonding and metal ion coordination. (69 pp.) 2010
141. Leivo, Kimmo: Gelation and gel properties of two- and three-component Pyrene based low molecular weight organogelators. (116 pp.) 2011
142. Martiskainen, Jari: Electronic energy transfer in light-harvesting complexes isolated from *Spinacia oleracea* and from three

photosynthetic green bacteria *Chloroflexus aurantiacus*, *Chlorobium tepidum*, and *Prosthecochloris aestuarii*. (55 pp.) 2011

143. Wichmann, Oula: Syntheses, characterization and structural properties of [O,N,O,X´] aminobisphenolate metal complexes. (101 pp.) 2011
144. Ilander, Aki: Development of ultrasound-assisted digestion methods for the determination of toxic element concentrations in ash samples by ICP-OES. (58 pp.) 2011
145. The Combined XII Spring Meeting of the Division of Synthetic Chemistry and XXXIII Finnish NMR Symposium. Book of Abstracts. (90 pp.) 2011
146. Valto, Piia: Development of fast analysis methods for extractives in papermaking process waters. (73 pp.) 2011
147. Andersin, Jenni: Catalytic activity of palladium-based nanostructures in the conversion of simple olefinic hydro- and chlorohydrocarbons from first principles. (78 pp.) 2011
148. Aumanen, Jukka: Photophysical properties of dansylated poly(propylene amine) dendrimers. (55 pp.) 2011
149. Kärnä, Minna: Ether-functionalized quaternary ammonium ionic liquids – synthesis, characterization and physicochemical properties. (76 pp.) 2011
150. Jurček, Ondřej: Steroid conjugates for applications in pharmacology and biology. (57 pp.) 2011
151. Nauha, Elisa: Crystalline forms of selected Agrochemical actives: design and synthesis of cocrystals. (77 pp.) 2012
152. Ahkola, Heidi: Passive sampling in monitoring of nonylphenol ethoxylates and nonylphenol in aquatic environments. (92 pp.) 2012
153. Helttunen, Kaisa: Exploring the self-assembly of resorcinarenes: from molecular level interactions to mesoscopic structures. (78 pp.) 2012
154. Linnanto, Juha: Light excitation transfer in photosynthesis revealed by quantum chemical calculations and exiton theory. (179 pp.) 2012
155. Roiko-Jokela, Veikko: Digital imaging and infrared measurements of soil adhesion and cleanability of semihard and hard surfaces. (122 pp.) 2012
156. Noponen, Virpi: Amides of bile acids and biologically important small molecules: properties and applications. (85 pp.) 2012
157. Hulkko, Eero: Spectroscopic signatures as a probe of structure and dynamics in condensed-phase systems – studies of iodine and gold ranging from isolated molecules to nanoclusters. (69 pp.) 2012
158. Lappi, Hanna: Production of Hydrocarbon-rich biofuels from extractives-derived materials. (95 pp.) 2012
159. Nykänen, Lauri: Computational studies of Carbon chemistry on transition metal surfaces. (76 pp.) 2012
160. Ahonen, Kari: Solid state studies of pharmaceutically important molecules and their derivatives. (65 pp.) 2012

161. Pakkanen, Hannu: Characterization of organic material dissolved during alkaline pulping of wood and non-wood feedstocks. (76 pp.) 2012
162. Moilanen, Jani: Theoretical and experimental studies of some main group compounds: from closed shell interactions to singlet diradicals and stable radicals. (80 pp.) 2012
163. Himanen, Jatta: Stereoselective synthesis of Oligosaccharides by *De Novo* Saccharide welding. (133 pp.) 2012
164. Bunzen, Hana: Steroidal derivatives of nitrogen containing compounds as potential gelators. (76 pp.) 2013
165. Seppälä, Petri: Structural diversity of copper(II) amino alcohol complexes. Syntheses, structural and magnetic properties of bidentate amino alcohol copper(II) complexes. (67 pp.) 2013
166. Lindgren, Johan: Computational investigations on rotational and vibrational spectroscopies of some diatomics in solid environment. (77 pp.) 2013
167. Giri, Chandan: Sub-component self-assembly of linear and non-linear diamines and diacylhydrazines, formulpyridine and transition metal cations. (145 pp.) 2013
168. Riisiö, Antti: Synthesis, Characterization and Properties of Cu(II)-, Mo(VI)- and U(VI) Complexes With Diaminotetraphenolate Ligands. (51 pp.) 2013
169. Kiljunen, Toni (Ed.): Chemistry and Physics at Low Temperatures. Book of Abstracts. (103 pp.) 2013
170. Hänninen, Mikko: Experimental and Computational Studies of Transition Metal Complexes with Polydentate Amino- and Aminophenolate Ligands: Synthesis, Structure, Reactivity and Magnetic Properties. (66 pp.) 2013
171. Antila, Liisa: Spectroscopic studies of electron transfer reactions at the photoactive electrode of dye-sensitized solar cells. (53 pp.) 2013
172. Kemppainen, Eeva: Mukaiyama-Michael reactions with α-substituted acroleins – a useful tool for the synthesis of the pectenotoxins and other natural product targets. (190 pp.) 2013
173. Virtanen, Suvi: Structural Studies of Dielectric Polymer Nanocomposites. (49 pp.) 2013
174. Yliniemelä-Sipari, Sanna: Understanding The Structural Requirements for Optimal Hydrogen Bond Catalyzed Enolization – A Biomimetic Approach.(160 pp.) 2013
175. Leskinen, Mikko V: Remote β-functionalization of β'-keto esters. (105 pp.) 2014
176. 12th European Conference on Research in Chemistry Education (ECRICE2014). Book of Abstracts. (166 pp.) 2014
177. Peuronen, Anssi: N-Monoalkylated DABCO-Based N-Donors as Versatile Building Blocks in Crystal Engineering and Supramolecular Chemistry. (54 pp.) 2014
178. Perämäki, Siiri: Method development for determination and recovery of rare earth elements from industrial fly ash. (88 pp.) 2014

179. Chernyshev, Alexander, N.: Nitrogen-containing ligands and their platinum(IV) and gold(III) complexes: investigation and basicity and nucleophilicity, luminescence, and aurophilic interactions. (64 pp.) 2014
180. Lehto, Joni: Advanced Biorefinery Concepts Integrated to Chemical Pulping. (142 pp.) 2015
181. Tero, Tiia-Riikka: Tetramethoxy resorcinarenes as platforms for fluorescent and halogen bonding systems. (61 pp.) 2015
182. Löfman, Miika: Bile acid amides as components of microcrystalline organogels. (62 pp.) 2015
183. Selin, Jukka: Adsorption of softwood-derived organic material onto various fillers during papermaking. (169 pp.) 2015
184. Piisola, Antti: Challenges in the stereoselective synthesis of allylic alcohols. (210 pp.) 2015
185. Bonakdarzadeh, Pia: Supramolecular coordination polyhedra based on achiral and chiral pyridyl ligands: design, preparation, and characterization. (65 pp.) 2015
186. Vasko, Petra: Synthesis, characterization, and reactivity of heavier group 13 and 14 metallylenes and metalloid clusters: small molecule activation and more. (66 pp.) 2015
187. Topić, Filip: Structural Studies of Nano-sized Supramolecular Assemblies. (79 pp.) 2015
188. Mustalahti, Satu: Photodynamics Studies of Ligand-Protected Gold Nanoclusters by using Ultrafast Transient Infrared Spectroscopy. (58 pp.) 2015
189. Koivisto, Jaakko: Electronic and vibrational spectroscopic studies of gold-nanoclusters. (63 pp.) 2015
190. Suhonen, Aku: Solid state conformational behavior and interactions of series of aromatis oligoamide foldamers. (68 pp.) 2016
191. Soikkeli, Ville: Hydrometallurgical recovery and leaching studies for selected valuable metals from fly ash samples by ultrasound-assisted extraction followed by ICP-OES determination. (107 pp.) 2016
192. XXXVIII Finnish NMR Symposium. Book of Abstracts. (51 pp.) 2016
193. Mäkelä, Toni: Ion Pair Recognition by Ditopic Crown Ether Based bis-Urea and Uranyl Salophen Receptors. (75 pp.) 2016
194. Lindholm-Lehto, Petra: Occurrence of pharmaceuticals in municipal wastewater treatment plants and receiving surface waters in Central and Southern Finland. (98 pp.) 2016
195. Härkönen, Ville: Computational and Theoretical studies on Lattice Thermal conductivity and Thermal properties of Silicon Clathrates. (89 pp.) 2016
196. Tuokko, Sakari: Understanding selective reduction reactions with heterogeneous Pd and Pt: climbing out of the black box. (85 pp.) 2016
197. Nuora, Piia: Monitapaustutkimus LUMA-Toimintaan liittyvissä oppimisympäristöissä tapahtuvista kemian oppimiskokemuksista. (171 pp.) 2016

198. Kumar, Hemanathan: Novel Concepts on The Recovery of By-Products from Alkaline Pulping. (61 pp.) 2016
199. Arnedo-Sánchez, Leticia: Lanthanide and Transition Metal Complexes as Building Blocks for Supramolecular Functional Materials. (227 pp.) 2016
200. Gell, Lars: Theoretical Investigations of Ligand Protected Silver Nanoclusters. (134 pp.) 2016
201. Vaskuri, Juhani: Oppiennätyksistä opetussuunnitelman perusteisiin - lukion kemian kansallisen opetussuunnitelman kehittyminen Suomessa vuosina 1918-2016. (314 pp.) 2017
202. Lundell Jan, Kiljunen Toni (Eds.): 22nd Horizons in Hydrogen Bond Research. Book of Abstracts. 2017
203. Turunen, Lotta: Design and construction of halogen-bonded capsules and cages. (61 pp.) 2017
204. Hurmalainen, Juha: Experimental and computational studies of unconventional main group compounds: stable radicals and reactive intermediates. (88 pp.) 2017
205. Koivistoinen Juha: Non-linear interactions of femtosecond laser pulses with graphene: photo-oxidation, imaging and photodynamics. (68 pp.) 2017
206. Chen, Chengcong: Combustion behavior of black liquors: droplet swelling and influence of liquor composition. (39 pp.) 2017
207. Mansikkamäki, Akseli: Theoretical and Computational Studies of Magnetic Anisotropy and Exchange Coupling in Molecular Systems. (190 p. + included articles) 2018.
208. Tatikonda, Rajendhraprasad: Multivalent N-donor ligands for the construction of coordination polymers and coordination polymer gels. (62 pp.) 2018
209. Budhathoki, Roshan: Beneficiation, desilication and selective precipitation techniques for phosphorus refining from biomass derived fly ash. (64 pp.) 2018
210. Siitonen, Juha: Synthetic Studies on 1-azabicyclo[5.3.0]decane Alkaloids. (140 pp.) 2018
211. Ullah, Saleem: Advanced Biorefinery Concepts Related to Non-wood Feedstocks. (57 pp.) 2018
212. Ghalibaf, Maryam: Analytical Pyrolysis of Wood and Non-Wood Materials from Integrated Biorefinery Concepts. (106 pp.) 2018

DEPARTMENT OF CHEMISTRY, UNIVERSITY OF JYVÄSKYLÄ
DISSERTATIONS PUBLISHED IN THE JYU DISSERTATIONS RESEARCH SERIES

1. Bulatov, Evgeny: Synthetic and structural studies of covalent and non-covalent interactions of ligands and metal center in platinum(II) complexes containing 2,2′-dipyridylamine or oxime ligands. (58 pp.) 2019. JYU Dissertations 70.
2. Annala, Riia: Conformational Properties and Anion Complexes of Aromatic Oligoamide Foldamers. (80 pp.) 2019. JYU Dissertations 84.
3. Isoaho, Jukka Pekka: Dithionite Bleaching of Thermomechanical Pulp - Chemistry and Optimal Conditions. (73 pp.) 2019. JYU Dissertations 85.